AD-A022 645

INFRARED VIDICONS EMPLOYING METAL-SILICON SCHOTTKY DIODE ARRAYS

James P. Spratt, et al

General Electric Company

Prepared for:

Air Force Cambridge Research Laboratories

1 October 1975

DISTRIBUTED BY:

NTIS
National Technical Information Service
U. S. DEPARTMENT OF COMMERCE

DDC
RECEIVED
APR 5 1976
RECEIVED
C

REPRODUCED BY
NATIONAL TECHNICAL
INFORMATION SERVICE
U. S. DEPARTMENT OF COMMERCE
SPRINGFIELD, VA. 22161

UNCLASSIFIED
Security Classification

DOCUMENT CONTROL DATA - R & D

(Security classification of title, body of abstract and indexing annotation must be entered when the overall report is classified)

Field	Entry
1. ORIGINATING ACTIVITY (Corporate author)	General Electric Company Space Division/Space Sciences Laboratory P.O. Box 8555, Philadelphia, Pennsylvania 19101
2a. REPORT SECURITY CLASSIFICATION	Unclassified
2b. GROUP	
3. REPORT TITLE	INFRARED VIDICONS EMPLOYING METAL-SILICON SCHOTTKY DIODE ARRAYS
4. DESCRIPTIVE NOTES (Type of report and inclusive dates)	Scientific. Final. For Period 3/27/74 to 9/26/75
5. AUTHOR(S) (First name, middle initial, last name)	James P. Spratt Ruth F. Schwarz George W. Racette
6. REPORT DATE	1 October 1975
7a. TOTAL NO. OF PAGES	130
7b. NO. OF REFS	9
8a. CONTRACT OR GRANT NO.	F19628-74-C-0142
b. PROJECT NO.	2444-n/a-n/a
c.	
d.	
9a. ORIGINATOR'S REPORT NUMBER(S)	
9b. OTHER REPORT NO(S) (Any other numbers that may be assigned this report)	AFCRL-TR-75-0446
10. DISTRIBUTION STATEMENT	A - Approved for public release; distribution unlimited.
11. SUPPLEMENTARY NOTES	This research was supported by the Defense Advanced Research Projects Agency. ARPA Order No. 2444.
12. SPONSORING MILITARY ACTIVITY	Air Force Cambridge Research Laboratories Hanscom AFB, Massachusetts 01731 Contract Monitor: Jerome Bloom/LQD

13. ABSTRACT

The results achieved under this program are as follows:

- A laboratory facility featuring a demountable high beam velocity camera tube and multi-purpose electronic console has been designed and built for evaluating infrared vidicon retinae.
- Infrared imagery has been successfully demonstrated with Schottky barrier retinae in the demountable camera tube.
- It has been shown that metal-silicon Schottky barrier diode arrays suitable for use as infrared retinae can be produced in a conventional silicon I.C. facility using standard processes.
- Quantitative studies have been begun to characterize this new approach to infrared imagery.
- A new high performance sealed-off camera tube has been designed and built for eventual use with these retinae. This tube features high beam landing voltage, meshless construction, and high beam current density. A subsequent report will deal with the details of this new tube.

DD FORM 1 NOV 65 1473 REPLACES DD FORM 1473, 1 JAN 64, WHICH IS OBSOLETE FOR ARMY USE.

Unclassified
Security Classification

Unclassified

Security Classification

14. KEY WORDS	LINK A		LINK B		LINK C	
	ROLE	WT	ROLE	WT	ROLE	WT
Infrared						
Vidicon						
Schottky Diodes						

Unclassified

Security Classification

TABLE OF CONTENTS

Section		Page
I	SUMMARY	1
	A. Program Objective	1
	B. Technical Approach	2
	C. Conclusions	3
II	TECHNICAL DISCUSSION	4
	A. Overall Description of Experiment	4
	1. Principles of Vidicon Operation	4
	a. High Beam Velocity Vidicon Operation	6
	b. Long Wavelength Cutoff Vs. Operating Temperature	9
	2. Description of Demountable Tube and Related Equipment	10
	a. Vacuum Subsystem	12
	b. Electronic Subsystem	12
	c. Cryogenic Subsystem	13
	3. Retina Design	14
	B. Experimental Apparatus	16
	1. Electronics	16
	a. Beam Formation	16
	i. Cathode Activation	
	ii. Filament Supply	
	iii. Voltage Supplies	
	iv. Focus and Alignment Coil Supplies and Regulators	
	v. Horizontal and Vertical Position	
	vi. Offset Controls	
	vii. Panel Meter	
	viii. Cathode Blanking/Variable Integration Period	
	b. Beam Deflection	22
	i. Sync Generator	
	ii. H & V Sweep Generator	
	iii. H & V Deflection Amplifier	
	c. Video Processor/Preamplifier	23
	i. Preamplifier	
	d. Display Subsystem	26
	i. C Scope	
	ii. A Scope	

TABLE OF CONTENTS

Section		Page
	2. Optics	26
	a. Refractive Elements	27
	b. Black Body Source	27
	c. Filters	27
	d. Accessories	27
C.	Retina Characteristics	28
	1. Retina Measurements Made Using Hard Wire Contact	31
	a. Current-Voltage-Temperature Measurements	33
	b. Retina Photoresponse Measurements	40
	c. Retina Spectral Response	41
	2. Retina Measurements Made Using Electron Beam Contact	41
	a. Saturated Values of Target Current	44
	b. Evidence for Beam Induced Conductivity in Exposed SiO_2 on Retina Surface	47
	c. Retina Photoresponse Measurements Using Electron Beam Contact	56
	i. Retina Dark Current Measurements Using Electron Beam Contact	
	ii. Retina Photocurrent	
D.	Imaging Results	64
	1. Qualitative Imagery Studies	64
	2. Development of Working Model to Explain Retina Performance	67
	a. I-V Characteristics Between Mesh and Back Surface S, If The Photosensitive Element is a Photoconductor	71
	b. I-V Characteristics Between Mesh and Back Surface S, if the Photosensitive Element is a Photodiode, Assuming that the SiO_2 Isolating the Diode is Electrically Inactive	77
	c. Retina I-V Characteristics and Imaging for the Case Where the SiO_2 is No Longer Considered Inactive	83
	i. Physical Model of Conduction Processes in the Oxide under the Influence of the Beam	
	ii. I-V Curves between Target Surface and Mesh	
	iii. I-V Curves between Target and Oxide	

TABLE OF CONTENTS

Section | Page

iv. I-V Relations of the Photodiodes
v. Imaging Properties of the Retina
d. Conclusions 120

APPENDIX 123

LIST OF ILLUSTRATIONS

Figure		Page
1	Schematic Diagram of High Beam Velocity Camera Tube	5
2	Equivalent Circuit of Picture Element	7
3	Demountable Camera Tube	11
4	Photographs of Retina at X1 and X1000 Magnification	15
5	Block Diagram of Electrical Subsystem for Demountable Camera Tube	17
6	Photo of Electronic Console	18
7	Circuit for Activating Cathodes and Activation Schedule	20
8	Schematic Diagram of a Schottky Diode under Bombardment by an Electron Beam, I_B	28
9	Equivalent Circuit for the Element in Figure 8	30
10	Equivalent Circuit of High Beam Velocity Vidicon Retina	32
11	Schematic of Schottky Barrier Array Retina (and with Metal Overlay)	34
12	Electron Potential Diagram of Metal - P Silicon Schottky Diode, and Metal-Oxide - P Silicon Interface	35
13	Reverse I-V Characteristics of Retina #10P102D (Dark)	37
14	Reverse I-V Characteristics of Retina 10P102D	39
15	Normalized Short Circuit Current Vs. Open Circuit Voltage Difference (Retina 10P102D)	42
16	Modified Fowler Plot for Relative Spectral Response Vs. Photon Energy (Retina 10P102D)	43
17	Normalized Target Current vs. V_{SM} ($T = 300^{o}K$, $V_{MK} = 250V$)	45
18	Saturated Target Current Vs. V_{MK}	48

LIST OF ILLUSTRATIONS

Figure		Page
19	Normalized Target Current vs. V_{TK}	49
20	Metal Target - Oxide Contact	51
21	Normalized Target Current Per Unit Length of Diode Perimeter Vs. Normalized Target Voltage	55
22	$\frac{I_T}{I_B}$ Vs. V_{SM} for Retina 10P115	58
23	Target Current, I_T Vs. V_{SM} for Various V_{MK}	59
24	Normalized I_T Vs. V_{SM} at Various Light Levels	61
25	Retina Photocurrent Vs. Radiance	62
26	Photo of Image of GE Stencil	66
27	Electron Potential Diagram between the Mesh and the Back Surface, S, of the Photosensitive Element	68
28	Target to Mesh I-V Characteristic	69
29	I_{TM} Vs. V_{TM} for Various Values of the Photocurrent RH	74
30	Superposition of Figures 28 and 29	75
31	I_{TM}, the Signal Current, Vs. Increasing Light Level	76
32	I_{TM} - V_{TM} Curves of the Photodiode Vs. Light Level	79
33	A Superposition of Figures 32 and 28	80
34	A Qualitative Description of I_{TM}, the Signal Current, Vs. Light Level H	82
35	View of Pd_2Si - Oxide Surface as Seen by Electron Beam	84
36	Energy Distribution of Electrons in the Pd_2Si	86
37	Energy Distribution of Electrons in the Oxide	87
38	Metal-Oxide Interface	88

LIST OF ILLUSTRATIONS

Figure		Page
39	Electron Potential as a Function of Distance Between Composite Surface and Mesh	90
40	(a) $\frac{I_{TM}}{I_B}$ Vs. $\frac{V_{TM}}{\overline{V}}$ and (b) $\frac{I_{OM}}{I_B}$ Vs. $\frac{V_{TM}}{\overline{V}}$	96
41	$\frac{I_{OM}}{I_B}$ Vs. $\frac{V_{0T}}{\overline{V}}$ for Constant Values of $\frac{V_{TM}}{\overline{V}}$	97
42	$\frac{I_{OM}}{I_B}$ Vs. $\frac{V_{0T}}{\overline{V}}$ for Constant Values of $\frac{V_{OM}}{\overline{V}}$	98
43	$\frac{I_{OM}}{I_B}$ Vs. $\frac{V_{TM}}{\overline{V}}$ for Constant Values of $\frac{V_{OM}}{\overline{V}}$	99
44	$\frac{I_{TM}}{I_B}$ Vs. $\frac{V_{TM}}{\overline{V}}$ for Constant Values of $\frac{V_{OM}}{\overline{V}}$	100
45	$\frac{I_S}{I_B} = \frac{I_{OM} + I_{TM}}{I_B}$ Vs. $\frac{V_{TM}}{\overline{V}}$ for Constant Values of $\frac{V_{OM}}{\overline{V}}$	102
46	Average Signal Current $\frac{\langle I_S \rangle}{I_B}$ Vs. $\frac{V_{TM}}{\overline{V}}$	104
47	$\frac{I_{T0}}{I_B}$ Vs. $\frac{V_{0T}}{\overline{V}}$	106
48	Average Current Off the Oxide Vs. $\frac{V_{TM}}{\overline{V}}$	108
49	Average Signal Current Vs. $\frac{V_{TM}}{\overline{V}}$	109
50	Experimental Data of $\langle I_S \rangle$ vs. V_{TM} at Room Temperature and Cold, in the Light and in the Dark	110

LIST OF ILLUSTRATIONS

Figure		Page
51 (a)	$\frac{I_{ST}}{I_B}$ as a Function of Light Level Superimposed on $\frac{I_{TM} + I_{T0}}{I_B}$ or $\frac{\langle I_S \rangle}{I_B}$ Vs. $\frac{V_{TM}}{\overline{V}}$	112
51 (b)	$\frac{I_{TS}}{I_B}$ as a Function of Light Level Superimposed on $\frac{I_{TM} + I_{T0}}{I_B} = \frac{\langle I_S \rangle}{I_B}$	113

I. SUMMARY

A. Program Objective

The research described herein was conducted to demonstrate the utility of silicon integrated circuit technology in addressing problems of cost and reliability in infrared imaging systems. Such systems have, in the past, employed arrays of individual detectors (used in conjunction with mechanical scanners) to respond to the instantaneous radiation flux from the corresponding point in object space as the scene is scanned. Separate pre-amplifiers are often employed for each detector. Furthermore, the detectors themselves employ exotic semiconductor materials tailored to the specific spectral interval of interest, so that little commonality is achieved in the development of devices. The result is a technology characterized by impressive performance but plagued by high system costs and less than optimum reliability. If new and novel approaches to infrared imagery could be developed which would provide comparable performance at reduced cost and with improved reliability, the impact on military infrared technology would be substantial.

Silicon technology has, in recent years, produced a revolution in electronics well known to all in the fields of engineering and science. It has found little application in the infrared area, however, since silicon does not normally respond to infrared radiation of wavelength $\gtrsim$ 1 μm. If a suitable photoresponsive mechanism in the range beyond 1 μm could be developed for use in silicon devices, the full weight of a very impressive materials technology could be brought to bear on infrared imagery, and the dual problem of high cost and insufficient reliability might be solved. Internal photoemission(1) in metal-silicon Schottky barrier diode structures has long been known to permit the detection of infrared radiation of wavelength longer than the fundamental absorption edge in silicon. After comparison with alternative infrared photoresponsive mechanisms for use with silicon, this was selected as the one offering the greatest opportunity for success. The detailed properties of the physical process of internal photoemission dictated the direction which would be pursued in applying it to infrared imagery.

B. Technical Approach

Internal photoemission in metal-silicon Schottky barrier diodes is characterized by a relatively low quantum efficiency (~ 0.1%), so that imagers employing such devices must employ more efficient sampling techniques than those used in conventional infrared line scanners in order to achieve comparable sensitivity. One well known way to achieve more efficient sampling is to employ frame time integration. Television systems for the visible portion of the spectrum typically use this method to enhance sensitivity before readout. Contrast in this application is typically 20% or better, so that the minimum detectable signal is set, not by fluctuations in the signal or the background, but rather by a fixed noise source such as the input stage of the preamplifier. If one attempts to apply this technique to the infrared, where low contrast conditions exist because of thermal radiation from the background, several problems arise, viz:

- Detector saturation by background photon flux.
- Non-uniformity in responsivity, when operating against a high background, generates a fixed pattern "noise," which while not truly random, limits the ability to detect low level signals conveniently.

Analysis has shown[2] that these two problems can, with proper care, be controlled sufficiently to permit the use of metal-silicon Schottky barrier retinae, operated in the storage mode, out to the 3-5 μm spectral range. (This wide range of operation is possible because of the high degree of uniformity which silicon technology permits in the fabrication of Schottky barrier mosaics.) Consequently, storage mode operation of metal-silicon Schottky barrier diode arrays was selected as the approach to be pursued.

Storage mode operation of diode arrays can be achieved in "hard wire accessed arrays," and in "electron beam accessed arrays." The latter approach was pursued at the Space Sciences Lab of General Electric Co., with the goal of producing an infrared vidicon employing as a retina a mosaic of palladium-silicon Schottky diodes. This particular metal was selected because it produces, on P-type silicon, a barrier sufficiently low (0.35 ev) to permit detection out to 3.54 μm-sufficiently far to demonstrate the basic feasibility of the approach while at the

same time not posing the more serious experimental problems of a 5 μm tube. The first consideration addressed under this program was the selection of the mode of vidicon operation to be pursued. Conventional vidicon camera tubes use electron beams which land at a few volts potential to charge individual picture elements down to cathode potential. In tubes employing diode mosaics for the retina, diode polarity is selected to assure that such charging reverse biases the diodes so that dark current is kept to a minimum. In the vidicon under discussion here, diode polarity is dictated by the desired long wavelength cutoff. This polarity results in a forward biased diode when used with a low landing velocity electron beam. Consequently, a high velocity electron beam readout is required. In this mode of operation, the beam lands with an energy sufficiently high to dislodge secondaries with a yield $\delta > 1$. These secondaries flow to a nearby collector, with the result that individual picture elements charge positively with respect to this collector (and hence to the underlying P-type silicon). Thus, the technical approach selected was to demonstrate the feasibility of infrared imagery using an infrared vidicon tube employing a high velocity beam to interrogate a mosaic of Pd-P type Si Schottky diodes.

C. Conclusions

The results achieved under this program are as follows:

- A laboratory facility featuring a demountable high beam velocity camera tube and multi-purpose electronic console has been designed and built for evaluating infrared vidicon retinae.

- Infrared imagery has been successfully demonstrated with Schottky barrier retinae in the demountable camera tube.

- It has been shown that metal-silicon Schottky barrier diode arrays suitable for use as infrared vidicon retinae can be produced in a conventional silicon I.C. facility using standard processes.

- Quantitative studies have been begun to characterize this new approach to infrared imagery.

- A new high performance sealed-off camera tube has been designed and built for eventual use with these retinae. This tube features high beam landing voltage, meshless construction, and high beam current density. A subsequent report will deal with the details of this new tube.

II. TECHNICAL DISCUSSION

Four topics will be discussed in detail in this section of the report. These are:

- Overall description of experiment
- Experimental apparatus
- Retina design and characterization
- Imaging results

A. Overall Description of Experiment

1. Principles of Vidicon Operation

The experiment described herein was designed to demonstrate the feasibility of infrared imagery using a vidicon tube in which a high velocity beam is used to interrogate a mosaic of palladium-P type silicon Schottky barrier diodes. The essential elements in such a vidicon camera tube are shown schematically in Figure 1. These are the electron gun section, beam deflection section, and the retina section. The electron gun section typically contains a thermionic cathode and several other electrodes for forming and modulating an electron beam. The scanning section contains coils (electromagnetic deflection) or plates (electrostatic deflection) for deflecting the beam across the retina surface in a prescribed fashion. The retina section consists of a photosensitive surface which can be charged (by the scanning beam) relative to its opposite (window) side. Light incident on the window side of the retina will discharge the photosensitive surface, necessitating the flow of additional current to recharge the retina during the next scan. This recharging current thus varies in time in a manner which is synchronized with the spatial position of the scanning beam, and hence the spatial pattern of incident light. It constitutes the video signal. This current (I_S) flows for a time t_R, the dwell time of the beam on a given picture element. During this time the potential of this picture element is restored to its equilibrium value. The charge deposited in the process is

$$Q_D = I_S t_R \qquad (1)$$

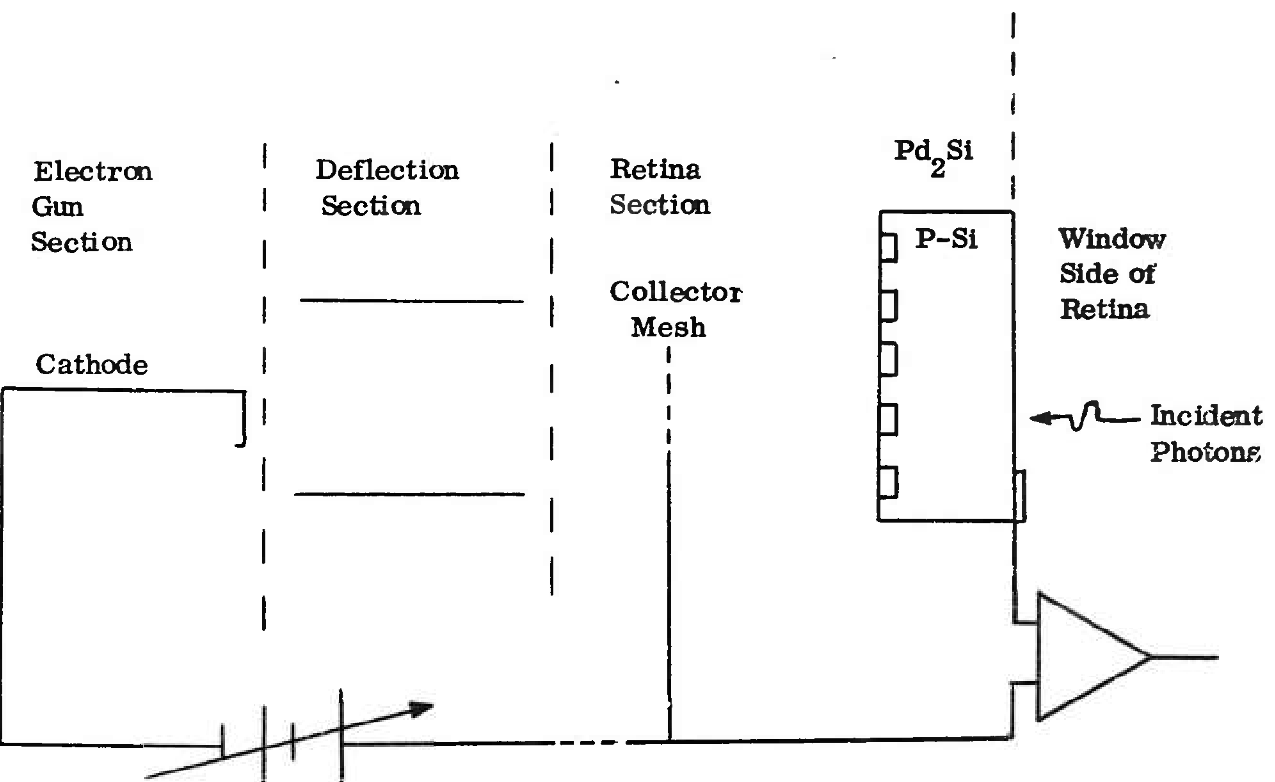

Figure 1. Schematic Diagram of High Beam Velocity Camera Tube.

The charge leaked off that picture element by light (Q_L) during the frame time, t_f, is (neglecting dark current)

$$Q_L = I_P t_f = q\, y\, i_{ph} \tag{2}$$

where I_P = photocurrent

q = electronic charge

y = quantum efficiency

i_{ph} = photon flux (photons/picture element/second)

In the cyclic state, $Q_D = Q_L$, so that

$$I_S = I_P \frac{t_f}{t_R} = q\, y \frac{t_f}{t_R} i_{ph} \tag{3}$$

If t_f = 1/30 second, and t_R = 1 μsec, a storage mode gain of $\frac{t_f}{t_R} = 3 \times 10^4$ results to offset the effect of low quantum efficiency inherent in metal-silicon Schottky diodes for radiation of wavelength beyond the fundamental edge of silicon. The equivalent circuit of such an idealized picture element is shown in Figure 2. It can be seen that attainment of the high storage mode gain assumes that the leakage of charge off the capacitor in the absence of light is minimal. To assure that this condition is met it is necessary that the voltage applied to the diode be of the proper polarity (reverse bias), and that the operating temperature be such that the thermally generated leakage current is low. These two requirements and their implications are discussed below.

a. High Beam Velocity Vidicon Operation

To permit the scanning beam to land on the retina, the common side of any diode mosaic must be biased positively with respect to the cathode. The floating side of the retina will then be charged by the beam to a potential relative to the cathode (and hence to the common side of the diode mosaic) which depends on the velocity with which the beam lands on the floating surface. Conventional camera tubes use electron beams which land at a few volts potential relative to the cathode. If the common side of the diode mosaic is N-type, slow electrons such as these

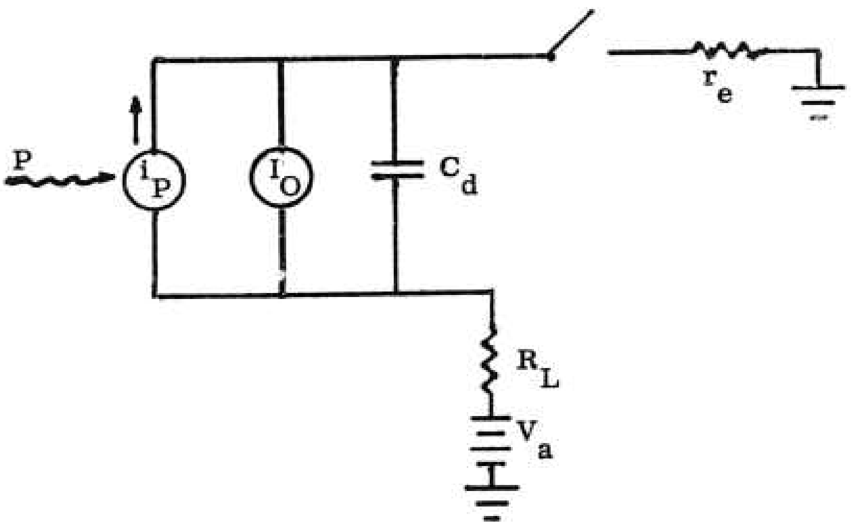

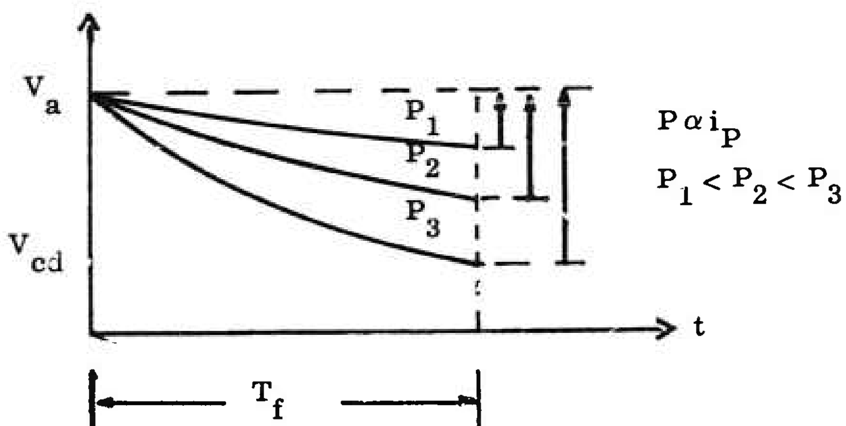

C_d = diode capacitance

I_O = diode reverse leakage

i_P = photocurrent

P = photon flux

r_e = beam resistance

R_L = load resistance

T_f = frame time

V_a = applied voltage

V_{cd} = voltage across C_d

Figure 2. Equivalent Circuit of Picture Element.

charge the floating side of the retina to a voltage sufficiently negative with respect to the cathode to make it impossible for additional electrons to land. Thus P^+ islands on N material become reverse biased, permitting storage over a full frame time (N^+ islands on P material would become forward biased, and full frame time storage would be impossible). Since the spectral range of both P^+-N and N^+-P mosaics is identical, diode polarity can be selected to permit low beam velocity scanning. Metal-silicon Schottky barrier diodes, however, have an additional constraint placed on them. In order to achieve the desired long wavelength cutoff in the infrared vidicon retina, a metal-silicon system must be chosen which has a low value of barrier height, ϕ_o. This is most easily achieved using high work function metals (such as Pd_2Si) on P-type silicon. Such a choice, however, results in a diode polarity opposite to that normally used in semiconductor diode retinae. Consequently, these mosaics must be scanned with electron beams which land with an energy sufficiently high to dislodge secondary electrons with a yield $\delta > 1$. An individual Pd_2Si island will therefore charge positively under a fast beam to a potential, V_{FT}, determined by the mesh (mesh stabilized operation) rather than to a potential determined by the cathode, as occurs in low beam velocity scanning. V_{FT} can be determined for the highly idealized case of a homogeneous retina as follows. Assuming that the secondary electrons are Maxwellian one obtains the following equations[3];

$$I_M = \int_{V_{FT}}^{\infty} \frac{di_S}{dV_Z} \, dV_Z = i_S \exp(-V_{FT}/\overline{V}) \qquad (4)$$

where I_M = current of secondary electrons going to the mesh

i_S = secondary electron current generated at the floating target

V_Z = energy component of secondaries normal to plane of target

$\overline{V}$ = average energy of secondaries

The net current supplied by the beam to the floating target is the difference between the primary beam landing and the secondaries going to the mesh, which is

$$I_T = I_B - I_M = I_B - i_S \exp(-V_{FT}/\overline{V})$$

$$= I_B \left[1 - \delta \exp(-V_{FT}/\overline{V})\right]; \quad V_{FT} \geq 0 \tag{5}$$

$$= I_B (1 - \delta) \qquad ; \quad V_{FT} \leq 0 \tag{6}$$

where $i_S = \delta I_B$

I_B = beam current

The floating target will charge to a voltage V_{FT} such that $I_T = 0$, if possible. This will produce

$$V_{FT} = \overline{V} \, \ln \delta \tag{7}$$

where V_{FT} is positive relative to the mesh. Thus if the common side of the diode mosaic is biased negatively with respect to the mesh, the net voltage between the Pd_2Si island and P silicon is such that the diode is reverse biased. If we neglect interactions between the Pd_2Si islands and the SiO_2 between these islands, a fast beam scanned across the diode mosaic in raster fashion will charge the metal to V_{FT}. Photocurrents can then discharge the target surface down toward mesh potential during the frame time, so that a signal will be generated between retina and mesh when the beam returns to a given spot during the next scan.

b. Long Wavelength Cutoff Vs. Operating Temperature

The quantum efficiency (y) of the internal photoemission process in metal-silicon Schottky diodes is low, as shown by the following equation[1]

$$y = C A \frac{\left(h\nu - \emptyset_o\right)^2}{h\nu} \quad ; \; h\nu \geq \emptyset_o \tag{8}$$

where C = constant $\approx$ 0.2/ev

A = optical absorptance in metal

$\emptyset_o$ = height of metal-silicon barrier in e.v.

If the barrier height is selected to permit detection out to a cutoff wavelength λ_o ($\lambda_o = 1.24/\emptyset_o$), the reverse leakage current I_o is affected, since[4]

$$I_o = A^* T^2 \exp\left(-q\varnothing_o/kT\right) \quad (9)$$

where A^* = modified Richardson constant.

The reverse leakage current must be such that the charge leaking off a diode in a frame time is less than the charge on the diode

$$I_o t_f \leq C_D V_D \quad (10)$$

where C_D = diode capacitance
V = voltage across diode

It must also be less than the maximum charge which the beam can deposit in one read time, t_R.

$$I_o t_f \leq I_B (\delta - 1) t_R \quad (11)$$

where $I_B (\delta - 1)$ is the maximum current which the fast beam can deposit on the retina (cf. equation (5)).

t_R is the time the beam dwells on an individual picture element.

Because of the high specific capacity of diodes, and the limitations on beam current available in camera tubes, equation (11) is a more difficult condition to meet. Using this equation, the temperature to which the retina must be cooled for a given long wavelength cutoff can be determined. For the retina design used herein, operating temperatures $< 110^oK$ are required.

2. Description of Demountable Tube and Related Equipment

To permit the evaluation of different retina designs and different electron beam scan configurations, a demountable camera tube was designed and built. This tube permits a retina to be scanned on one side with a suitable fast beam of electrons (with provision for collecting secondaries), while the opposite side is being exposed to the optical image. Retina cooling is achieved by radial heat flow to a suitable heat sink. Figure 3 depicts such a demountable camera tube, showing the main features of the system. The vacuum, electronic, and cryogenic subsystems are discussed below.

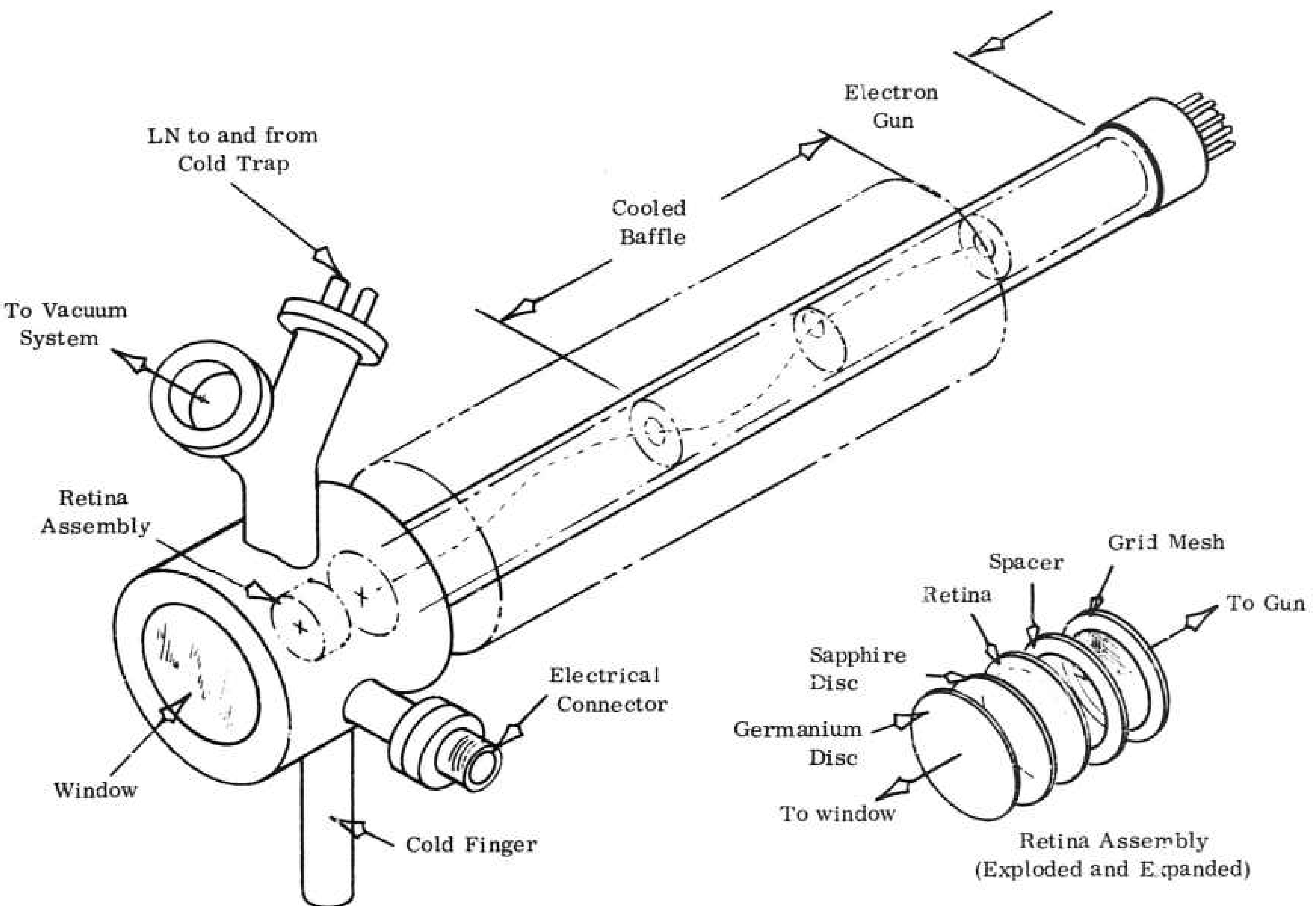

Figure 3. Demountable Camera Tube

a. Vacuum Subsystem

One of the major problems encountered in operating a demountable camera tube is that of establishing and maintaining good emission from the thermionic cathode used in the electron gun despite the need for repeatedly opening the system to change retinas. The approach used in this program was to use standard electron guns of the type employed in the GE Z7966 3-inch image orthicon camera tube. Such tubes were obtained from the factory, with the image section removed, before the cathode was activated. The problem then became one of activating the cathode in situ, and protecting the cathode after activation by good vacuum technique. The more important features of the vacuum system are described here.

The vacuum system employs a Welch 2-stage Duo-Seal mechanical pump of 25 L/M capacity, with a cold trap to reduce oil contamination of the camera tube. The high vacuum pump used is a Hughes 30 L/sec ion pump, which is sufficiently fast to handle the 3-liter volume of the tube adequately. (Pressures in the neighborhood of 3×10^{-7} Torr are readily obtained). After roughing the system, and before turning on the ion pump, the glass part of the system is baked overnight with heating tapes to drive off adsorbed water. Then the cathode barrel is heated using an R.F. induction heater. Power is slowly increased until the barrel glows dull red, then it is reduced sufficiently to eliminate the incandescence and allowed to bake for 1 hour. The tube is then cooled and the ion pump is turned on. To prevent condensation of residual water vapor on the retina, a 120 cm^2 Meissner trap is pre-cooled. Using this large surface to cryo-pump, system pressure can quickly be reduced from 3×10^{-7} Torr to 3×10^{-8} Torr.

b. Electronic Subsystem

The electrical and electronic functions needed to operate the demountable tube include those associated with beam forming and deflection, video processing, and display, in addition to the required power supplies and monitoring equipment. These are discussed in Section II-B below. Aspects of the electronics peculiar to the demountable tube itself deal with cathode activation and the baffle. Figure 3 shows a cooled baffle in the gun portion of the tube, designed to baffle optical

radiation from the hot cathode. This baffle consists of two on-axis apertures separated by an off-axis aperture located one node from each. By applying equal and opposite d.c. deflection fields in each chamber of the baffle, the electron beam can be threaded thru, while optical radiation from the beam defining aperture in the gun section is completely blocked. After emerging from the baffle, the beam can be deflected in the normal fashion to produce a raster scan. (The baffle structure is made of alumina in the deflection section, while copper is sufficient for the baffle section, since the use of d.c. deflection fields there prevent eddy current losses from being a problem.)

The cathode used in the demountable tube is a standard oxide cathode, activated in situ using conventional activation procedures. It has been found that once activated, a cathode will usually permit 5 to 10 exposures to ambient pressure before emission degrades substantially.

Early in the program, the decision was made to operate the tube with the cathode at system ground potential, and the retina assembly above ground. This was done to avoid possible problems with the cathode blanking circuit and to simplify isolation between cathode and filament. In hindsight this was a mistake, since it complicates retina cooling immeasurably to have the retina several hundred volts above the heat sink. A system redesign to correct this should be considered.

c. Cryogenic Subsystem

Figure 3 shows a cold finger originally designed to provide retina cooling. Experience showed, however, that such a feature was unable to cool the retina sufficiently, by itself, and was unnecessary when flowing liquid nitrogen was used to cool the retina holder as well as the Meissner trap.

The retina assembly shown in Figure 3 was designed to facilitate retina cooling. The germanium disc serves as a cooled long pass filter. The sapphire disc, in intimate contact with the retina, increases lateral heat flow to the cold retina holder, while at the same time providing needed electrical insulation between the silicon target and the retina holder, which is at system ground potential.

3. Retina Design

The particular material system selected for this purpose was palladium on P-type silicon. Palladium forms a stable silicide having a barrier height of 0.34 ev on P-silicon, giving a long wavelength cutoff of 3.65 μm. The mask set used produced a 34 mm diameter array of 8 μm square diodes on 10 μm centers. Cuts were made in this pattern in a 0.5 μm thermal oxide grown on 2-inch wafers of P-type silicon of two different resistivities, 3 ohm-cm and 10 ohm-cm. Palladium of two different thicknesses (500 Å and 5000 Å) was deposited and sintered at 270°C for 5 minutes in 50:50 H_2, N_2. Unreacted palladium was then etched off without removing the Pd_2Si, leaving the desired diode pattern. Ohmic contact to the P-region consisted of an annular ring, 0.125 inch wide and 2 inches O.D. of sintered platinum on the side of the wafer opposite to the diode array. (The forward voltage drop calculated for the Pt-Si contact at 1 μA is 70 mev.) Figure 4 shows a photograph of a finished retina at X1 and X1000.

P-N junction diode array vidicon targets suffer from problems of surface inversion which shorts adjacent diodes. This problem will not bother cooled Schottky diode vidicon targets for two reasons:

(1) There are no means for generating minority carriers in the bulk to re-supply an inverted surface. Thermal generation is minimal, especially at the target operating temperature of 77°K. Optical generation of minority carriers requires photons of $\lambda < 1.1$ μm, which are filtered out by means of a germanium pre-filter.

(2) In the case of adjacent metal islands sitting at different potentials, any minority carriers initially present at the surface will flow to the appropriate island, but the other island cannot serve as a source of additional minority carriers, since its barrier to minority carriers is higher than its barrier to majority carriers.

As a result of this freedom from surface inversion, it appears that these retinae will not require a resistive sea. In view of the lack of information on the properties of resistive sea at 77°K, this development is a happy one.

A more detailed discussion of retina characteristics is given in Section II-C below.

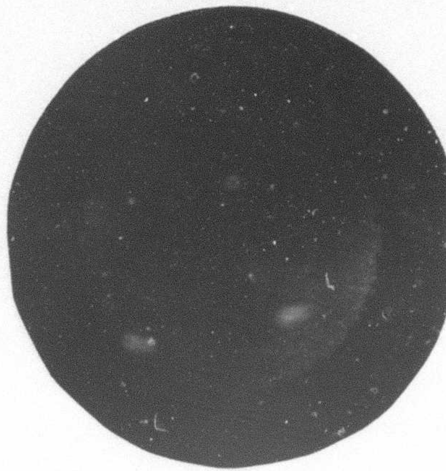

Figure 4. Photographs of Retina at X1 and X1000 Magnification

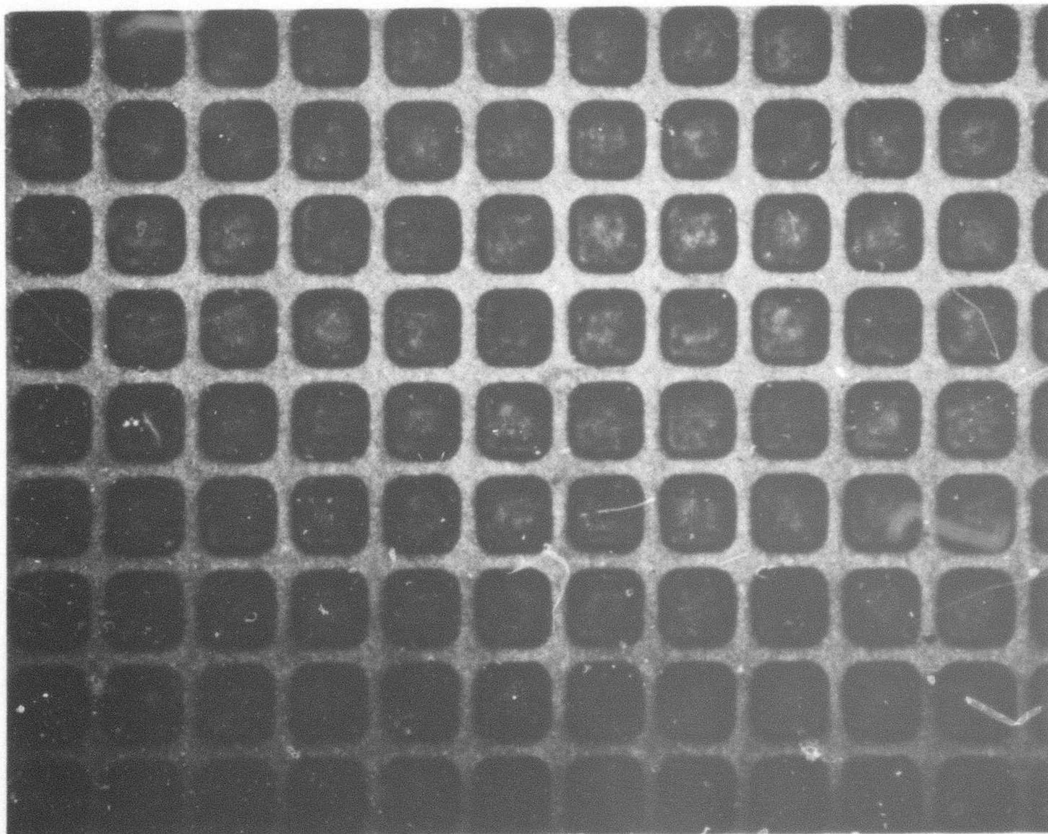

B. Experimental Apparatus

In addition to the demountable camera tube described above, the experimental apparatus used in this program consisted primarily of an electronics console, and an optical bench. The former supplied to the demountable tube the functions of beam forming and deflection, video processing, and display. The latter was designed to permit measurement of retina response and initial imaging experiments. Once the feasibility of imaging was demonstrated, and sufficient experience obtained with retina behavior under a high velocity scanning beam to warrant quantitative studies, the optics was upgraded to permit measurement of tube transfer characteristic, square wave response, resolution element size, etc.

1. Electronics

Figure 5 shows the block diagram of the electronic subsystem used in this experiment. It supplies four functions, viz. beam forming, deflection, video processor, and display, all contained in the test console shown in Figure 6. The details of each of these blocks is given elsewhere,[5] and is summarized below.

a. Beam Formation

The beam formation functions supplied by the electronics console include the following:

- Cathode activation
- Filament supply
- Voltage supplies for G1, G4, G6, mesh and retina
- Focus and alignment coil current supplies and regulators
- H & V position
- Offset controls (these control fields used to thread beam thru baffle)
- Panel mounted meter and rotary switch permitting all D.C. tube currents and voltages to be monitored readily
- Cathode blanking/Variable integration period control

Each of these functions is discussed below:

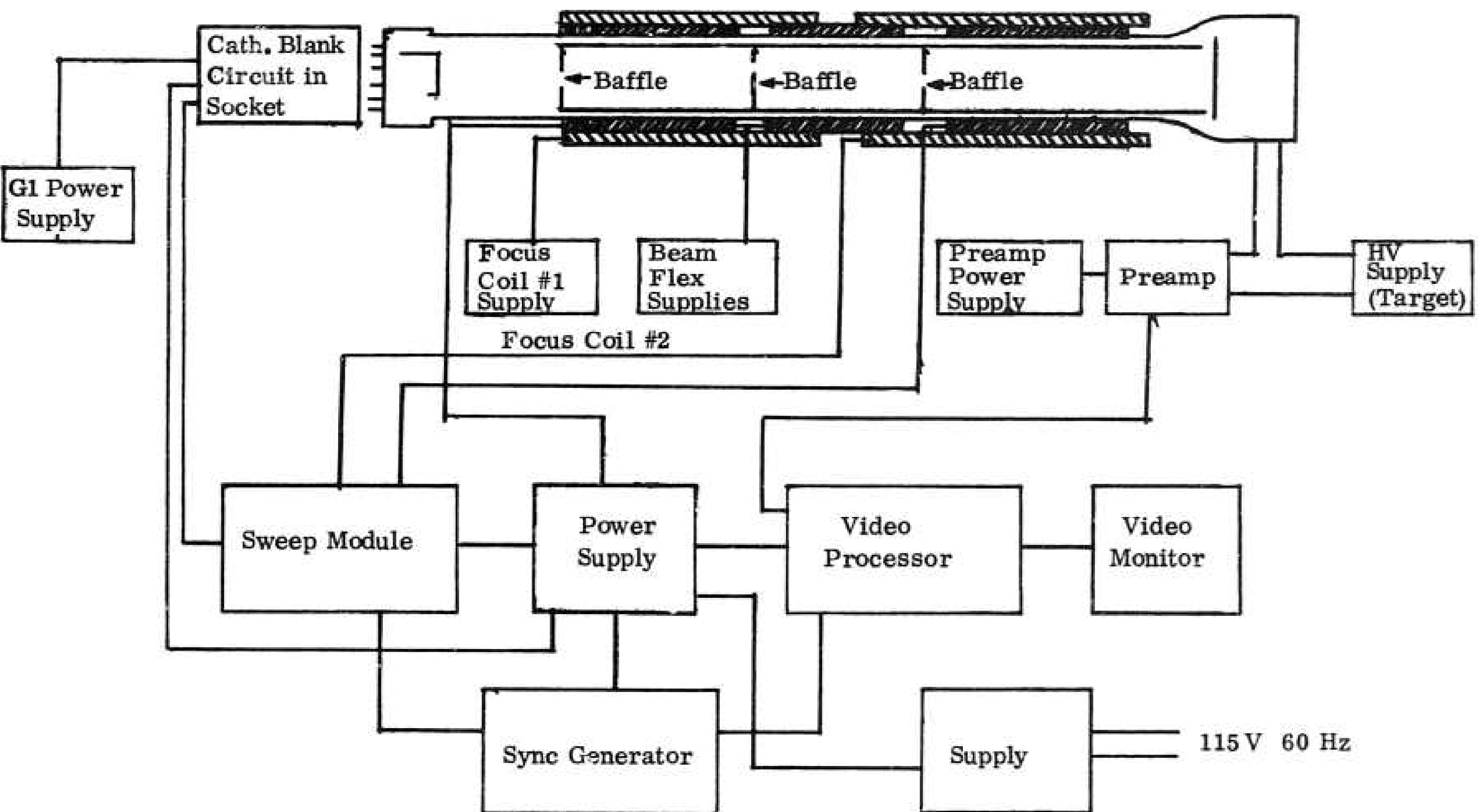

Figure 5. Block Diagram of Electrical Subsystem for Demountable Camera Tube.

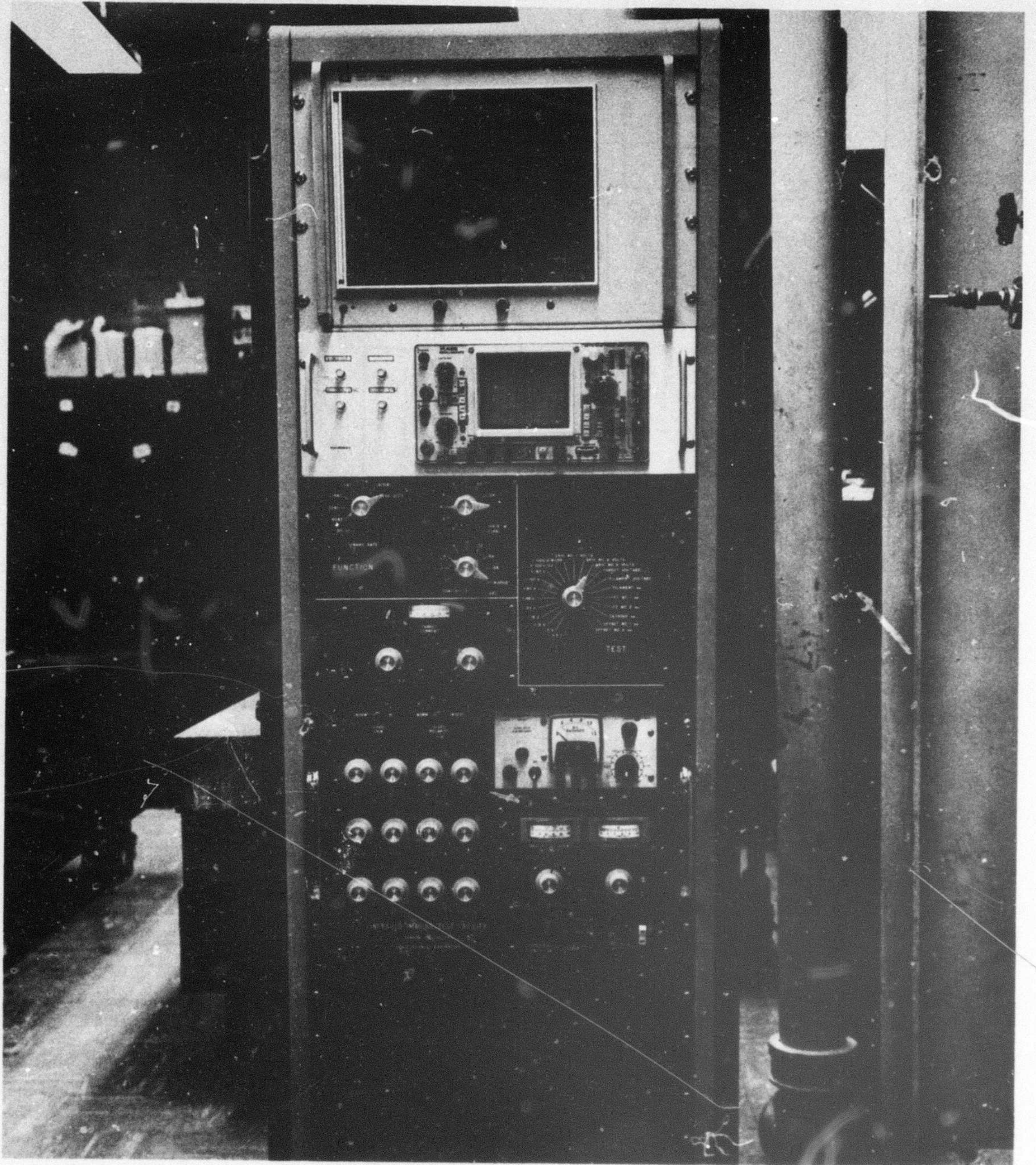

Figure 6. Photo of Electronic Console.

i. Cathode Activation

The cathodes used in the demountable tube are activated in situ using the circuit and schedule shown in Figure 7. The filament (heater) current and G1 voltage are supplied by the electronics console, and the progress of activation is monitored there by observing cathode current I_k on the digital panel meter.

ii. Filament Supply

Commercial GE Z7966 3-inch I. O. tubes require 0.6 amps filament current in operation. The less than optimum cathode activation conditions imposed by the use of a demountable tube force the use of higher values, especially after repeated cycling. Thus, filament current is continuously variable over the range from 200 ma (filament standby current level) to 1 ampere (maximum filament operating current).

iii. Voltage Supplies

G1 is the control grid of the demountable tube. When varied over the range from -10 volts to +1, it varies cathode current (I_k), and hence beam current, from cutoff to saturation.

G4 is the designation assigned to the copper baffle. It is operated between +130 and +185 volts above cathode potential (system ground).

G6 is the designation assigned to the metallization on the inside of the ceramic section of the baffle nearest the retina. It is operated +25 volts above the mesh, to assist in collecting secondaries generated off the mesh by the fast beam.

The mesh most frequently used is a 750 line per inch copper structure formed by electroforming and stretched over a stainless steel frame in such a way that the mesh can be brought arbitrarily close to the retina surface. It has a transparency factor of 61%, and can be biased anywhere over the range from 0 volts to 1000 volts above system ground.

The retina contact can be biased anywhere from -40 volts to +40 volts relative to the mesh.

2-Hour Bake at 350°C

Time (Minutes)	Heater Current	I_k
10	.4	0
10	.5	0
10	.6	0
3	.7	10-50 μA
2	.8	1 mA
3	.7	700 μA
2	.8	1.5 mA
3	.7	1 mA

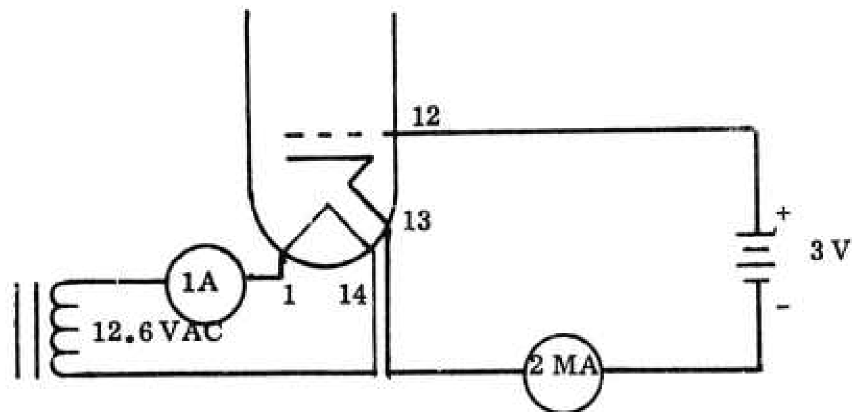

Figure 7. Circuit for Activating Cathodes and Activation Schedule.

iv. Focus and Alignment Coil Supplies and Regulators

Two focus coils are used in the demountable system because of the extra tube length necessitated by the baffle. Regulation is achieved thru the use of a conventional differential D.C. amplifier which compares the voltage drop produced by the focus current flowing thru a precision resistor to a fixed regulated voltage source. Each supply can be varied over the range 0.55 to 1.1 amps D.C.

The alignment coil requires a small direct current to compensate for misalignment of the gun. We have never found it necessary to use the alignment coil.

v. Horizontal and Vertical Position

These controls permit the horizontal and vertical center of the scan to be adjusted by passing a direct current thru the H & V deflection coils.

vi. Offset Controls

These controls permit the direct current fed to the offset (vertical direction) coils to be varied, enabling the electron beam to be threaded through the baffle of the demountable tube.

vii. Panel Meter

Because of the need for extreme flexibility in research equipment of this type, provision was made for monitoring a wide range of parameters which in a practical demonstration system would be fixed. A twenty-three (23) position switch allows selection of 23 test points whose readings appear on a digital panel meter. The test points include D.C. power supply voltages, camera tube electrode voltages and essential current readings. A variety of signal conditioning circuits is required to permit all these quantities to be displayed on the same meter.

viii. Cathode Blanking/Variable Integration Period

To guard against retina burn in the event of sweep failure, a camera blanking circuit was employed which drives the cathode positive with respect to G1, into cutoff when sweep ceases. (This control circuit can be bypassed if unscanned measurements are desired.) The same circuit permits a switch selected integration period. In this mode the beam can be cut off for a specified number of frames

(2^n fields where $0 \leq n \leq 7$) after which the retina can be read out in a separately specified number of frames (2^m fields where $0 \leq m \leq 7$). This capability permits the effects of retina leakage to be determined readily.

b. Beam Deflection

The deflection functions supplied by the console include the following:

Sync generator

H & V Sweep Generator

H & V Deflection Amplifier

i. Sync Generator

The sync generator selects the desired frame and line rates. In the standard mode, the horizontal frequency is 15.750 kHz, and the vertical frequency 60 Hz with a positive 2:1 interlace for a 30 frames/sec picture rate. In the variable mode, the vertical frequency can be reduced from 60 Hz to 1.875 Hz in six discrete steps of ratio 2X. In this case there are 525 lines, non-interlaced, per frame. To view images in this mode an X-Y monitor is required (instead of the standard TV monitor), so there is no need for the 2:1 interlace feature. The low frame rates will result in picture flicker anyway, even if interlace were used, and removing it will result in smoother pictures and eliminate some of the interlace problems normally associated with television display systems.

ii. H & V Sweep Generator

The horizontal (H) and vertical (V) sweep generator generates the necessary H and V sawtooth voltages to drive the X-Y display and the H&V deflection amplifier. The output of the sweep generator is a fixed sawtooth amplitude for each frame and line rate selected. The frame and line rate selection is made in the sync generator. The sync generator supplies the necessary H and V sync pulses to drive the H&V sweep generator.

The sweep generator sawtooth output has a controlled offset that is used for picture centering or picture offset. This is possible because of the D.C. deflection amplifier which is direct coupled to deflection yoke.

iii. H & V Deflection Amplifier

The horizontal (H) and vertical (V) deflection amplifier converts the voltage sawtooth input from the H&V sweep generator to a current sawtooth to drive the horizontal and vertical deflection coils on the vidicon camera tube.

The horizontal deflection amplifier limits line rate and essentially the frame rate of the system. The deflection amplifier limits its flyback voltage peak to approximately 35 volts. With a low inductance yoke (50 microhenry) a sweep of 3 amperes is required for one-half deflection or 6 amperes for full deflection and a flyback period of 10 to 12 microseconds. To reduce the flyback time, a higher flyback voltage limit or a lower inductance yoke is required. A lower inductance yoke would require a higher sweep current sawtooth.

The deflection amplifier includes offset power supply voltages. Instead of the ±35 volt supply a +50V and -20V supply is used to increase the flyback voltage limit, but it requires additional power dissipation at the quiescent point because of the offset.

The limit of line rate 60 x 525 = 31.5 kHz was selected to allow approximately a 2 to 1 active to blanking time ratio. Higher frame rates would increase line rate and result in the blanking (flyback) period being a large portion of the total line scan period. Since the deflection yoke is D.C. coupled to the deflection amplifier, the low frequency scan rate poses no such problem.

c. Video Processor/Preamplifier

The functions supplied in this area are those involved in amplifying and conditioning the video signal to the level necessary to operate conventional TV monitors. The preamplifier, several versions of which are described below, amplifies the low-level video signal from the nanoampere level extracted from the retina to several hundred millivolts, at which it is passed on to the video processor. The bandwidth can be tailored to be sufficient to the resolution the retina is capable of, and no more.

The video processor amplifies the output of the preamplifier to 0.7 to 1.0 volts peak video, as required to drive the monitor. In addition, the video processor

includes peaking circuits to compensate for bandpass roll-off effects which might be present in retina or preamplifier. Also included is a D.C. restorer, and the circuitry needed to add to the video the blanking levels for zero black level. Video processor output can be either composite or non-composite, and can be supplied either normal or inverted.

i. Preamplifier

One of the key tasks of this program is the determination of the preamplifier configuration best suited for use with Schottky diode retinas used in high beam velocity, direct target readout, vidicons. The preamplifier must be A.C. coupled, to separate the video from the high D.C. voltage at which the retina rides. We can assume that, between mesh and retina leads, the preamplifier will see the diode capacitance in series with the capacitance from metal islands to mesh. The latter should, for typical mesh spacings, be in the neighborhood of 10 pf or less. Thus, parasitic capacitance to ground between retina and preamp input should be the dominant pre-amp input load factor. Since in a demountable system, such parasitics are difficult to control, it is not clear whether adequate system frequency response can be obtained with a high input impedance preamplifier. It may be necessary to resort to low input impedance configurations, even if system noise figure is degraded somewhat in the changeover. If extremely small target to mesh spacings are used, mesh capacitance can rise substantially, making low Z_{in} preamplifiers essential. (See Appendix)

Preamplifier evaluation has not been completed as yet, but two modifications of low Z_{in} configurations have been studied. One (referred to henceforth as type "A" preamp) is a transimpedance amplifier with a buffer stage on the output. The second (type "B") employs a grounded base input stage to achieve low Z_{in}. No feedback is used to reduce open loop gain. Instead, emitter regeneration is used to control gain stability. Table 1 gives some important parameters of these two preamplifiers. This data was obtained as follows: Using a bar generator, the transimpedance was determined by measuring the output voltage for a given input current. Then, the wideband peak-to-peak noise was determined under given conditions of capacitive loading on the input. Using this value of output noise, the equivalent rms output noise voltage was obtained[6]. From the rms output noise and the transimpedance, the rms input current noise was obtained. (For each value of C_{in}, gain and bias

Table I

Transimpedance Amplifier with Video Buffer

	$C_{in} = 0$	$C_{in} = 300$ pf	$C_{in} = 1000$ pf
Transimpedance	1.2×10^6	1.3×10^6	1.4×10^6
Output Noise (peak-to-peak)	30 mV	50 mV	70 mV
Output Noise (rms)	5 mV	8.3 mV	12 mV
Input Noise (rms)	4.2 na	6.4 na	7.1 na

Grounded Base Pre-amplifier

	$C_{in} = 0$	$C_{in} = 300$ pf	$C_{in} = 1000$ pf
Transimpedance	0.55×10^6	------	0.51×10^6
Output Noise (peak-to-peak)	15 mV	------	40 mV
Output Noise (rms)	2.5 mV	------	6.7 mV
Input Noise (rms)	4.6 na	------	13 na

were re-adjusted for stability, so that the values obtained for R_T are not the same.) Studies are continuing on both of these pre-amplifier types, as well as candidate high input impedance designs.

d. Display Subsystem

The display subsystem consits of an A scope (for displaying waveforms and individual lines of video) and a C scope (for displaying images), both mounted in the electronics rack. It also consists of a line selector, and video tape recorder with separate display, all separate from the electronics rack.

i. C Scope

The television display is a Hewlett-Packard HP-1300. It is basically an X-Y display that requires sawtooth inputs for vertical and horizontal scan. [illegible] alternate video processor video output includes the composite video output signal to drive a conventional 525 line, 2 to 1 interlace, 30 frames/sec television monitor. This output is useful, when the vidicon camera is in the standard TV mode.

ii. A Scope

A dual input oscilloscope, Tektronix Model R432 is used to select a frame and/or field of video as well as a line selector video. The line or lines of video displayed upon the oscilloscope will be shown on the TV display monitor via a bright or dark line.

2. Optics

The optical subsystem for use in this facility is designed to permit the measurement of resolution, uniformity, and spectral response of infrared vidicon retinae mounted in the demountable camera tube. Refractive optics are used which were designed for minimum chromatic aberration over the range $1.8\ \mu m \le \lambda \le 3.5\ \mu m$. These optics are mounted on an optical bench coaxial with the demountable tube. This bench also supports the filter assembly, precision apertures, stencil patterns, irises, etc. The black body source is positioned axially with the system at the opposite end of the optical bench. The parameters of interest of the optical subsystem are as follows:

a. Refractive Elements

Two Servo Corporation Ge-Si achromat doublets, four inches in diameter, with twelve inch focal length, are used, providing an F/3 capability. (The price paid for achieving the demountable feature in the test facility is a retina position which is much deeper into the tube from the front window than desired. As a result, the maximum usable F number for external optics is F/3.) These lenses have 0.2 milliradian resolution on axis, and 0.4 milliradian at the edge of a one inch field of view. They are coated for maximum transmission over the range $2\ \mu m \leq \lambda \leq 5\ \mu m$.

b. Black Body Source

Temperature range

$50^{o}C$ to $1000^{o}C$

Stability (long term)

$\pm 0.5^{o}C$

Apertures

1.0, 0.6, 0.4, 0.2, 0.1, 0.05, 0.025, and 0.0125 inch diameter

c. Filters

Neutral density

Densities - 0.15, 0.3, 0.5, 1.0, 2.0 plus blank substrate

Substrate - quartz

Calibration - % transmittance vs. λ from 0.2 to 2.5 μm

Size - 2 inch square

Bandpass

Center λ - 1.8 μm, 1.9 μm, 2.0 μm, 2.1 μm, 2.2 μm, 2.3 μm
2.4 μm, 2.5 μm, 2.6 μm, 2.7 μm, plus blank substrate

Bandpass - 0.1 μm

Size - 1 inch diameter

d. Accessories

Various pinhole patterns and stencils of the type used in determining spatial resolution are available.

C. Retina Characteristics

The single most important task in this whole area of research was that of demonstrating that mosaics of metal silicon Schottky barrier diodes, fabricated in a conventional integrated circuit facility, could in fact produce images at wavelengths longer than the fundamental edge in silicon. To accomplish this task, several requirements must be imposed on the retina, which can best be described by considering the schematic diagram of a Schottky diode under a fast electron beam (Figure 8).

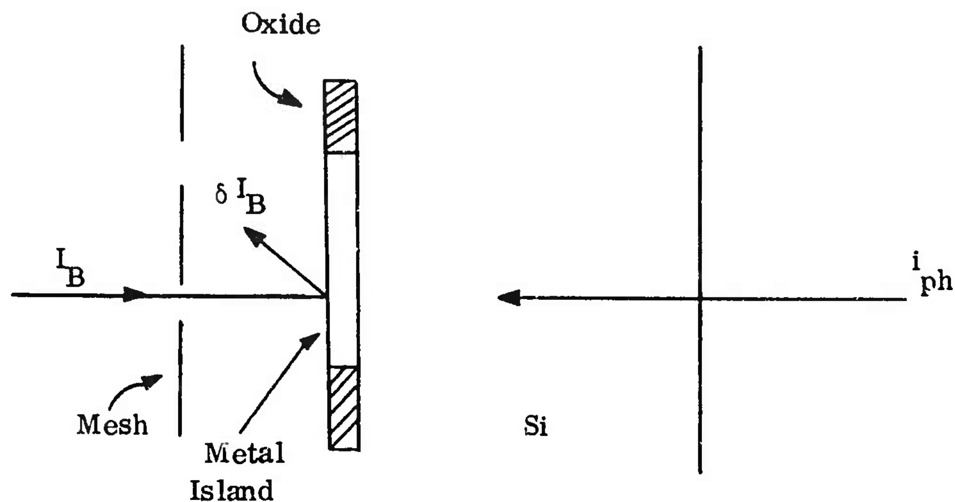

Figure 8. Schematic Diagram of a Schottky Diode under Bombardment by an Electron Beam, I_B

This beam is assumed to generate δI_B secondaries where δ is greater than 1. The number of these secondaries which can escape to the mesh is determined by the target to mesh voltage, V_{TM}. If the secondaries are assumed to have a Maxwellian energy distribution with an average energy $\overline{V}$, then the current of secondary electrons which can escape to the mesh is given by

$$I_{sec_{TM}} = \delta I_B \exp \frac{-V_{TM}}{\overline{V}} \tag{12}$$

Of these, I_B will be equal and opposite to the primary beam flowing to the target from the cathode. There thus appears to be a current of electrons, I_B, flowing from cathode to mesh, and a net positive current flow from target to mesh given by

$$I_{TM} = I_B - \delta I_B \exp \frac{-V_{TM}}{\overline{V}}$$

$$= -I_B(\delta - 1) + \delta I_B \left(1 - \exp \frac{-V_{TM}}{\overline{V}}\right) \tag{13}$$

The current in the first term on the right of equation (13) is independent of the target to the mesh voltage and behaves like a current generator driving a positive current from mesh to target if δ is greater than 1. The second term on the right of equation (13) represents a current controlled by the target to mesh voltage. This is describable in an equivalent circuit by a voltage dependent resistor, r_b, in parallel with the current generator described by the first term. For a Maxwellian energy distribution, r_b is by definition

$$1/r_b \equiv \frac{d\left\{\delta I_B \left(1 - \exp \frac{-V_{TM}}{\overline{V}}\right)\right\}}{d_{V_{TM}}}$$

$$= \frac{\delta I_B}{\overline{V}} \exp \frac{-V_{TM}}{\overline{V}} \tag{14}$$

There is also a target to mesh capactiance, C_{TM}, in parallel with r_b and the current generator $I_B(\delta - 1)$. An equivalent circuit for the particular element shown in Figure 8, may thus be described by Figure 9. Here the diode is represented by the parallel combination of a resistance r_D, a capacitance C_{TS}, and a current generator, RH where H is the radiant power incident on the diode, and R is the responsivity of the diode in amps/watt.

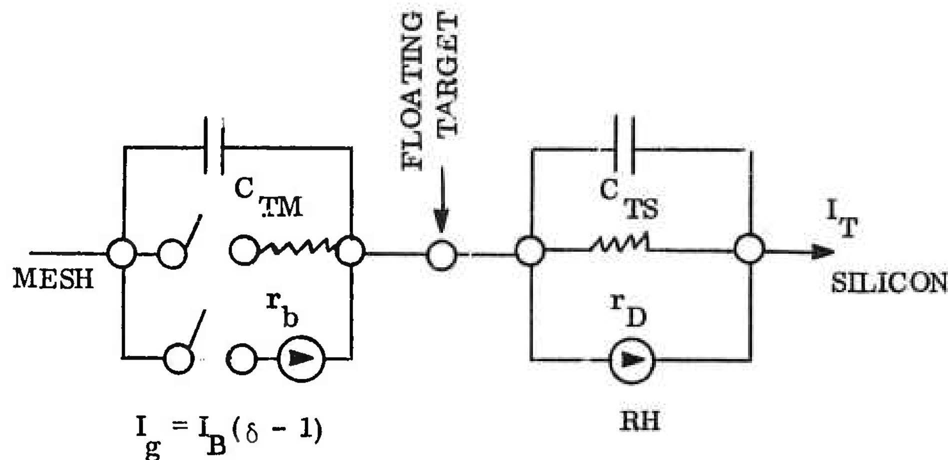

Figure 9. Equivalent Circuit for the Element in Figure 8

The switches in the mesh to target loop are closed during the read time, t_R, when the electron beam is on the diode, and are open during the remainder of the frame time, $t_f - t_R$, which we shall refer to as the storage time.

If in the steady state, no current were flowing out the Si, the current, $(\delta - 1)I_B$, would flow through the resistance r_b, and the voltage V_{TM0} would be determined from (13) as

$$I_B(\delta - 1) = \delta I_B\left(1 - \exp\frac{-V_{TM0}}{\overline{V}}\right)$$

which yields

$$V_{TM0} = \overline{V} \, \ln \delta \tag{15}$$

In the operation of the tube,

$$O \lesssim V_{TM} \lesssim V_{TM0} \tag{16}$$

Thus from equations (14), (15), and (16)

$$\frac{\bar{V}}{\delta I_B} \lesssim r_b \lesssim \frac{\bar{V}}{I_B} \tag{17}$$

For δ not too different from unity, r_b does not vary appreciably over the operating range of the tube, and the equivalent circuit of Figure 9 is conceptually quite useful. r_D and C_{TS} will both be voltage dependent, but these dependences are reasonably well understood.

If there are a total of N diodes on the target, the equivalent circuit of the mesh to Si loop is represented by N loops like Figure 9 in parallel, plus a mesh to Si capacitance, C_{MS} also in parallel with these loops. Thus the entire mesh to Si circuit appears as shown in Figure 10. Characterizing retinas for use in this program requires determining the values of the components shown in the equivalent circuit of Figure 9, and determining the ranges in tube bias levels over which this equivalent circuit applies. This can be done either by actually measuring the target current of the tube as a function of landing voltage, silicon to mesh voltage, light level, etc., or by a combination of these tube measurements and measurements on the retina itself using hard wire contacts instead of electron beam contact. The former is preferable, since only for this case can we be sure that the measurement conditions are identical to the conditions encountered in operation. The latter type of measurement can however be useful if interpreted correctly.

1. Retina Measurements Made Using Hard Wire Contact

Figure 9 shows the importance of the leakage resistance of the diode, r_D, and diode responsivity, R, in determining retina performance. It is desirable to perform measurements of r_D and R on retinas with a metal layer (later removed) connecting a number of elemental diodes into one large "diode," if it can be shown that such measurements provide data relevant to the case where contact is made

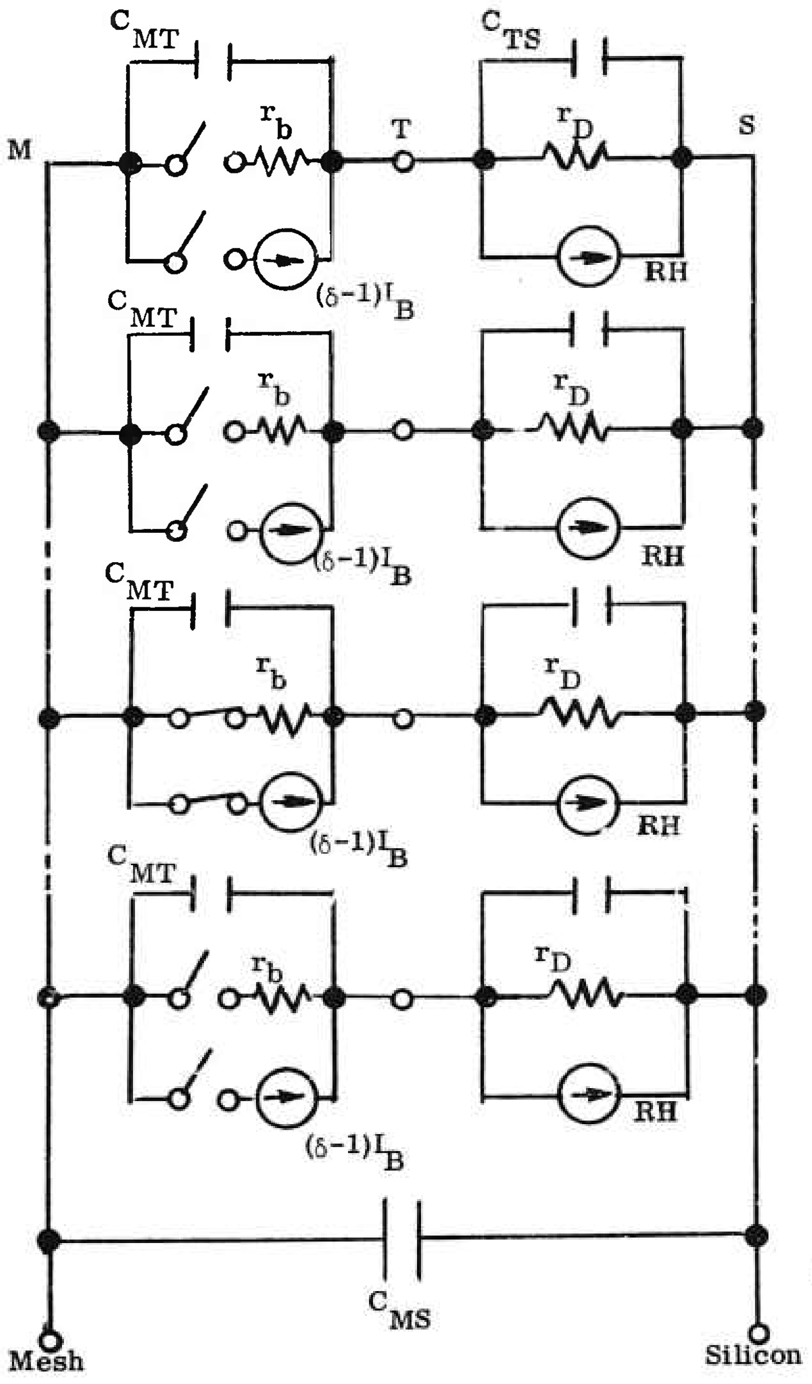

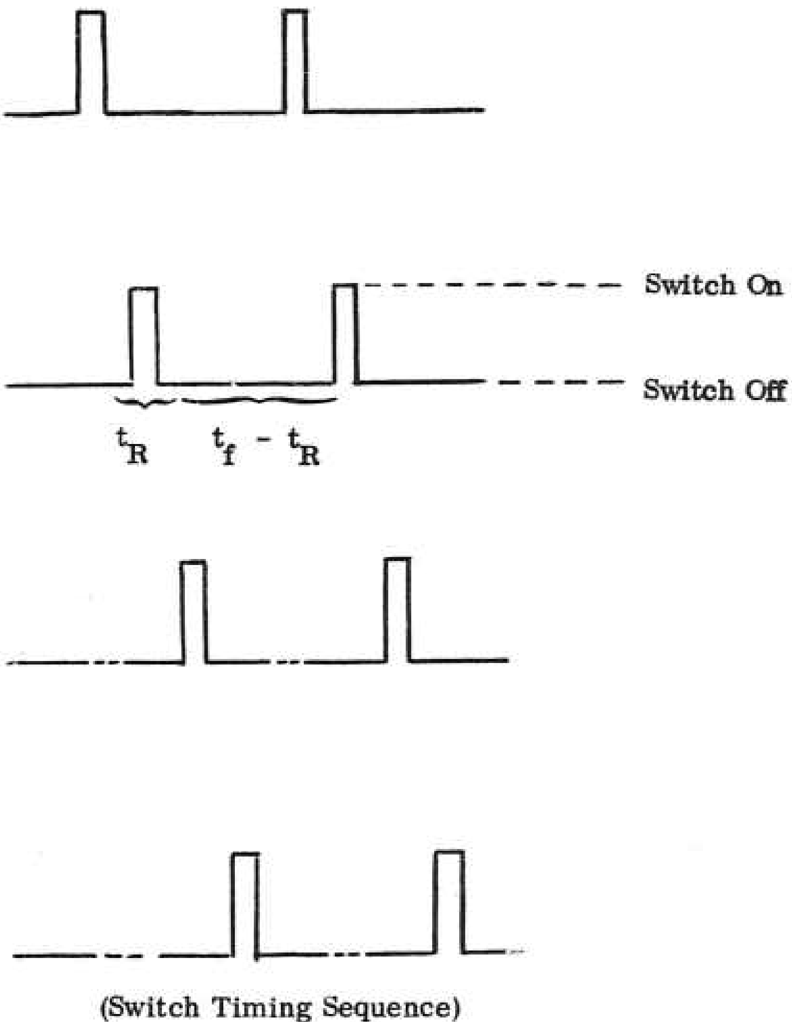

Figure 10. Equivalent Circuit of High Beam Velocity Vidicon Beam.

with an electron beam. Figure 11A is a schematic of a metal silicon Schottky barrier array vidicon target as it might be used in a camera tube. Figure 11B is a schematic of the same device with a metal overlay.

To determine the effect of the large perimeter to area ratio of an overlaid device on its current-voltage characteristic, it is necessary to examine the electron energy diagram at the perimeter of a metal island. Figure 12 shows such a diagram where the metal contacts the silicon directly (M-S contact), and where the oxide layer sits between the metal and the silicon (M-O-S contact). Figure 12A shows these two diagrams for zero applied bias. The M-S contact is characterized by a barrier height $\emptyset_o$. In the M-O-S contact, the energy difference between the metal Fermi level (F.L.) and the valence band edge is given by the silicon surface potential, $\emptyset_s$. $\emptyset_s$ is determined by the charge concentration in the oxide, work function difference, etc., and may be less than $\emptyset_o$. Electrons at the Fermi level in the metal on plane AA' in Figure 11B will see a barrier height $\emptyset_o$ in the x-direction, and $\emptyset_s$ in the y-direction. As the metal bias is varied relative to the silicon, $\emptyset_s$ varies while $\emptyset_o$ is constant. This occurs since the metal F.L. is the same in both the M-S and M-O-S contact, the semiconductor Fermi level is the same in both cases, and some of the potential difference appears across the oxide in the M-O-S case while all of it drops across the depletion layer in the M-S case. Thus, if $\emptyset_s (V=0) < \emptyset_o$, current flow at the periphery will dominate the diode.

On the other hand, if the I-V characteristic obtained for the device of Figure 11B is a well behaved Schottky diode, then this would indicate that the large perimeter-to-area ratio was posing no special problem, and r_D can be determined from measurements made with hard wire contact.

a. Current-Voltage-Temperature Measurements

I-V-T measurements have been made on structures prepared as shown in Figure 11B. Forward characteristics obtained in this case agreed well with the theoretical relationship given by[4]

$$I_F = AA^* T^2 \exp - (q\emptyset_B/kT) \left[\exp \frac{qV_F}{nkT} - 1\right] \qquad (18)$$

Figure 11

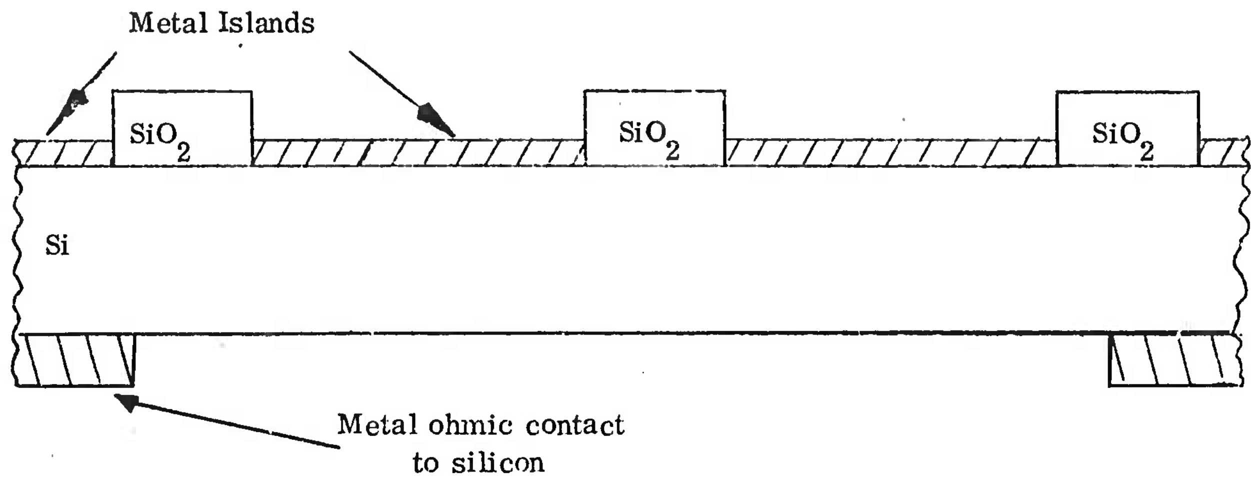

A. Schematic of Schottky barrier array retina

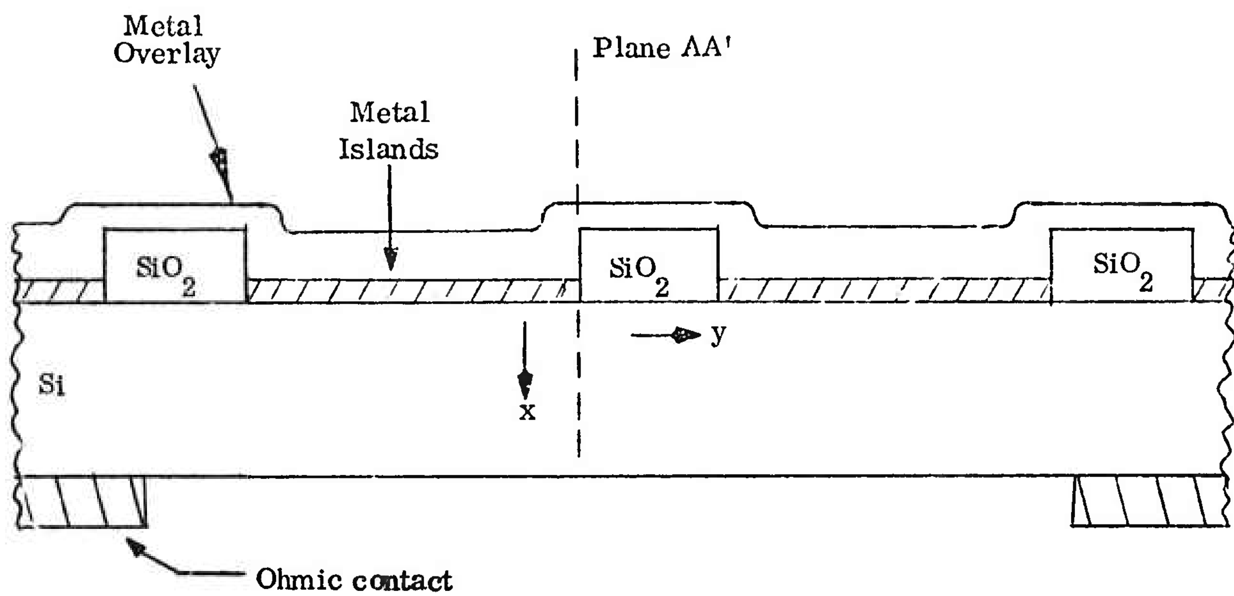

B. Schematic of Schottky retina with metal overlay

Figure 12

Electron potential diagram of Metal - P silicon Schottky diode, and Metal-oxide - P silicon interface

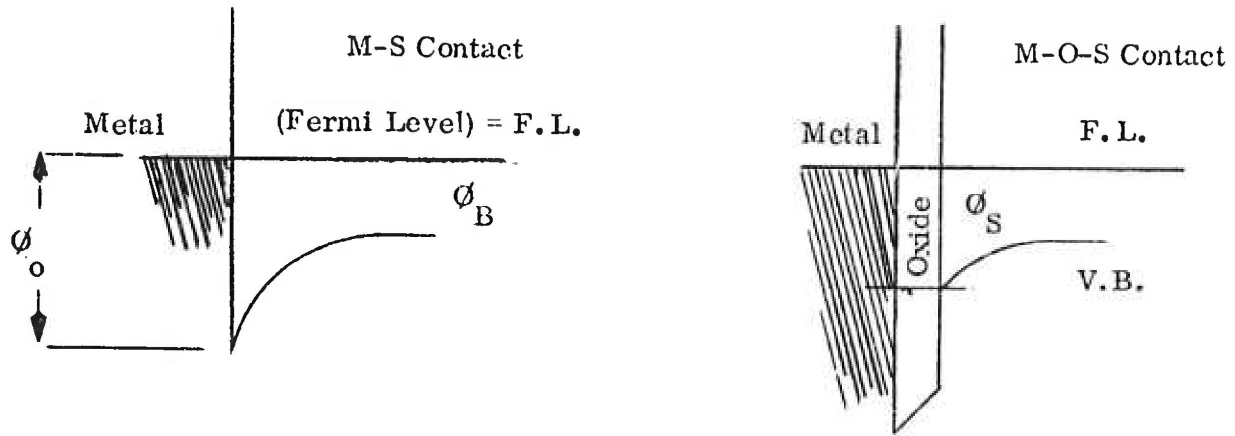

Figure 12A. Zero Applied Voltage

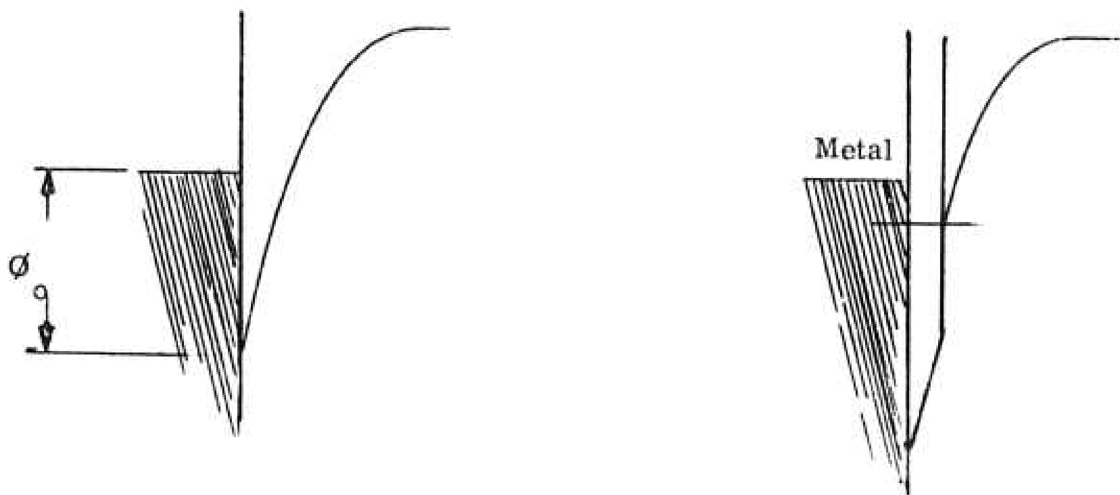

Figure 12B. Reverse Bias Case

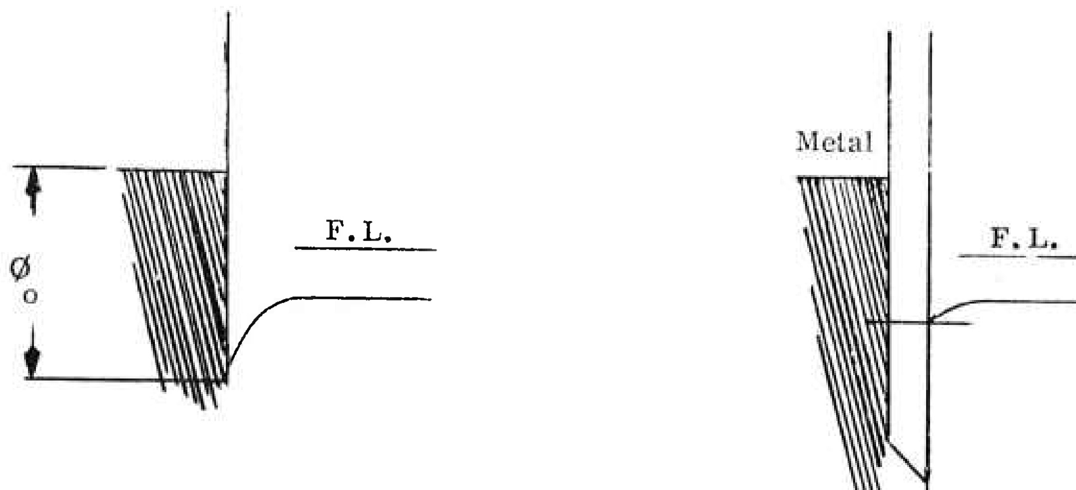

Figure 12C. Forward Bias Case

where

I_F, V_F = forward current, voltage

A = diode area

A^* = Modified Richardson constant
= 30 amps/$cm^2/(^oK)^2$ for P-Si

ϕ_B = barrier height

n = diode ideality factor

Table II shows typical values obtained for n and ϕ_B on three such diodes at $T = 77^oK$.

Table II

Retina No.	Area (cm^2)	n	ϕ_B (e.v.)
10P102D	3.24	.06	0.364
10P105	1.82	1.05	0.333
10P108	5.8	1.06	0.344

[With the assumption that the n value for a given diode is independent of temperature, it is possible (using n values obtained for $T = 77^oK$) to use such a diode as a thermometer for determining how well the retina is being cooled in the demountable tube. Such measurements have been used to show that in operation the retina temperature is consistently below 100^oK, and with care can be made as low as 90^oK.]

Reverse I-V-T measurements on these devices are much more complex, and show the importance of edge effects at island boundaries. Figure 13 shows reverse I-V curves at a number of temperatures. Bistable action is observed, with a low current branch being followed out to $V_R \approx 5\text{-}6$ V at which point switching occurs to the high current branch. If the reverse voltage is then decreased, the leakage current follows the upper branch down toward zero. It is interesting to note that the low current branch appears to display thermally activated currents, while the high current branch shows leakage currents which decrease with increasing temperature.

Figure 13

Reverse I-V Characteristics of Retina #10P102D (Dark)

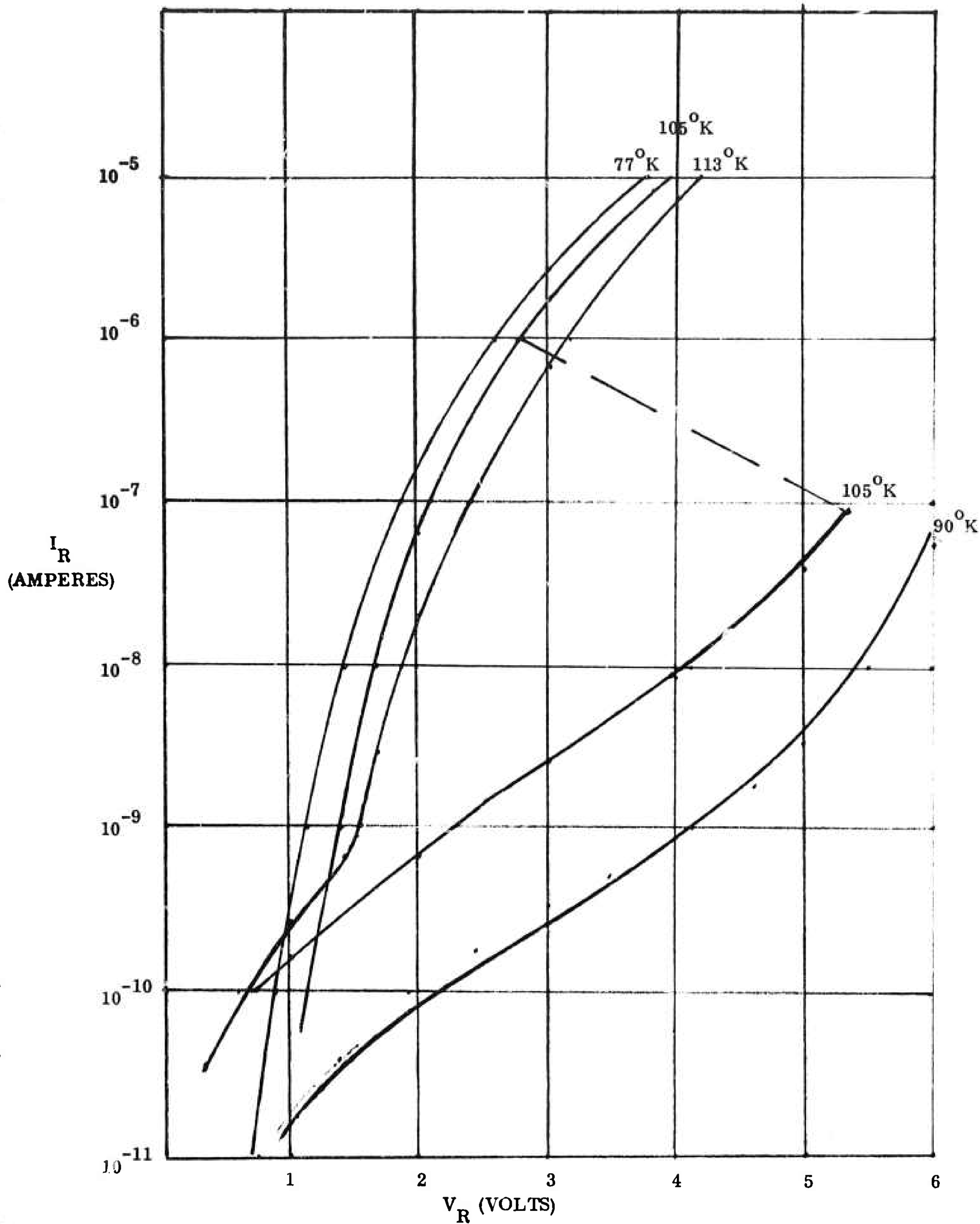

The reverse leakage current I_R which is theoretically predicted for metal-silicon Schottky diodes is given by the equation[4]

$$I_R = AA^*T^2 \exp - (q\phi_B/nkT) \exp \frac{+q}{nkT} \left[\frac{qE}{4\pi K\epsilon_o}\right]^{1/2} \tag{19}$$

where

E = maximum field strength in junction

K = dielectric constant of silicon

ϵ_o = permittivity of free space

It can be shown[4] that

$$E = \frac{2qN_A}{K\epsilon_o}\left[\left(V_R + V_{bi} - \frac{kT}{q}\right)\right]^{1/2} \cong \left[\frac{2qN_A\left(V_R + \phi_B\right)}{K\epsilon_o}\right]^{1/2}$$

where V_{bi} = build in potential

This equation is plotted in Figure 14 using the values for n and ϕ_B obtained from forward biased measurements of retina 10P102. Measured values of I_R from the lower branch of Figure 13 are shown for comparison. It is clear from this figure that a substantial amount of excess reverse current is seen under dark conditions. This is not surprising in view of the very high perimeter to area ratio of these devices. (It has been found[7] that diffused guard rings are necessary to suppress edge effects in metal-silicon Schottky diodes. Only then can the theoretically predicted reverse leakage current be observed.)

The upper branch observed in Figure 13 can be tentatively explained as follows. For zero and positive applied voltages, the silicon surface potential ϕ_S is greater than ϕ_o, the Schottky barrier height. Thus, the latter dominates the diode I-V characteristic. Under reverse bias, however, high fringing fields are built up, so that excess reverse leakage occurs. When sufficiently high edge fields are achieved, avalanche effects begin. The minority carriers produced are trapped at the silicon-silicon dioxide interface, between metal islands. When the silicon surface there is inverted, $\phi_S = E_g - 2\phi_B$, where ϕ_B = bulk Fermi level. Electrons in this surface inversion layer are prevented from moving laterally into the portion of the silicon conduction band under the metal by a lateral potential barrier of height

Figure 14

Reverse I-V Characteristics of Retina 10P102D

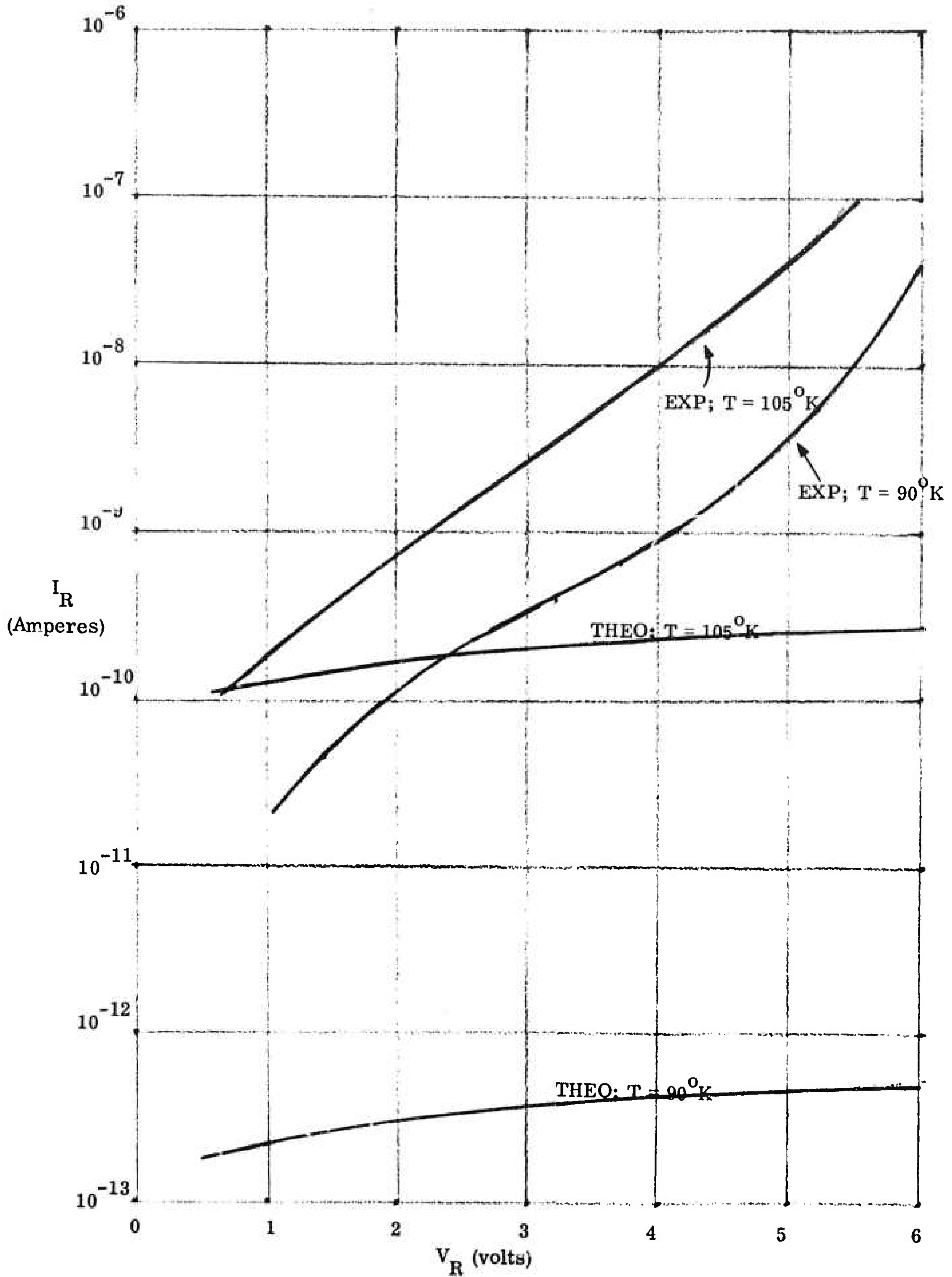

$(E_g - 2\phi_B) - \phi_o$

Thus, as long as the reverse bias is applied, this inversion layer persists. Its presence increases the edge electric field, so that the diode now follows the upper branch of the I-V characteristic until the reverse voltage is reduced to zero, permitting the inversion layer to collapse. If reverse bias were again applied, the lower branch of the I-V curve would be again observed.

In summary, I-V-T measurements made on overlaid metal-silicon Schottky diode mosaics show good agreement with theory in the forward direction, but substantial deviation from theory in the reverse direction because of strong edge effects.

b. Retina Photoresponse Measurements

I-V measurements were taken on retina 10P102D in the demountable tube at various light levels, using narrowband spectral filters to verify the predicted Schottky spectral response. It was found that the I-V characteristic for the overlaid diode was given, as expected, by

$$I = I_o \left[\left(\exp \frac{qV}{nkT} \right) - 1 \right] - I_L \tag{20}$$

where

I_L = RH

R = responsivity in amps/watt

H = radiant power on retina

By measuring short circuit current (I_{SC}) and open circuit voltage (V_{OC}) one can obtain quantitative data on junction temperature, similar to that obtained from I-V-T data. To do this, one first measures I_{SC} and V_{OC} with only thermal background radiation present. Then, the experiment is repeated for various values of H (and hence I_L) over and above background. One can show that

$$\ln \frac{I_L}{I_b} = \frac{q(V_{OCL} - V_{OCb})}{nkT} ; \tag{21}$$

where I_b = background generated short circuit current

V_{OCb} = background generated open circuit voltage

Figure 15 shows a plot of log (I_L/I_b) vs. $(V_{OCL} - V_{OCb})$. Using the value of n obtained for this retina from I-V measurements at 77°K (n = 1.06), one can obtain T from a least squares fit to this data. (T = 99.5°K)

c. Retina Spectral Response

To assure that the retinas to be used in imaging experiments were showing the response expected of metal-silicon Schottky diodes, spectral measurements were taken on one such device overcoated with metal as shown in Figure 11B to make one large diode. The measurements were taken with the retina in the demountable tube with a sapphire disc in close contact with the retina on a window side to facilitate cooling the thin (0.015") silicon wafer. The relative response is shown in Figure 16 in a modified Fowler plot. The solid line is the response predicted for the palladium-silicon system using the barrier height determined for this device from I-V data. It would appear from this data that interference effects are taking place in the gap between the sapphire disc and the silicon retina, but that otherwise the retina is behaving as expected.

2. Retina Measurements Made Using Electron Beam Contact

Having verified that the Schottky diode portion of the equivalent circuit of Figure 9 is applicable to the retinas being used, experiments were begun to study the target to mesh portion of Figure 9. The terminal parameters available to study these quantities are shown in Table III.

Table III

Terminal Name	Parameter Symbol	Eq. Circuit Parameter Affected
Beam Current	I_B	I_g, r_b
Target Current	I_T	
Mesh to Cathode Voltage	V_{MK}	δ, r_b
Silicon to Mesh Voltage	V_{SM}	r_b

Figure 15

Normalized Short Circuit Current Vs. Open Circuit Voltage Difference (Retina 10P102D)

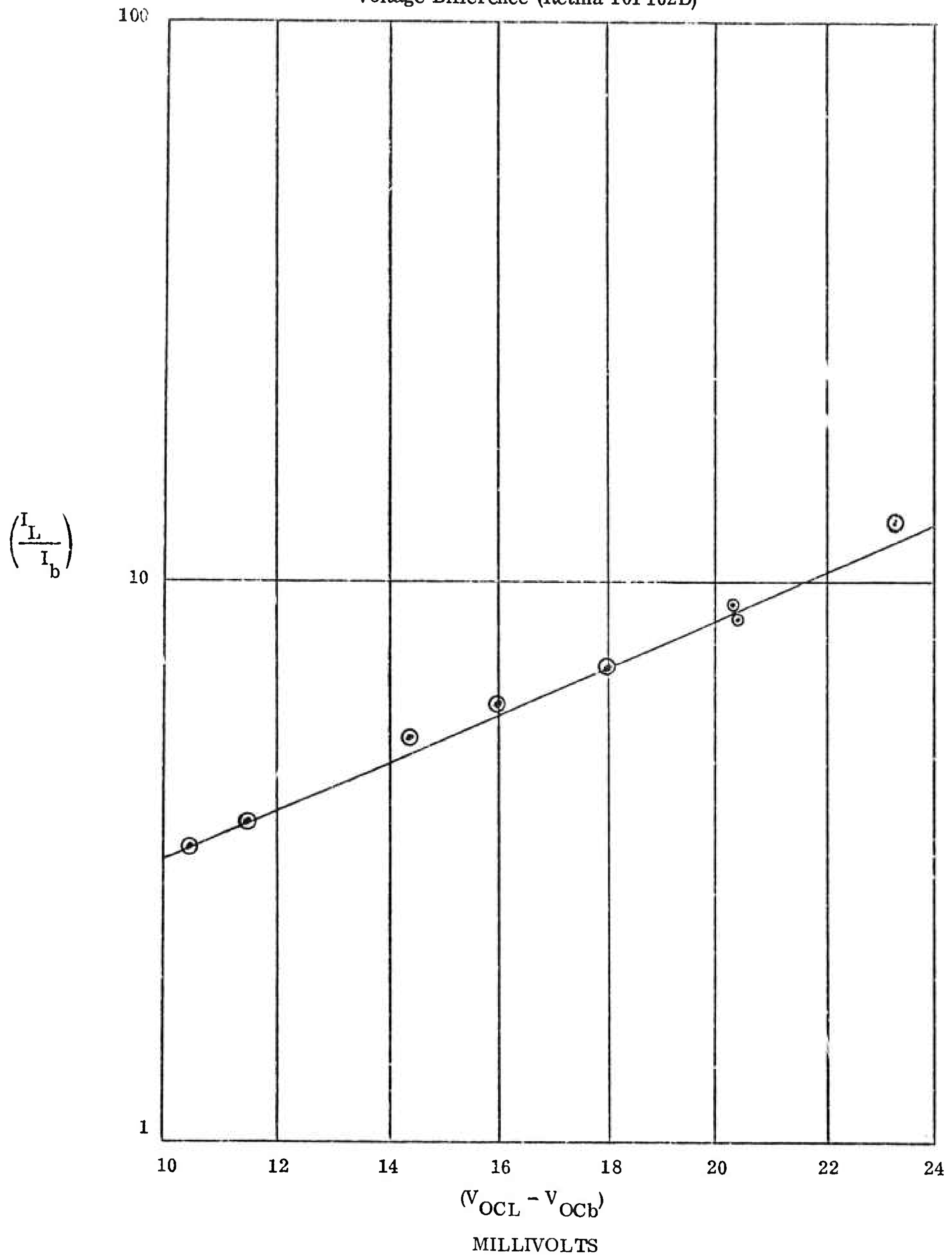

Figure 16

Modified Fowler Plot for Relative Spectral Response vs. Photon Energy (Retina 10P102D)

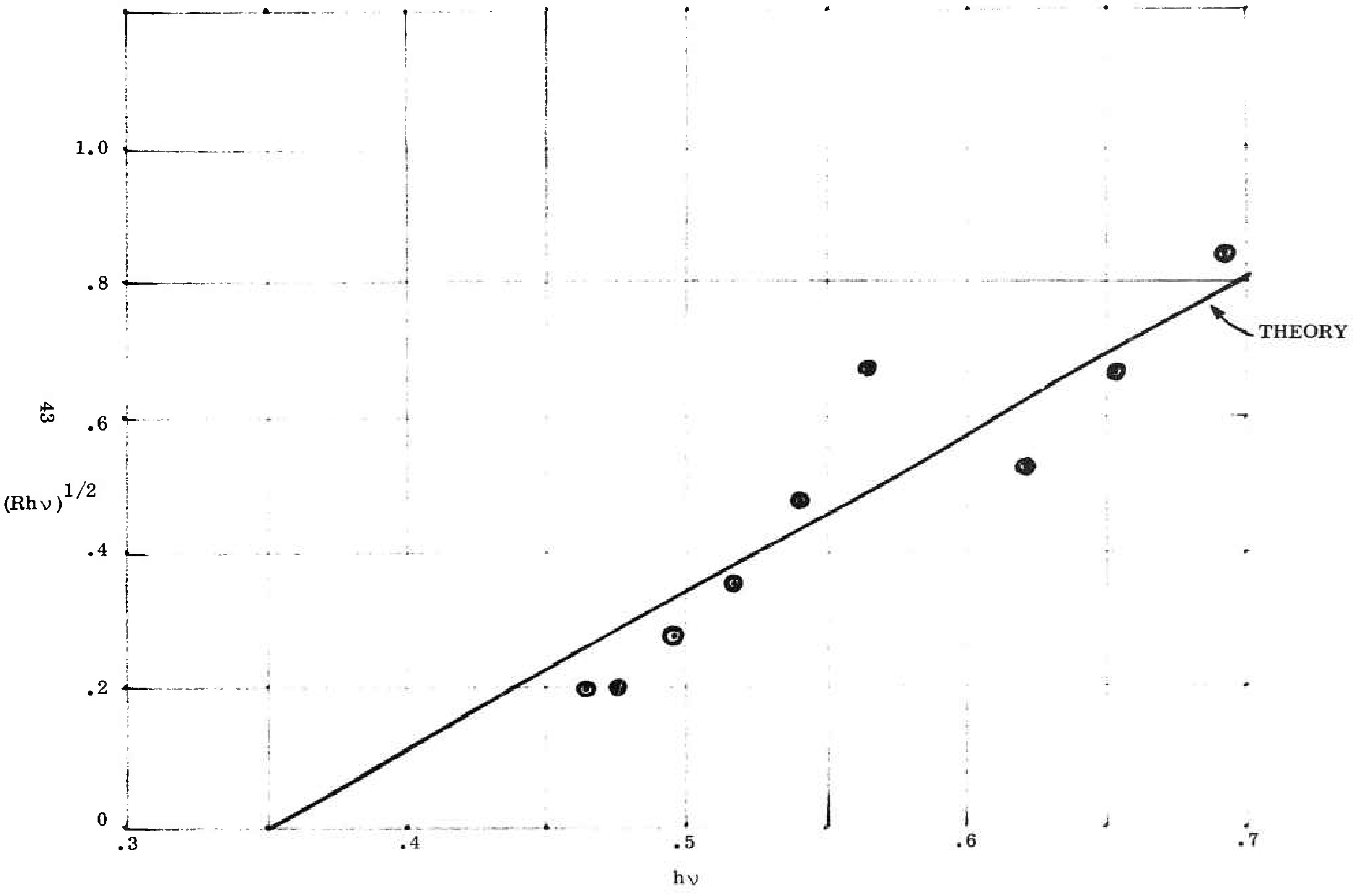

It has been found that meaningful and reproducible results are best obtained when the measured target current, I_T, is normalized to the total beam current (determined by adding algebraically the total currents carried by all electrodes able to divert beam current from the retina). This obviates the need to hold cathode emission constant during a given run, or between different runs. Furthermore, the raster scan being applied should be such that the retina is underscanned, or else substantial retina edge effects result. Under these conditions, measurements of I_T vs. V_{SM} at room temperature (where r_D of Figure 9 is very low) permit the study of retina to mesh interaction under a fast beam. Figure 17 is a typical plot of such data obtained on retina 10P104. It can be seen that when the silicon (and hence at room temperature the metal islands) is positive relative to the mesh (first quadrant of Figure 17) the target current saturates at a value essentially equal to the beam current. Since the mesh transparency is only 61%, the mesh must be intercepting part of the incident beam, and emitting secondaries, some of which fall onto the retina and add to the total target current. (The presence of mesh secondaries complicates the analysis of beam-retina interaction, since they land on the target with low energy and don't generate secondaries off the retina.) Since the retina is positive relative to the mesh in this quadrant, retina secondaries cannot escape to the mesh, and the net target current consists of electron flow out the retina lead (positive current flow according to our convention).

Figure 17 also shows that when the voltage between the metal islands and the mesh is negative (third quadrant), the sign of the target current corresponds to electron flow into the tube via the retina lead. This implies that the fast beam is generating secondaries on the retina with a yield $\delta_M > 1$, and that these secondaries escape to the mesh when $V_{SM} \ll 0$. Useful information can be obtained about the magnitude of the secondary emission currents from an analysis of the current values at which I_T saturates for large positive and large negative values of V_{SM}.

a. Saturated Values of Target Current

Consider the structure shown in Figure 8. A fraction f_M of the incident beam lands on the mesh and generates secondaries. For $V_{SM} \gg 0$, some of

Figure 17

Normalized Target Current vs. V_{SM} ($T = 300^{o}K$, $V_{MK} = 250$ V)

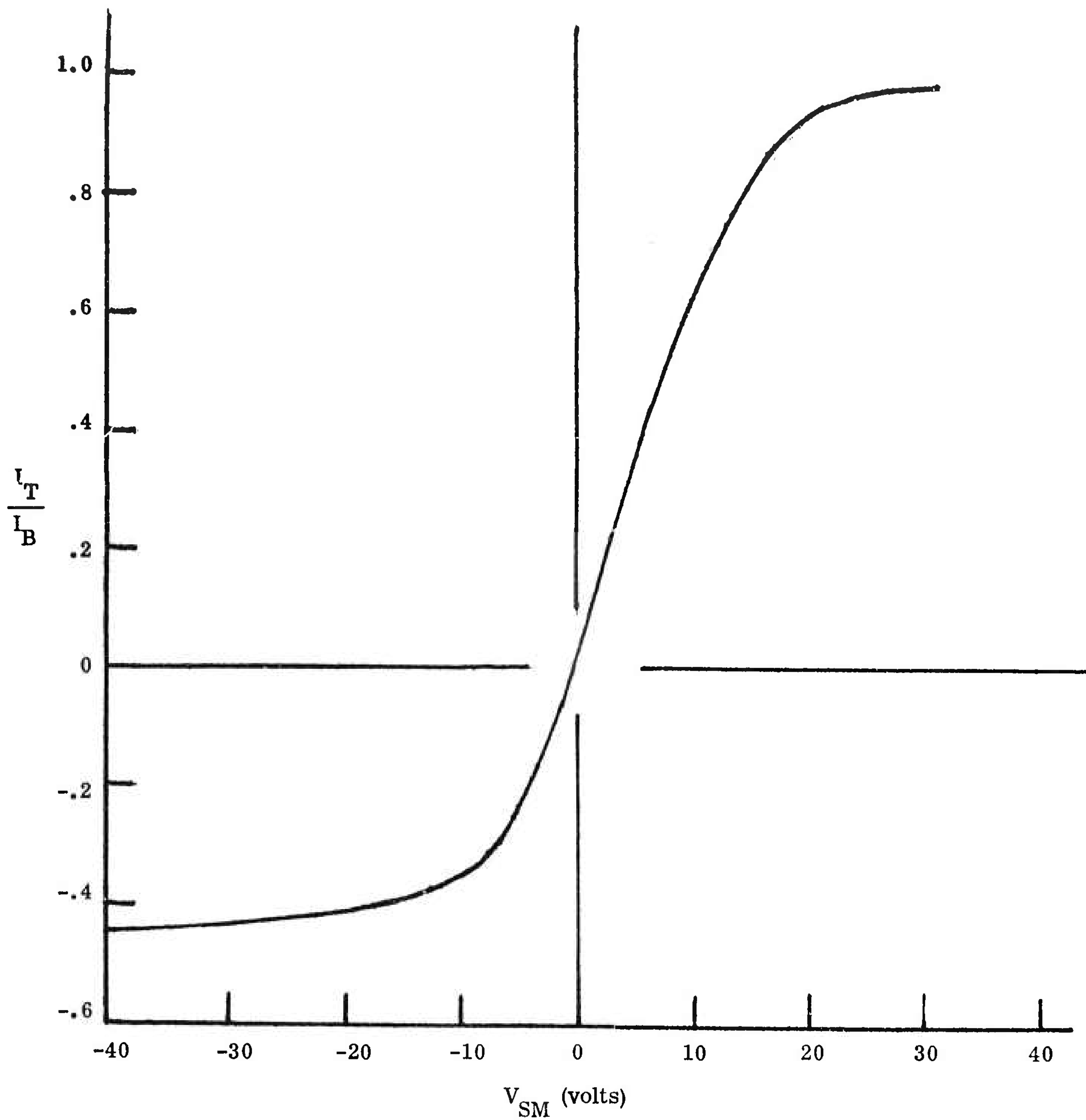

these secondaries can pass thru the mesh and land on the retina, the balance going to a remote cylindrical electrode maintained at all times at +25V relative to the mesh. If we describe the yield of the mesh for secondaries going to the retina by means of the coefficient δ'_{MK}, we find that a fraction $(1 - f_M)$ of the beam current continues thru the mesh unimpeded, while the remainder is removed from the fast beam and replaced with a slow component $f_M \delta'_{MK}$. This slow component is too low in energy to create secondaries when it lands on the retina, so it tends to make the fast electrons less effective.

Of the fast electrons that pass thru the mesh, a fraction f_T land on the metal islands on the retina ($f_T = 0.64$ for diode pattern used). The remainder falls on the exposed oxide. If we assume that the net current flow off the oxide surface is zero, the primaries landing there must generate an equal number of secondaries which, for $V_{SM} \ll 0$. are collected by the mesh. For $V_{SM} \gg 0$, they will be collected by the metal islands. These oxide secondaries are also unable to create secondaries, since they land on the collecting surface with low energy. Finally, the fraction of the original fast beam which can generate secondaries off the metal islands is

$$f_T (1 - f_M)$$

For $V_{SM} \gg 0$, these are unable to escape, while for $V_{SM} \ll 0$, they all escape to the mesh. By such reasoning it can be shown that the saturated values of target current should be as follows:

$$I_T/I_B = (1 - f_M) + f_M \delta'_{MK}; \quad V_{SM} \gg 0 \tag{22}$$

$$I_T/I_B = (1 - f_M) f_T (1 - \delta_{TK}); \quad V_{SM} \ll 0 \tag{23}$$

Substituting known values for f_M and f_T into these equations, one finds from data such as that shown in Figure 17 that $\delta'_{MK} \approx 1$ (which seems reasonable in view of the inefficient collection geometry), and that δ_{TK} can be as high as 2.1 at 250 volts beam voltage. The secondary emission constants of palladium silicide are not known, but most metals show peak values of δ of the order of 1.5, and these values occur for beam voltages substantially higher than 250 V. Thus, it appears that

the secondary emission yield off the retinas used in this program is higher than might have been expected (equation 23 would predict $I_T = 0.12\ I_B$ for palladium at 250 V, while Figure 17 shows that $I_T = 0.45\ I_B$ was measured). We shall show later that this, along with other data, forces one to the conclusion that the net current flow off the top of the exposed oxide is not zero, but that current transport from the metal islands into the oxide permits the oxide to play an important role in retina-beam interaction.

The effect of retina temperature and beam landing voltage (V_{MK}) on the saturated values of target current are also of interest. Equation (22) would indicate that I_T ($V_{SM} >> 0$) would vary with temperature and voltage as the secondary emission yield of the copper mesh does, i.e., I_T ($V_{SM} >> 0$) would be expected to show no strong dependence on either variable. This in fact is what is observed (Cf. Figure 18A). I_T ($V_{SM} << 0$) should depend on T and V_{MK} as δ_{TK}, the secondary emission yield of the target. Figure 18B shows a comparatively strong dependence on both T and V_{MK}. Once again there is indication that the secondary emission characteristics of the retina surface are more like those of an insulator than a metal.

b. <u>Evidence for Beam Induced Conductivity in Exposed SiO_2 on Retina Surface</u>

At low values of beam landing voltage ($V_{MK} < 100$ volts) hysteresis effects were observed in the measurement of I_T. This data is best presented by plotting I_T (normalized as before to I_B, the total beam current) vs. the total target to cathode voltage (V_{TK}). Figure 19 shows such a plot for retina 10P113. The data was taken with the retina at room temperature, and with the electron beam unscanned (beam landing on the same spot on the retina throughout the measurement), although similar data has been obtained with the retina cold, and with the beam being scanned in the normal raster fashion.

Several points of interest can be noted from Figure 19. First, the average retina yield (δ_{TK}) of secondary electrons is greater than one for both branches of the curve for $V_{TK} \gtrsim 75$ volts. (This follows from the fact that the sign of the target current is negative.) Second, $\delta_{TK} > 1$ for $V_{TK} \gtrsim 30$ volts for the lower

Figure 18

Saturated Target Current vs. V_{MK}

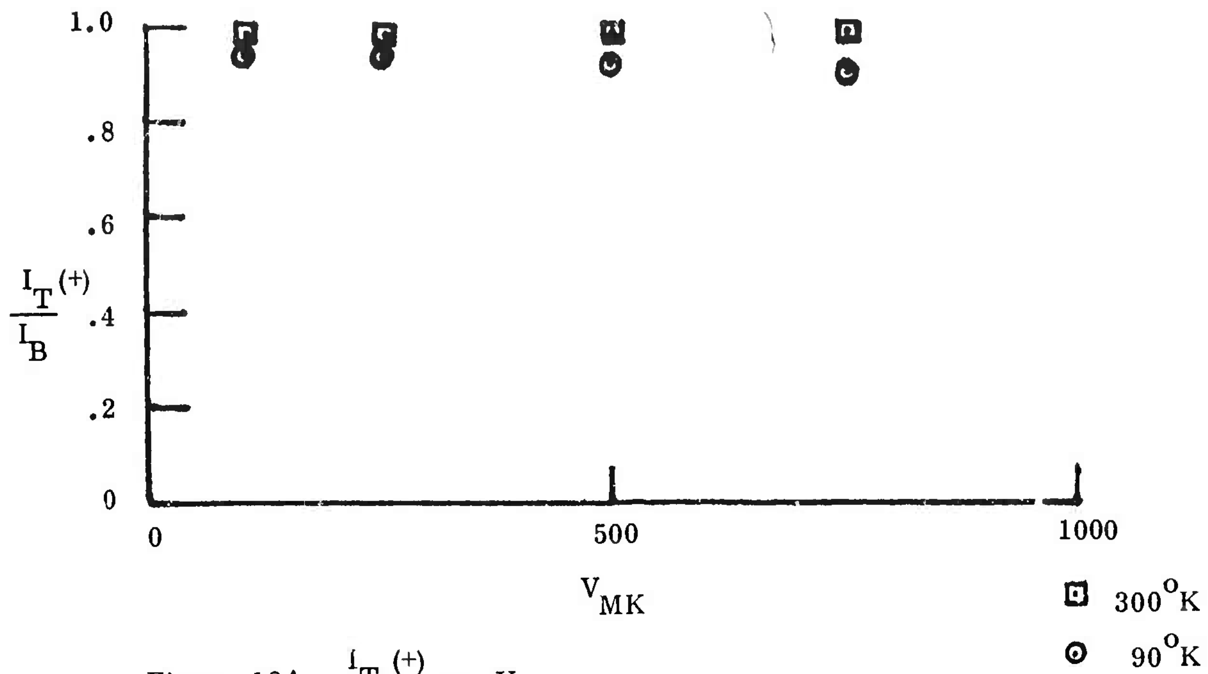

Figure 18A. $\frac{I_T}{I_B}(+)$ vs. V_{MK}

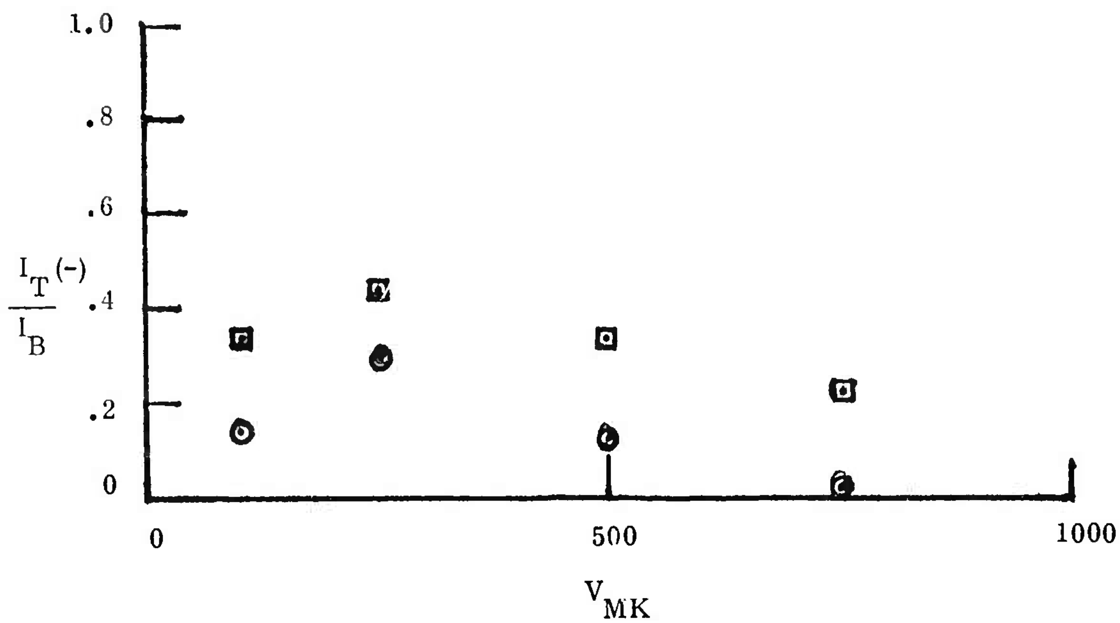

Figure 18B. $\frac{I_T}{I_B}(-)$ vs. V_{MK}

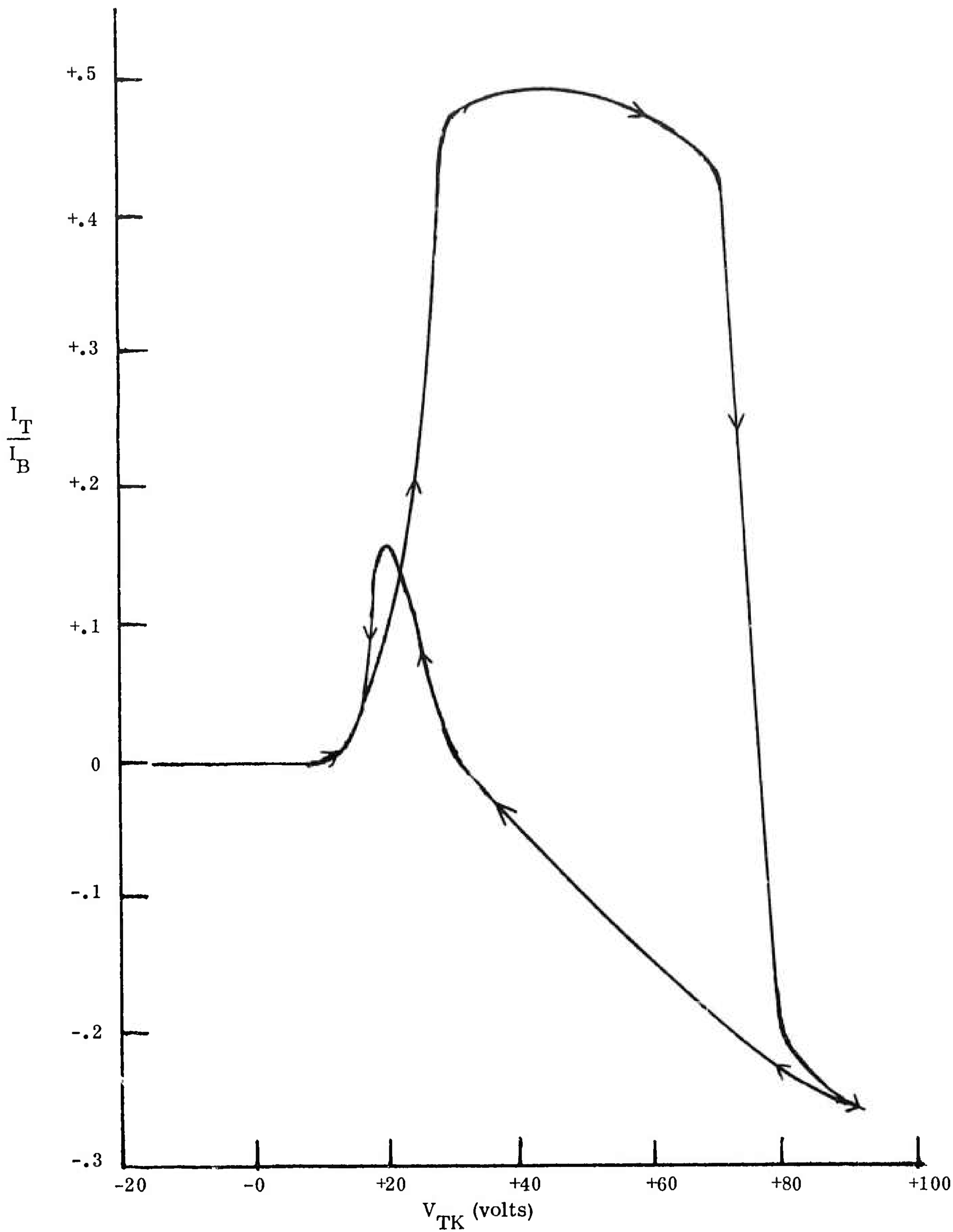

Figure 19. Normalized Target Current vs. V_{TK}
(Unscanned, $T = 300^\circ K$)

branch. Both of these points are surprising in view of the fact that the landing voltage at which $\delta \rightarrow 1$ is. for metals, usually in the neighborhood of 100-300 volts. On the other hand, silicon dioxide has a value of 30 volts for the first crossover voltage (V_C), and δ reaches a maximum of 2.1 to 2.9 for a voltage of 400-440 volts.[8] Both the data of Figure 19 and that of 18B are in closer agreement with the properties of SiO_2 than with those of any known metal (including palladium and silicon).

The third point of interest in the data of Figure 19 lies in the fact that the data was obtained on a D.C. basis. The conventional methods used to determine the secondary emission properties of insulators involve A.C. techniques, since the secondary electrons cannot be replaced by normal conduction processes, so that the targets charge to whatever potential will permit them to have no net current. (Insulators charge to cathode potential if $V_{TK} < V_C$, and to a voltage $\overline{V} \ell n \delta$ above mesh potential if $V_{TK} > V_C$). It is obvious that for the SiO_2 to be playing the role in secondary emission from the retina which the data of Figures 18B and 19 would indicate, it must be conducting (at least in the presence of the beam), and there must be a contact to it capable of supplying electrons to the conduction band of the oxide to replace those lost by secondary emission. If we assume that the beam does induce conductivity in the oxide, and that the metal-oxide interface, while under the beam, is capable of supplying electrons to the conduction band of the oxide, it becomes relatively straightforward to explain the hysteresis shown in Figure 19.

To determine the potential of the surface of the SiO_2 between adjacent metal islands in the array, consider the situation which exists when the retina is scanned by the beam while at room temperature. Because of the low barrier heights required in the metal-silicon Schottky barriers for the desired infrared cutoff, the diode impedance at room temperature is low, and the metal island can, in this case, be regarded as sitting at silicon potential relative to the cathode (V_{TK}). If this potential is increased from zero, while maintaining the mesh at a slight positive potential relative to the silicon, it is desired to calculate the potential at which the SiO_2 surface will float in the geometry used in these retinae. It can be shown that the oxide surface, if it were completely isolated electrically from the target, can

sit in two stable states; viz, at a potential slightly negative with respect to the cathode potential where the beam has been cut off, or at a potential slightly positive relative to the mesh where secondaries are being emitted to the mesh at a rate just equal to the beam current. In actual practice, the oxide surface is in contact with the target, where the target metal joins the oxide (Cf. Figure 20).

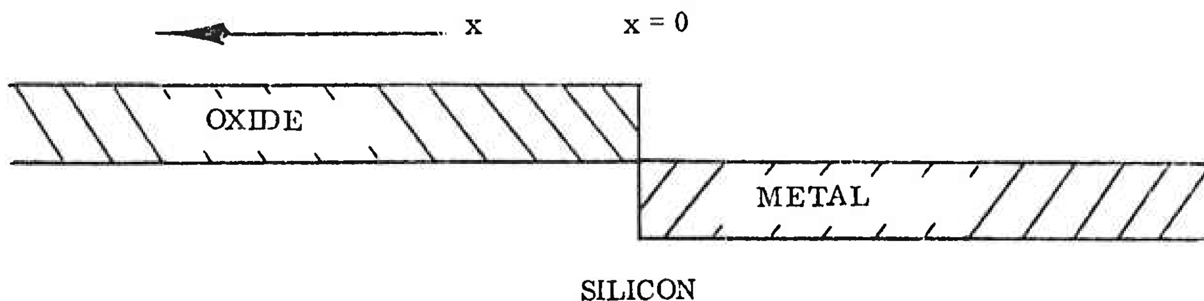

Figure 20. Metal Target-Oxide Contact

Therefore the potential of the oxide surface immediately adjacent to the metal must sit at the metal target potential, and the beam must supply a net flow of electrons in or out of the oxide in this region depending on whether $j_b \left[\delta (V_T) - 1\right]$ is less than or greater than zero. Here $\delta (V_T)$ is the secondary emission ratio of the oxide if the oxide surface sits at target potential. If the electrons are generated in the oxide with sufficient energy to escape as secondaries, it would seem that while the beam is landing, there should be electrons in the conduction band of the oxide, at least in a thin skin near the surface. These electrons can conduct laterally along the surface. Therefore, the oxide would have a sheet conductance σ under the influence of the beam. The lateral current/unit width in the oxide surface would then be given by

$$j = -\sigma \frac{dV}{dx} \quad \text{, where } \sigma \text{ is in mhos} \tag{24}$$

if lateral voltage gradients (dV/dx) occur. The derivative of the lateral current would be given by

$$\frac{dj}{dx} = -j_b \left[1 - \delta (V)\right] \tag{25}$$

where j_b = beam current density.

In actual practice, σ is no doubt a function of V, the landing voltage, however for this discussion, we will assume it is constant. Further let us assume that, for $V \approx V_C$ $\delta(V) = V/V_C$ where V_C is the voltage for which δ goes to unity. Then (24) and (25) may be combined to give

$$\sigma V_C \frac{d^2 (V/V_C)}{dx^2} = j_b \left[1 - \frac{V}{V_C}\right] \tag{26}$$

If the oxide is assumed to be semi-infinite in extent, then as we increase the target voltage above cathode

$$V = V_{TK} \text{ at } x = 0$$

and (27)

$$\frac{dV}{dx} = 0 \text{ at } V \approx 0,$$ which occurs a distance W away from the metal-oxide boundary (the voltages are measured relative to cathode). The solution to (26) which satisfies the boundary conditions (27) is

$$\frac{V - V_C}{V_C} = \left(\frac{V_T - V_C}{V_C}\right)\left[\frac{\sin Ax \sin AW + \cos Ax \cos AW}{\cos AW}\right] \tag{28}$$

where $A = \sqrt{\frac{j_b}{\sigma V_C}}$; $\cos AW = \left[1 - \frac{V_T}{V_C}\right]$

If one combines equations (28) and (24) to calculate the current flowing across the metal oxide interface at x = 0, we find that the current per unit width of this interface is given by

$$j = \left[j_b \sigma V_C \left(\frac{2V_T}{V_C} - \frac{V_T^2}{V_C^2}\right)\right]^{1/2} = \left[j_b \sigma V_T \left(2 - \frac{V_T}{V_C}\right)\right]^{1/2} \tag{29}$$

This current has a real solution for $0 \leq V_T/V_C \leq 2$. Several ranges of V_T/V_C are of interest, viz.

Case I: $V_T/V_C \leq 1$

Under these conditions, the potential of the top of the oxide varies from $V = 0$ far from the metal to $V = V_T$ at $x = 0$, but at no place along the oxide surface can it lose more electrons by secondary emission than it acquires from the incident beam. Since the oxide surface near $x = 0$ is prevented from charging to cathode potential to stop the beam from landing, we are forced to conclude that an electron flow takes place from oxide to metal in an amount given by equation (29).

Case II: $1 \leq V_T/V_C \leq 2$

In this range, the oxide adjacent to the metal is sufficiently positive to have $\delta \geq 1$. Thus, some electrons can be lost from the oxide by secondary emission to offset those landing from the beam. As soon as we travel some distance from the metal, however, the potential of the top of the oxide drops below V_C, and an "unfavorable trade balance" for electrons is encountered. Again, the boundary conditions of equation (27) force a current flow given by equation (29) to take place at the metal-oxide interface to prevent oxide charging.

Case III: $V_T/V_C \geq 2$

If the target voltage is increased above $2V_C$, there can only be a net flow of electrons from the target to the oxide. The oxide would no longer be able to charge down to cathode potential, but would have to charge to potentials more positive than the target in order to carry a net electron current away from the metal-oxide interface and hence into vacuum by secondary emission. As we move away from this interface, the oxide surface continues to go more positive until it reaches approximately the mesh potential at which point the losses via secondary emission equal the incident beam current. (This assumes that the mesh is more positive than the target.) Once V_T exceeds $2V_C$, the boundary conditions described in (27) must then be changed to

$$\left.\begin{aligned} V &= V_T \quad \text{at } x = 0 \\ &\text{and} \\ \frac{dV}{dx} &= 0 \quad \text{at } V = V_M \end{aligned}\right\} \qquad (30)$$

The solution to (26) and (30) is again the same as (28) except that now

$$\cos AW = \frac{V_T - V_C}{V_M - V_C} = \frac{V_T - V_C}{V_T + (V_M - V_T) - V_C} \tag{31}$$

When equation (31) is substituted into equation (28), the current flow across the metal-oxide interface may be calculated to be

$$j = -\left[j_b \sigma V_C \frac{(V_M - V_T)^2 + 2(V_T - V_C)(V_M - V_T)}{V_C^2} \right]^{1/2} \tag{32}$$

If V_T were now reduced from a value $> 2V_C$ to values $< 2V_C$, the current density per unit width of metal-oxide interface may continue to be negative until V_T is reduced to a value

$$V_T = V_C - \frac{(V_M - V_T)}{2} \tag{33}$$

Thus, there would be a hysteresis effect in the current carrier by the metal-oxide interface. Equations (32) and (29) are plotted in Figure 21 for $(V_M - V_T)/V_C = 1/3$. The arrows indicate the current flow as a function of the direction in which V_T is changed.

The relationship between the current carried by the metal-oxide interface, and the measured target current is as follows. A fraction f_T of the incident beam lands on metal islands, giving rise to a flow of secondaries to the mesh such that the net contribution to target current is

$$f_T (1 - \delta_{TK})$$

Since for these low voltages, δ_{TK} for the metal islands is < 1, this contribution is always positive. A fraction $(1 - f_T)$ of the incident beam lands on the oxide, giving rise to a flow of secondaries to the mesh just equal to the total current replenished by the flow of j current per unit length times the island perimeter, P where j is given by equation (32). Thus, for a beam diameter such that N diodes are under the beam at one time, NjP amperes of secondary electrons can flow off the oxide to the mesh on a D.C. basis, provided that the oxide has been biased

Figure 21
Normalized target current per unit length of diode perimeter vs. normalized target voltage

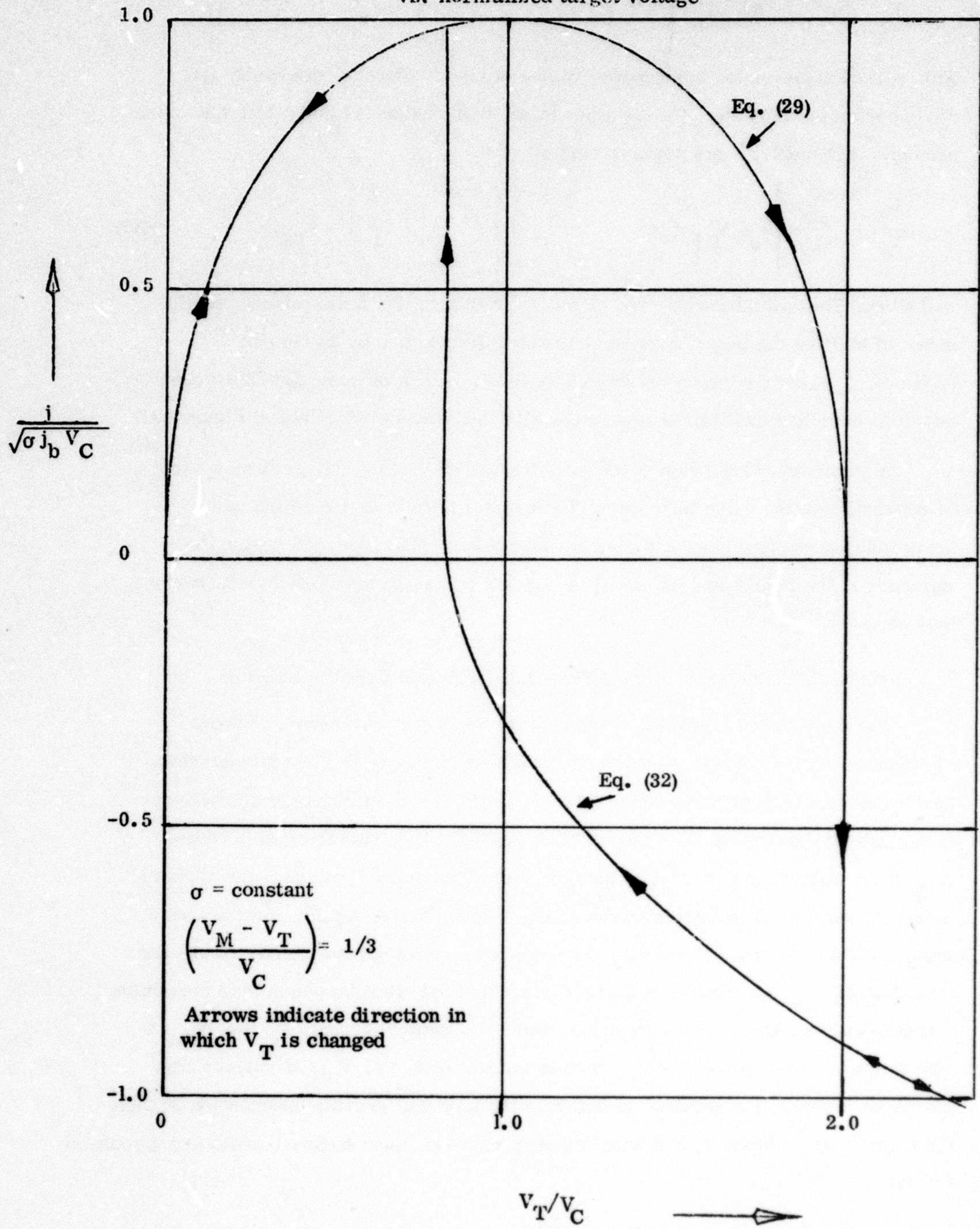

onto the lower branch of Figure 21. Thus, the net target current will be

$$\frac{I_T}{I_B} = f_T (1 - \delta_{TK}) - \frac{PN}{I_B}\left[j_b \sigma V_C \left\{ \frac{(V_M - V_T)^2 + 2(V_T - V_C)(V_M - V_T)}{V_C^2} \right\} \right]^{1/2} \quad (34)$$

This will be negative for appropriate values of beam induced conductivity (σ), diode perimeter (P), etc. On the other hand, if the oxide is biased onto the upper branch of Figure 21, a net positive current of

$$\frac{I_T}{I_B} = \frac{PN}{I_B}\left[j_b \sigma V_C \left(\frac{2 V_T}{V_C} - \frac{V_T^2}{V_C^2} \right) \right]^{1/2} + f_T (1 - \delta_{TK}) \quad (35)$$

will flow. Thus, the beam current flowing directly to the metal islands has the effect of shifting the target current toward positive values by an amount $f_T (1 - \delta_{TK})$ from the curve shown in Figure 21. It can be seen that this would result in excellent qualitative agreement with the experimental data of Figure 19.

In summary, D.C. data on target current vs. landing voltage forces one to conclude that the oxide between adjacent metal islands on the retina has a beam induced conductivity, and that the metal-oxide interface can, under the influence of the fast beam, re-supply electrons lost from the oxide by secondary emission.

c. Retina Photoresponse Measurements Using Electron Beam Contact

The previous two sections dealt with the secondary emission properties of Schottky barrier retinas deduced from measurements of D.C. target current, performed (usually) at room temperature. Under these conditions the impedance of the Schottky diode can be assumed to be negligible, so that the entire values of V_{SM} falls across the vacuum gap between metal and mesh (or across the parallel path between silicon and mesh, through the silicon dioxide layer). As the retina temperature is reduced, however, the impedance of the Schottky diode rises, and a portion of V_{SM} can drop across the diode. It should then be possible to determine the dark current of the retina by measuring D.C. target current, I_T, vs. V_{SM} at low temperatures. Furthermore, measurements of I_T vs. V_{SM} at various light levels up to that value required to saturate the tube will provide information on tube dynamic range, linearity, and absolute responsivity. Such measurements are discussed below.

i. <u>Retina Dark Current Measurements Using Electron Beam Contact</u>

Figure 22 is a plot of I_T vs. V_{SM} for retina 10P115, obtained with the retina at operating temperature ($T < 100^{\circ}K$). Curve 1 was obtained under "dark" conditions, i.e., no radiation was intentionally introduced. (Thermal radiation from tube surfaces at room temperature, such as the quartz window, cannot presently be excluded). Curve 2 was taken under saturated light conditions, i.e., at light levels sufficiently high that no further increases in I_T occurred. Neglecting the slight separation between the curves for large negative values of V_{SM} (not yet explained), the shape of the curves is as expected. I_T on curve 1 is limited by diode impedance for low negative values of V_{SM}. As $|V_{SM}|$ increases, however, diode impedance begins to decrease until, for $|V_{SM}| > 25$ volts, it has decreased to the point where beam impedance again limits I_T. Thus, measurements of I_T vs. V_{SM} at operating temperatures provide information on diode dark current under actual operating conditions. Figure 23 shows such curves for retina 10P104 for several different values of beam landing voltage. This data shows that the value of V_{TM} at which I_T changes sign is dependent upon V_{MK}. This is not surprising, since the crossover point depends in a complicated way on δ'_{MK} and δ_{TK}, the secondary emission yields of the mesh and the retina surface (Cf. equations (55) and (56) below). It is clear, however, that the diode voltage drop is zero at the crossover point V_0, and the diode becomes reverse biased as V_{SM} is decreased below V_0. Figure 23 shows that substantial evidence of high diode impedance is seen out to $V_{SM} = -10$ volts for $V_{MK} = +250$ volts, but at higher values of V_{MK}, the diode impedance decreases, and has essentially vanished at 750 volts V_{MK}. This would be expected if the metal islands (or the SiO_2) were sufficiently thin that at high voltages, a fraction of the beam could penetrate thru this layer and enter the silicon, there discharging the diode by the creation of hole-electron pairs. Care must be exercised, therefore, in estimating retina leakage current from target current measurements, since V_{MK} plays an important role.

Considering the 250 volt curve in Figure 23, it can be seen that the diode leakage at $V_{SM} = -10$ volts must be 12 na or less. This is quite low, considering that the scanned area was 5.8 cm^2, and shows that Schottky retina leakage can be reduced to a sufficiently low level, under actual conditions of retina temperature

Figure 22

$\frac{I_T}{I_B}$ vs. V_{SM} for Retina 10P115

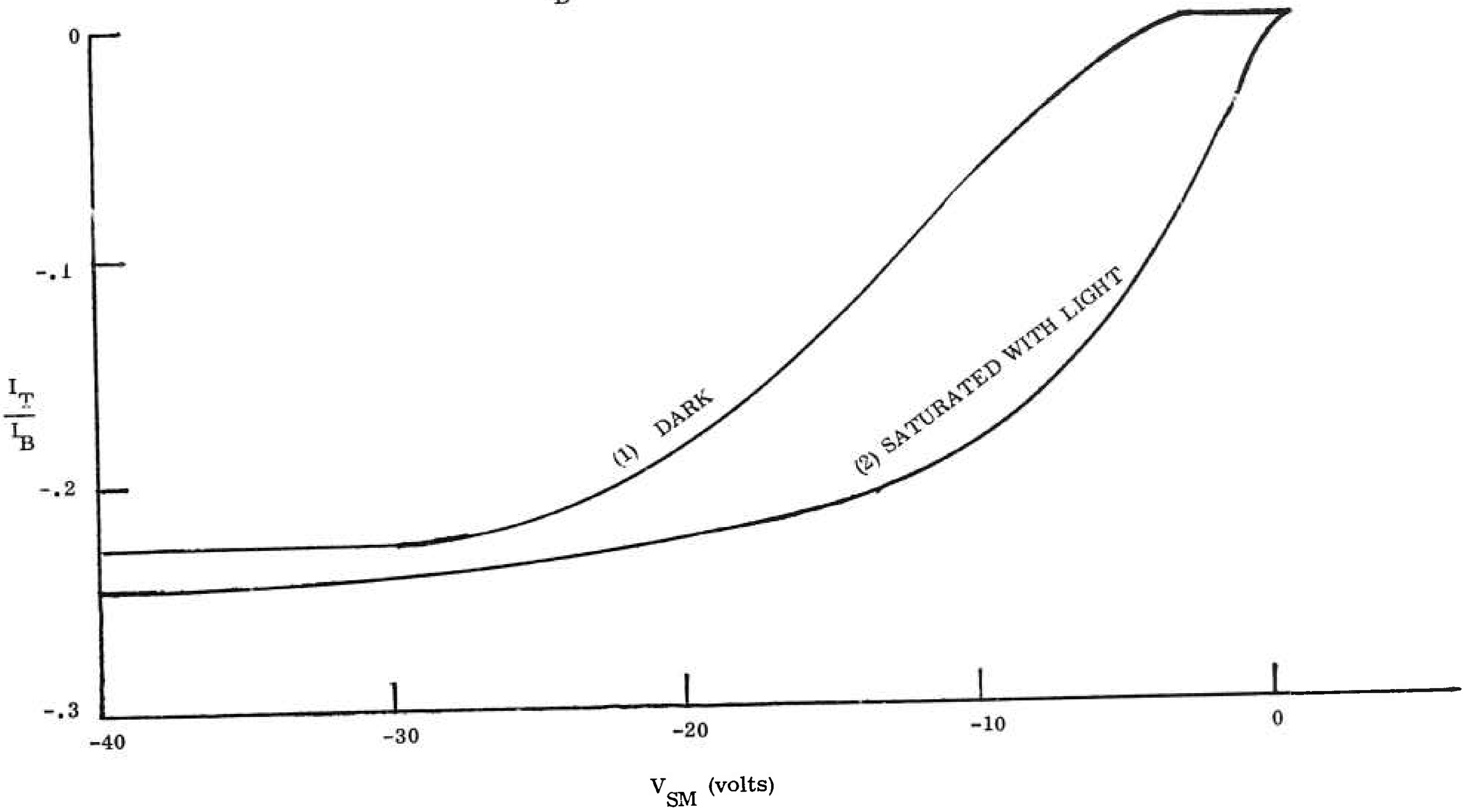

Figure 23

Target Current, I_T vs. V_{SM} for Various V_{MK}

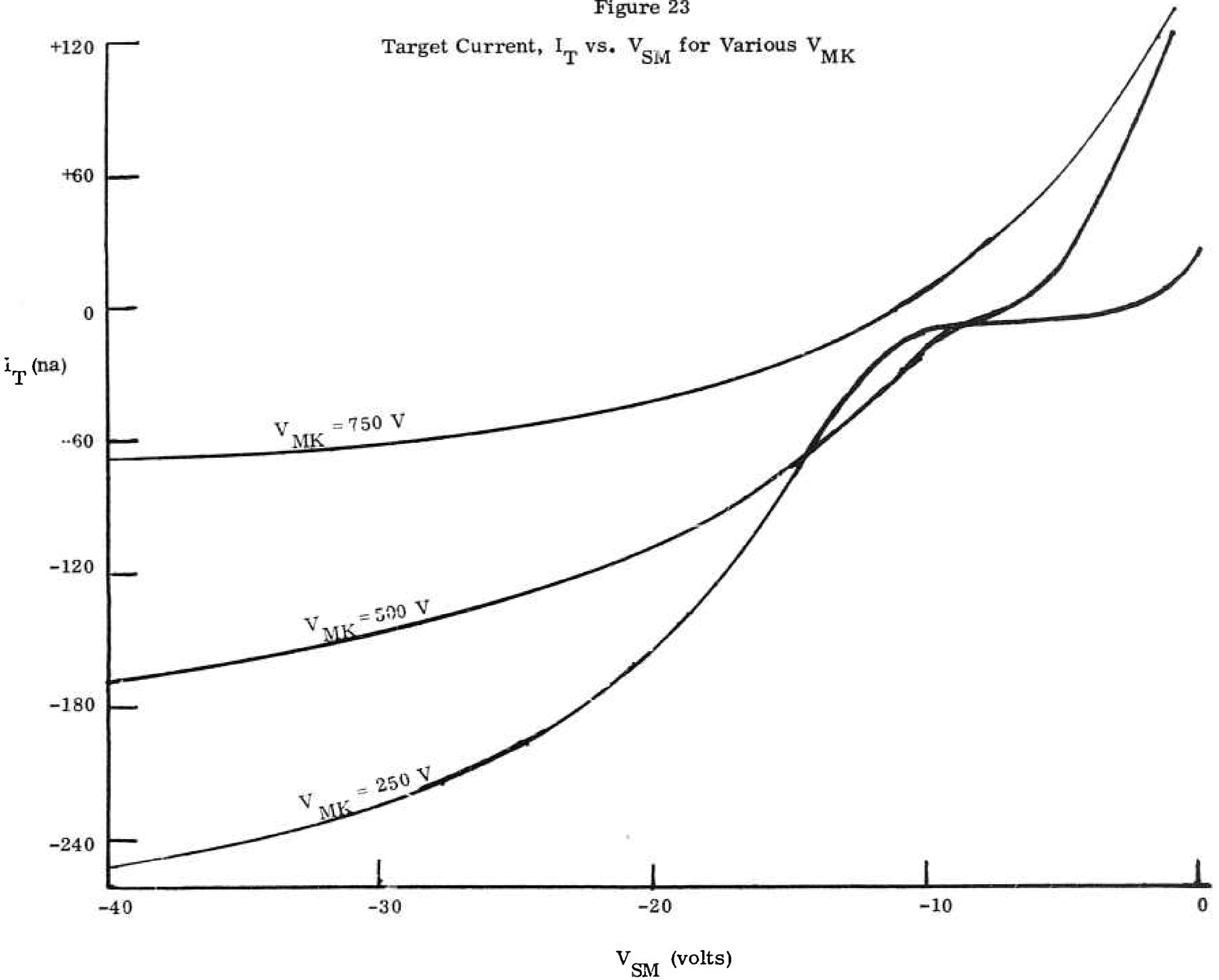

and high velocity scanning, to permit vidicon operation. Future retina designs will concentrate on maintaining this low leakage over a wider range of V_{SM} (higher breakdown diodes) and a wider range of V_{MK} (thicker metal islands, thicker oxides, closer control over surface scratches).

ii. Retina Photocurrent

Measurements of I_T vs. V_{SM} at various light levels permit the determination of tube responsivity, linearity, and dynamic range. Figure 24 is a plot of such data obtained on retina 10P115. Curve 0 is the dark curve, curves 1 thru 3 show I_T under illumination from an $800^{\circ}K$ black body (irradiances were $.1\ H_o$, $.5\ H_o$, and H_o, where $H_o = 8.9 \times 10^{-5}$ watts). Curve 4 is a saturated curve obtained using a microscope lamp operated sufficiently hot to saturate the retina. Several points can be made based on this data. First, the dynamic range of the retina is limited at the low end by retina dark current, I_{TD}, and at the high end by the maximum target current that the beam can supply. The latter quantity doesn't saturate with voltage until $|V_{SM}| > 20$ volts. Thus, it would be desirable if the retina dark current could be maintained at a low value until beam saturation occurs, since this would assure maximum dynamic range. This is equivalent to requiring that retina diode breakdown be ≥ 20 volts.

The second point to be made from the data of Figure 24 concerns the fact that retina 10P115 continues to show high retina impedance (low dark current) even though V_{MK} is 500 volts. At 250 volts, retina 10P115 was even better in this regard (data available, but not shown here because of space limitations). Retina 10P104, on the other hand, lost much of its diode impedance in raising V_{MK} from 250 volts to 500 volts. It is interesting to note that the metal film thickness t on these retinas is different ($t = 5000\ \mathring{A}$ for 10P115, $t = 500\ \mathring{A}$ for 10P104). Thus, this data supports a model which attributes increased retina leakage at high values of V_{MK} to penetration of a fraction of the fast beam thru the metal islands into the silicon. The third point to be made from the data of Figure 24 is the fact that retina responsivity and linearity can be obtained. Figure 25 is a plot of the photocurrent I_S at $V_{SM} = -10$ volts (target current minus dark current) normalized to the maximum photocurrent that can flow (saturated target current minus dark current). This data shows that the target photocurrent varies linearly with

Figure 24

Normalized I_T vs. V_{SM} at Various Light Levels

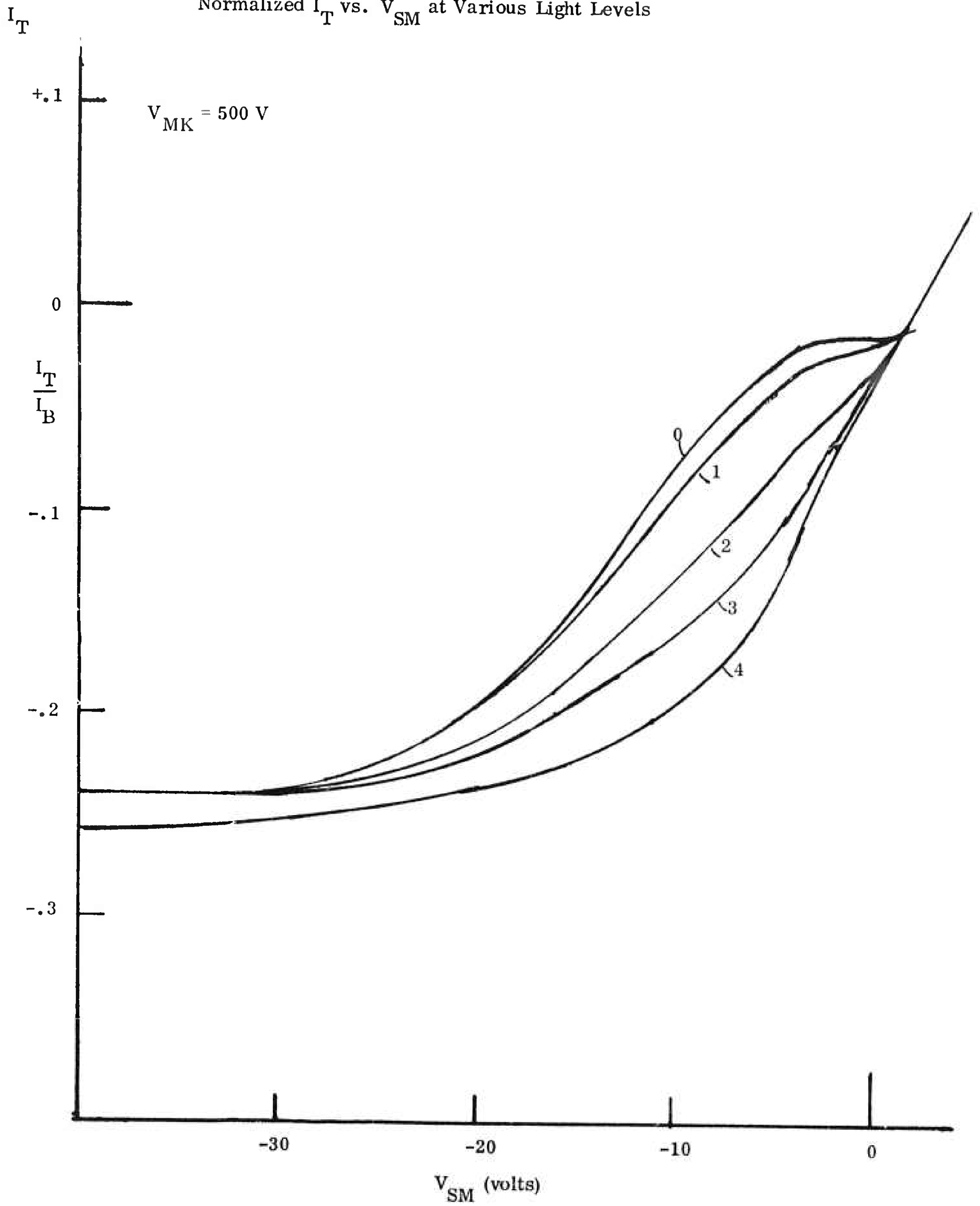

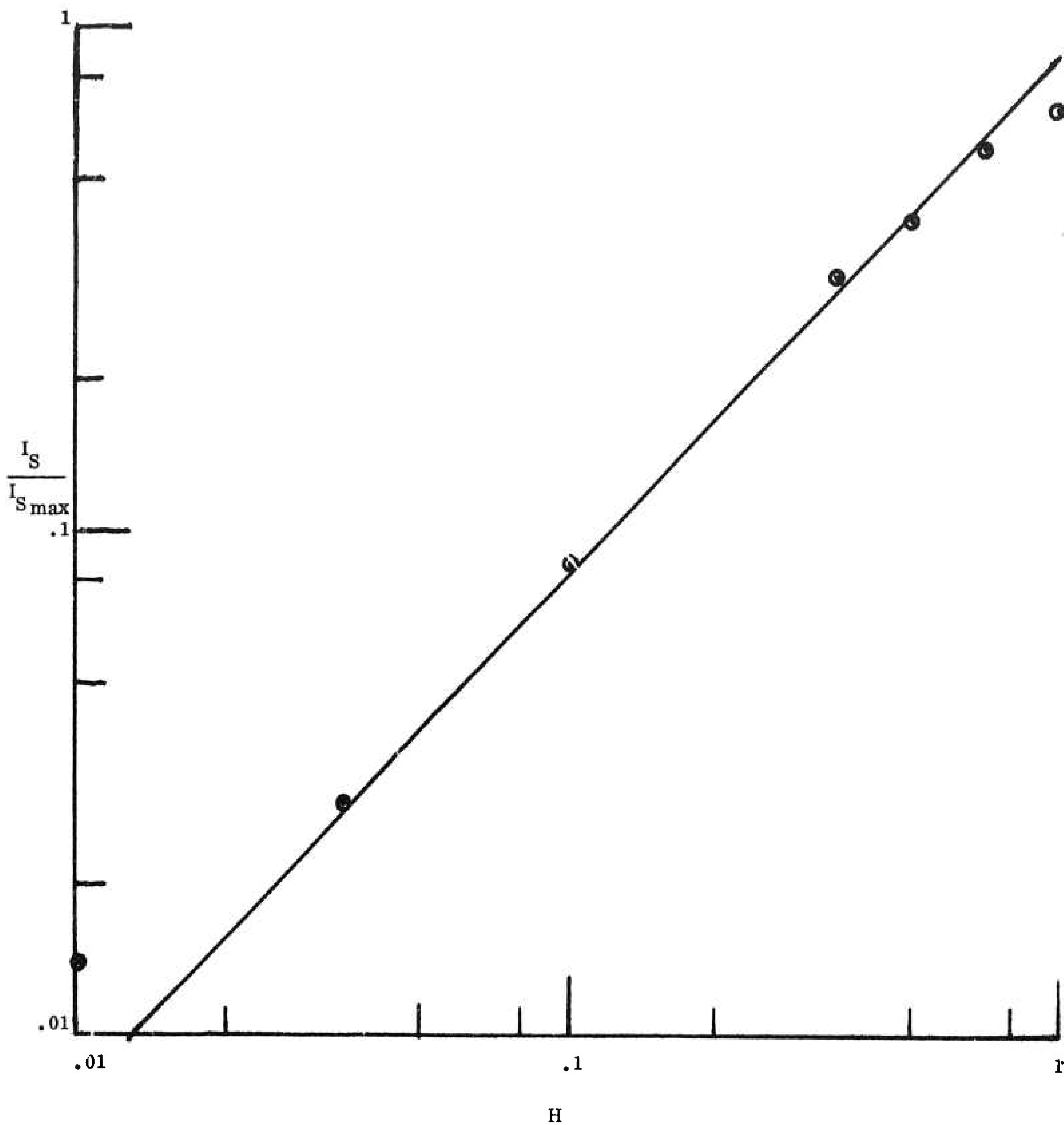

Figure 25. Retina Photocurrent vs. Radiance.

radiance ($\gamma = 1$, where $I_S = RH^{\gamma}$). Since $\gamma = 1$, it is possible to define a retina responsivity in amps/watt (R in the above equation). For retina 10P115, it was found that

$$R = 0.71 \frac{\text{ma}}{\text{watt}}$$

This compares very well with the responsivity calculated from equation (8) (calculation performed for $\lambda = 2.7\ \mu m$). The theoretical value for responsivity is given by

$$\mathcal{R} = \left(\frac{\text{amps}}{\text{watt}}\right) = \frac{y}{h\nu} = CA \frac{(h\nu - \phi_o)^2}{(h\nu)^2}$$

$$= CA \left[1 - \frac{\phi_o}{h\nu}\right]^2 \qquad (36)$$

Using the following parameter values

$C = .2/\text{ev}$

$A = .5$

$\phi_o = 0.354$

the values calculated for R is

$R = 5.2$ ma/watt

Due to the fact that the metal islands only occupy 64% of the surface of the retina, the maximum value that $\mathcal{R}$ could possibly have is

$$\mathcal{R}_{MAX} = 0.64\,\mathcal{R} = 3.3 \text{ ma/watt}$$

Thus, the responsivity under uniform illumination for this particular retina is somewhat less than the value theoretically predicted.

D. Imaging Results

Imaging experiments with metal-silicon Schottky barrier diode retinas have begun. Initial results are very promising, and clearly show that these retinas can produce high resolution images in the wavelength range beyond the silicon absorption edge (out to the long wavelength cutoff for internal photoemission of the Schottky diode). Because of the many new and novel features both of the retinas and of high beam velocity readout, complete characterization is a sizable undertaking. To speed up the process, it has been divided into three sub-tasks, viz. qualitative imagery studies, developing of working models to explain retina performance as determined from the qualitative studies, and finally, quantitative imagery studies using bias conditions, retina designs, etc., suggested by the working models. The last of these three sub-tasks will be performed during the next several months. The first two have been completed, and are described below.

1. Qualitative Imagery Studies

The previous section, entitled "Retina Characterization," described some of the factors of retina design and tube bias which are expected to influence the ability of metal-silicon Schottky diode mosaics to image in the infrared. These factors include the following:

Factors Expected to Influence Imaging

Retina Construction Factors	Tube Bias Factors
• Metal thickness	• V_{SM}
• Oxide integrity	• V_{MK}
• Diode breakdown	• Retina to mesh spacing
• Oxide conductivity under beam	• Beam current
	• Light level
	• Frame rate

In addition, other features of the system are expected to play a major role in imagery (e.g., preamplifier). In view of the large number of these factors, and the interplay expected between many of them, it seemed reasonable to determine

qualitatively which factors were most critical and what range of each factor was preferable. A number of retinas were examined for this purpose, and the major systematic dependencies were determined. The results of this survey are summarized below.

- Infrared imaging can be achieved with metal-silicon Schottky barrier diode retinae. Figure 26 is a photograph of such an im ge taken from the X-Y monitor described in Section B. This image was obtained by passing the radiation from a black body through a collimating lens, a stencil, and a 50 mil thick germanium filter, onto the retina. [The serrated outline is the edge of the diode mosaic pattern (Cf. Figure 4).]

- This imagery was achieved over the spectral range in which internal photoemission takes place at the metal-silicon interface. It was not due to absorption in the silicon. To verify this, a series of narrow spectral filters were inserted in the optical path. Imagery was only observed for wavelengths sufficiently long to be passed by the germanium ($\lambda \gtrsim 1.65\ \mu m$) filter, and shorter than the metal-silicon long wavelength cutoff ($\lambda \lesssim 3.5\ \mu m$).

- For small values of mesh-to-retina spacing (d = 0.002"), the anticipated "Dresner" type of high beam velocity imaging[9] (mode "A") was observed. In this mode, illuminated portions of the retina appear white, and dark regions appear black. This was observed for negative values of V_{SM} in the range of $4 \leq |V_{SM}| \leq 11$ volts.

- If V_{SM} was made more negative than the above range, the polarity of the image changed without any external circuit modifications being made (i.e., video polarity was not inverted electronically). This new mode of imagery (inverted mode, or mode "B") persisted to high values of V_{SM} ($|V_{SM}| = 40$ volts).

- If the mesh-to-retina spacing, d, were increased above 0.002", mode "A" imagery could no longer be observed. Mode "B" imagery, however, persisted to quite large values of d(d = 0.250"). In fact, it was observed with no mesh in the tube at all. Beam focus was poor when the mesh was not used, but imagery definitely was observed. (G6 electrode was still present, and biased positively.)

- The bias conditions required for imagery are as follows:

Reproduced from
best available copy.

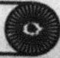

Figure 26. Photo of Image of GE Stencil

$V_{SM} \leq 0$ (optimum imagery in range $10 \leq |V_{SM}| \leq 25$)

$V_{MK} > 100$ V (optimum imagery in range $250\,V \leq V_{MK} \leq 500\,V$)

$T < 100^{o}K$ (photoresponse can still be detected for retina temperatures up to $120^{o}K$, but images wash out at $T = 110^{o}K$)

- As the light level is raised above the threshold for detecting images, a peak is observed in quality. Further increases in light level beyond this point degrade spatial resolution and contrast, until finally, at high light levels, the image is lost altogether.

- Similar behavior is observed if beam current is varied (keeping light level constant). At low beam currents, imaging cannot be detected. At intermediate levels, good images are seen. At high levels, imagery is lost.

- Transient effects, with time constants of the order of seconds are quite common. For example, if V_{SM} is reduced abruptly from -5 volts to -10 volts (for example), an image will often result which will fade out once the tube sits at the new bias level for several seconds.

2. Development of Working Model to Explain Retina Performance

If a positive D.C. bias supply V_{MK} is established between the mesh and cathode of a tube, then the electrons will arrive at the mesh with a kinetic energy of V_{MK}. A fraction $1 - f_M$ of these will pass through the mesh to the target, where they will land with a voltage given by $V_{MK} - V_{MT}$. Here V_{MT} is the voltage existing in the vacuum space between mesh and the floating target (Cf. Figure 27). (In the discussion which follows, the first subscript on V_{MT}, etc., will indicate the measurement point, and the second subscript will indicate the reference point. Thus, $V_{ST} = -V_{TS}$, etc.)

For a given value of V_{MK}, a constant current always flows out of the cathode and lands at the mesh plane. Therefore there appears to be a constant current in the mesh to cathode loop. The electron current flowing into the target lead is a function of V_{MT} and will look as shown in Figure 28. This curve has three essentially different regions of behavior. In region 1, the target is more negative than the cathode, and therefore if the electrons left the cathode with zero kinetic energy, they would never arrive at the target. Actually they leave the cathode with an exponential spread in energy determined by the temperature of the hot cathode.

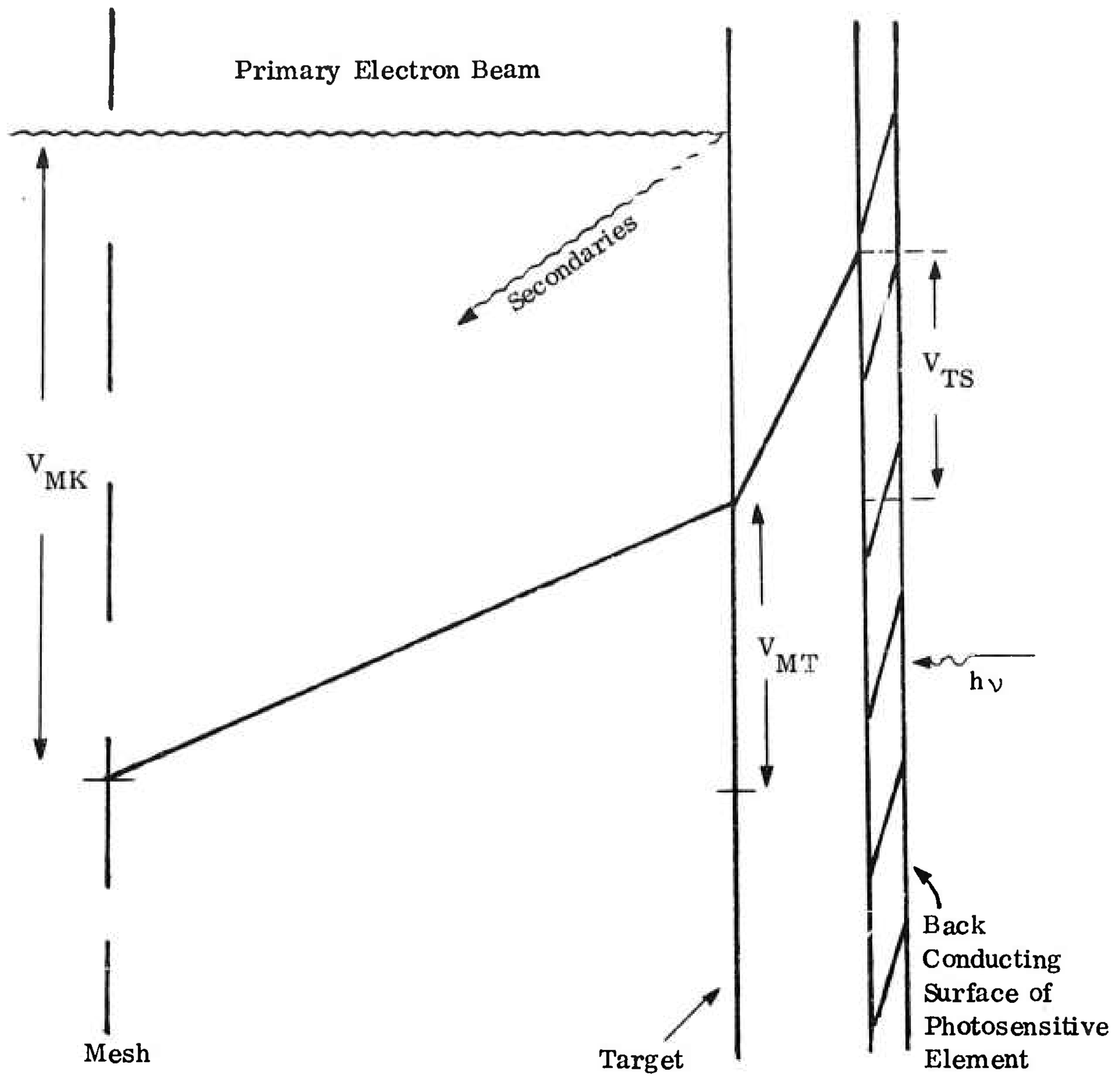

Figure 27. Electron Potential Diagram between the Mesh and the Back Surface, S, of the Photosensitive Element.

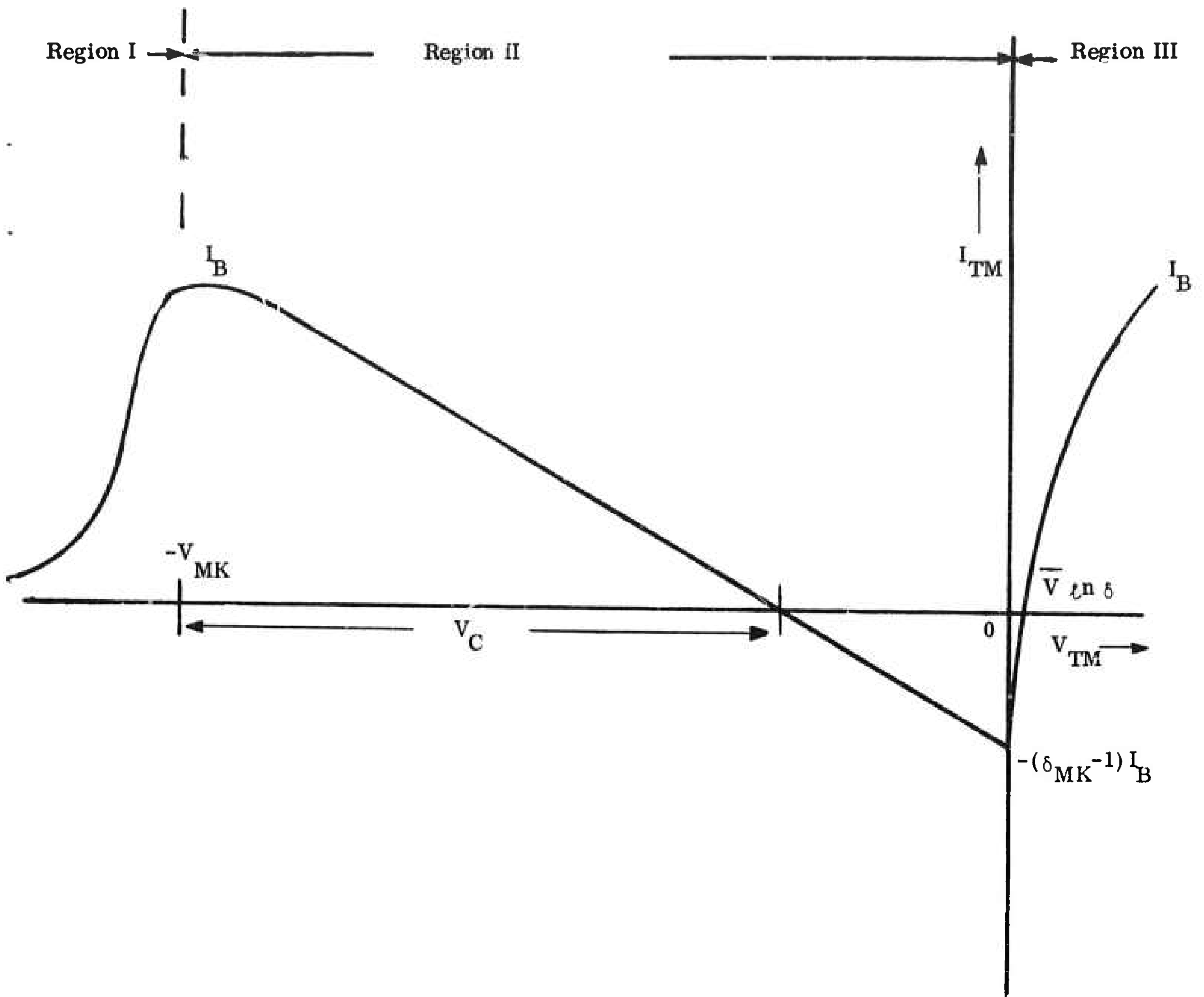

Figure 28. Target to Mesh I-V Characteristic.

Therefore the beam current will be cut off exponentially with voltage for $V_{TM} \leq -V_{MK}$. This is the so-called retarding potential region, or low beam landing characteristic region. In this region the beam impedance (the slope of the $I_{TM} - V_{TM}$ curve) is highly non-linear, but positive. Here the photosensitive surface can only be charged negatively, since there is always a net flow of electrons into the target element.

In region II the target to mesh voltage is negative, but less negative than the mesh to cathode voltage. Thus $(1 - f_M)$ primaries will land on the retina, and any secondaries which are generated will escape to the mesh. The landing voltage is given by $V_{MK} + V_{TM}$. Thus as V_{TM} gets less negative, the landing voltage increases and more secondaries are generated. Thus the net current leaving the target will decrease as V_{TM} becomes less negative. In this region the slope of the curve corresponds to a negative resistance. For $V_{MK} + V_{TM}$ greater than the first crossover voltage, V_C, where the secondary emission coefficient, δ, equals unity, the target to mesh current will become negative, corresponding to a net flow of electrons away from the target surface toward the mesh. We are particularly interested in this region, since this polarity of current can charge the target surface positive. In this region, we can approximate the beam characteristic by

$$I_{TM} \approx -(\delta - 1) I_B \left(1 + \frac{V_{TM}}{V_{MK} - V_C}\right) \tag{37}$$

$$\text{for } 0 \geq V_{TM} \geq -(V_{MK} - V_C)$$

Here δ is the secondary emission coefficient. Equation (37) assumes that δ is independent of the voltage, V_{TS}, existing across the photosensitive element. If the field associated with V_{TS} is not too high, this assumption ought to be reasonable.

In region III, the voltage existing between target and mesh is positive. Thus all the secondaries which are generated at the target surface cannot escape. If the mean spread in energy of the secondaries is $\overline{V}$, the current in this region is given by

$$I_{TM} \approx I_B \left[1 - \delta \; e^{\frac{-V_{TM}}{V}} \right] \tag{38}$$

for $V_{TM} \geq 0$

This region is that in which Dresner[9] envisions his high beam velocity vidicon to work. By modulating the voltage V_{TM} with light, he can modulate the number of secondaries which can escape to the mesh. Those secondaries which do not escape, will be retarded by the voltage V_{TM} and will land on a point on the target surface different from that where they were generated. In order to maintain coherence between the light and dark regions and the number of modulated secondaries, the field retarding the uncollected secondaries must be made high. Then the uncollected secondaries will land on the target surface close to their points of generation. The behavior of image tubes operating in these three regions can be understood by combining the tube I-V characteristic for the appropriate region with the I-V characteristic expected for the retina to be used.

a. <u>I-V Characteristics Between Mesh and Back Surface S, If The Photosensitive Element is a Photoconductor</u>

If the photosensitive element is a photoconductor, then the current flowing between the target and the back surface is of the form

$$I_{ST} = \frac{V_{ST}}{r_D} \left(1 + aH \right) \tag{39}$$

Here r_D is the dark resistance of the photoconductor, a is a constant, and V_{ST} is the bias between the floating target and the back contact. The current I_{ST} flows over the entire frame time, while the beam current flows only over the read time. Therefore, when the capacitive currents are included, we have that

$$I_{SM} \equiv I_{TM} = \frac{t_f}{t_R} < I_{ST} >_f = \frac{t_f}{t_R} \frac{< V_{ST} >_f}{r_D} \left(1 + aH \right)$$

$$= - \frac{t_f}{t_R} \left(\frac{< V_{TM} >_f + < V_{MS} >_f}{r_D} \right) \left(1 + aH \right) \tag{40}$$

Here the currents and voltages are averaged respectively over the frame and read times as indicated. If the internal capacitance of the target is large so that the photosensitive element cannot discharge significantly in a frame time, then the average voltages during the frame time cannot be very different than the average voltages during the read time. We then drop this averaging on either side of equation (40) and use it to determine the voltages in question. The only voltage which may not be properly accounted for in this way is the supply voltage V_{MS}. If the load resistor, R_L, between M and S is large, then V_{MS} could differ by large voltages during the frame time, as we move from dark to light areas. We may evaluate $\langle V_{MS} \rangle_f$ by averaging equation (40) over the entire frame time. Thus

$$\langle V_{MS} \rangle_f = V_{MS_O} + R_L \langle I_{SM} \rangle_f \tag{41}$$

and

$$\langle I_{SM} \rangle_f = -\frac{t_f}{t_R} \frac{\left(\langle V_{TM} \rangle_f + V_{MS_O} + R_L \langle I_{SM} \rangle_f \right)\left(1 + aH \right)}{r_D} \tag{42}$$

Then

$$\langle I_{SM} \rangle_f = -\frac{t_f}{t_R} \frac{\left(\langle V_{TM} \rangle_f + V_{MS_O} \right)\left(1 + aH \right)}{r_D \left(1 + \frac{t_f}{t_R} \frac{R_L \left(1 + aH \right)}{r_D} \right)} \tag{43}$$

Therefore from (43) and (41)

$$\langle V_{MS} \rangle_f = \frac{V_{MS_O} - \frac{t_f}{t_R} \frac{R_L}{r_D} \left(1 + aH \right) \langle V_{TM} \rangle_f}{1 + \frac{t_f}{t_R} \frac{R_L}{r_D} \left(1 + aH \right)} \tag{44}$$

and from (44) and (40)

$$I_{SM} \equiv I_{TM} = -\frac{t_f}{t_R} \frac{\left(V_{MS_O} + \langle V_{TM} \rangle_f\right)\left(1 + aH\right)}{r_D\left[1 + \frac{t_f}{t_R}\frac{R_L}{r_D}\left(1 + aH\right)\right]} \tag{45}$$

or since V_{TM} is nearly constant over a frame time

$$I_{TM} \approx -\frac{t_f}{t_R} \frac{\left(V_{MS_O} + V_{TM}\right)\left(1 + aH\right)}{r_D\left[1 + \frac{t_f}{t_R}\frac{R_L}{r_D}\left(1 + aH\right)\right]} \tag{46}$$

Equation (46) for I_{TM} is plotted as a function of V_{TM} and H in Figure 29.

It is interesting to note from equation (46) that the sensitivity of the target current to photocurrent is decreased by the presence of a load resistance, as the light level increases.

Figure 29 and Figure 28 must be combined to give the signal current I_{TM} as a function of photocurrent. By superimposing Figure 28 and 29, we thus obtain the locus of signal current vs. photocurrent. This is shown in Figures 30 and 31.

If V_{MS_O} the bias supply is made less negative than $(V_{MK} - V_C)$, then for low light levels, the photoconductor can be biased in such a way that V_{TM} is positive. (Cf. curves 0 and 1. Figure 30.) In this case severe redistribution should suppress imaging since target secondaries would return to the target. For higher light levels, the photoconductor I-V curve will cross the beam characteristic in region II. (Cf. curves 2, 3, and 4, Figure 30.) If V_{MS_O} is less than $(V_{MK} - V_C)$, the resistance of the photoconductor plus the effective load resistance, R_L, can be small compared to the beam resistance. Thus the signal can stably bias itself into this region of the curve, and imaging can be achieved. In this case the signal current out the lead, S, can be made negative corresponding to a net flow of electrons into S. This negative flow of electrons should decrease in absolute magnitude, with increasing light level giving rise to inverted video signals. In order to get significant modulation, the photoconductor must be able to withstand voltages of the order of $V_{MK} - V_C$, and

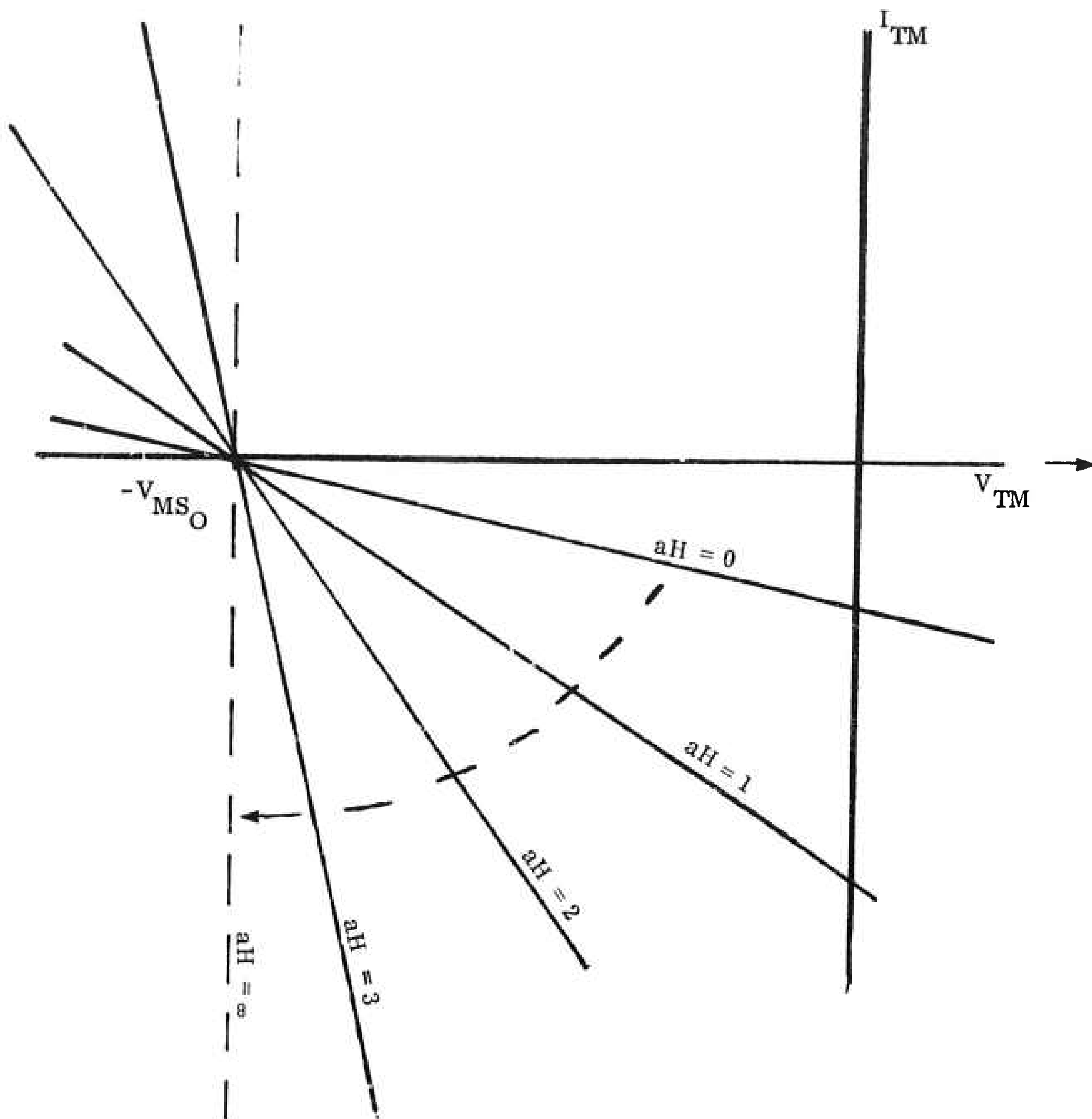

Figure 29. I_{TM} vs. V_{TM} for Various Values of the Photocurrent aH. The Slope of the I_{TM} Curves Increases with Increasing Photocurrent. All curves pass through the Bias Point $-V_{MS_O}$.

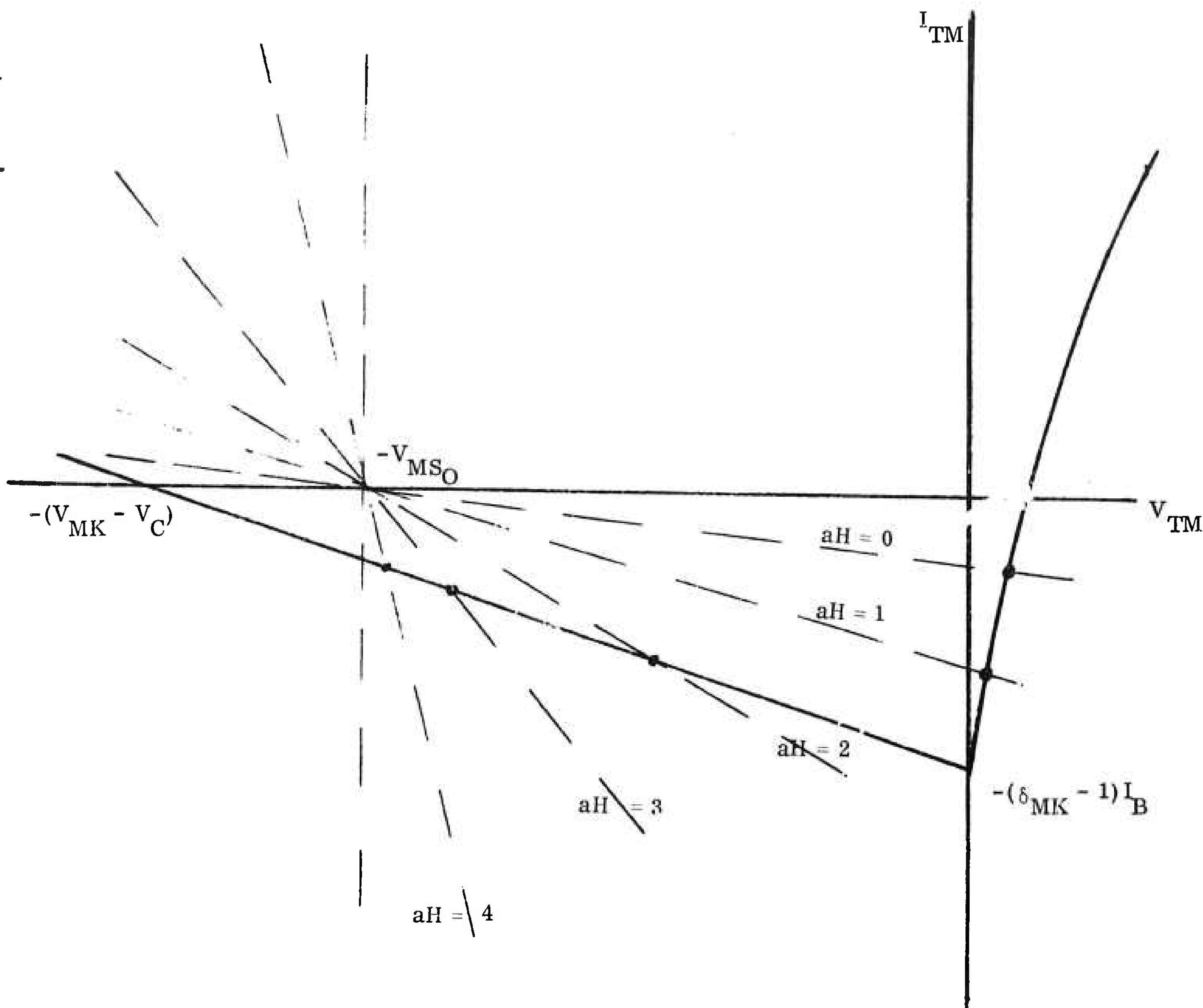

Figure 30. Superposition of Figures 28 and 29.

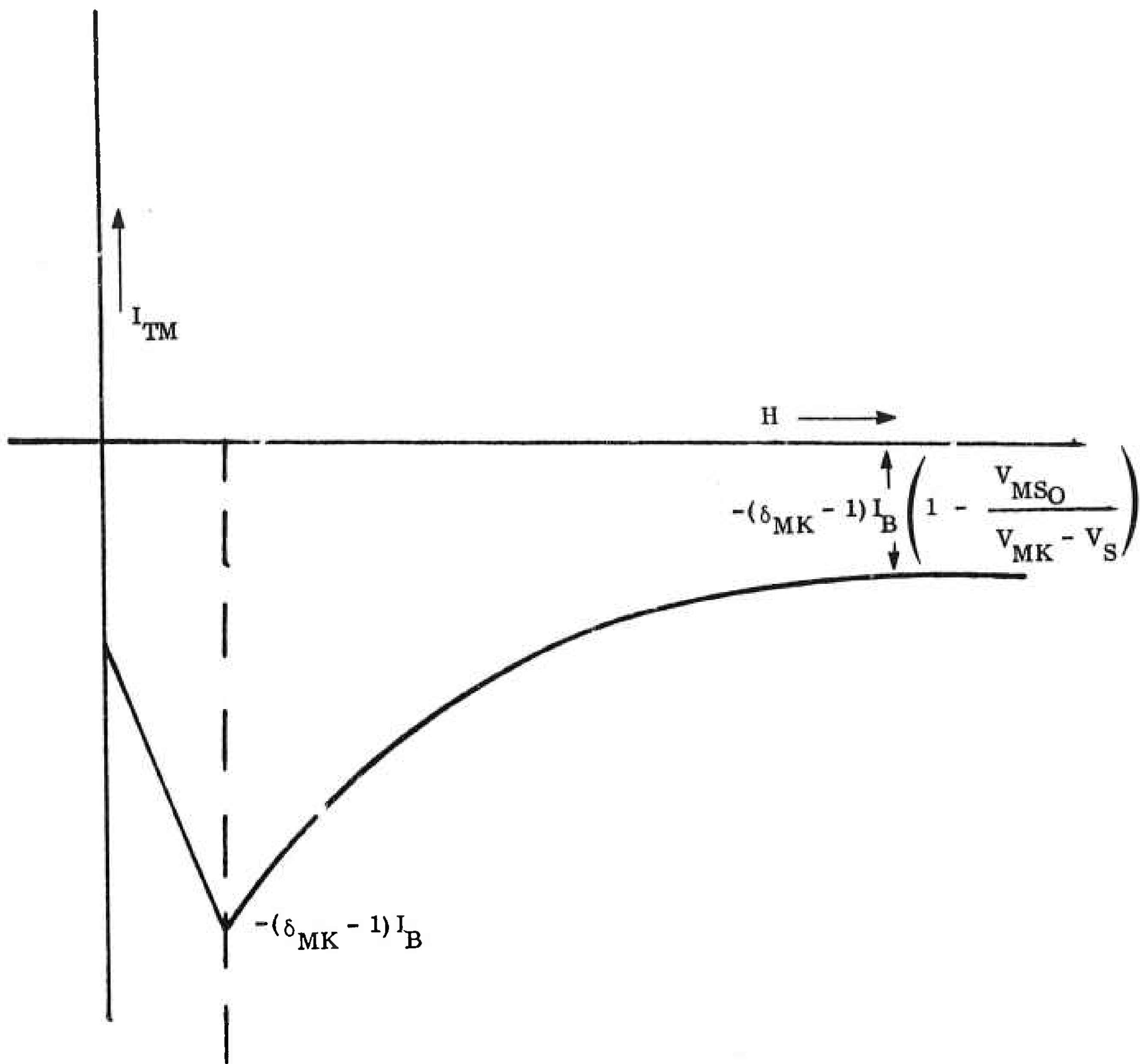

Figure 31. I_{TM}, the Signal Current, vs. Increasing Light Level.

$(V_{MK} - V_C)$ must be large enought that $(\delta - 1)$ is significant. If (46) is combined with (37), we have that

$$I_{TM} \approx \frac{-\left(\delta_{MK} - 1\right) I_B \left[1 - \left(\frac{V_{MS_O}}{V_{MK} - V_C}\right)\right]}{\left[1 - \left\{\frac{\left(\delta_{MK} - 1\right) I_B r_D \left(t_R/t_f\right)\left(1 + \frac{t_f}{t_R}\frac{R_L}{r_D}\left(1 + aH\right)\right)}{\left(V_{MK} - V_C\right)\left(1 + aH\right)}\right\}\right]} \qquad (47)$$

where

$$1 \geq \frac{V_{MS_O}}{V_{MK} - V_C} \geq \frac{(\delta_{MK} - 1) I_B r_D \left(t_R/t_f\right)\left(1 + \frac{t_f}{t_R}\frac{R_L}{r_D}\left(1 + aH\right)\right)}{(V_{MK} - V_C)(1 + aH)}$$

This analysis of imaging in a high beam velocity vidicon using a photoconductive retina helps to clarify some important features of these tubes. It can be seen that the sign of the target current does not determine video polarity. This quantity is defined by the change of target current with illumination. If $\Delta I_T/\Delta H$ is positive, illuminated regions of the retina appear white and dark regions appear black. If $\Delta I_T/\Delta H$ is negative, the inverse is true. Since retina current always increases in magnitude with illumination, video polarity will be determined by the portion of the tube I-V characteristic on which we operate. Regions I and III of Figure 28 will produce positive polarity, while region II will produce negative polarity.

b. I-V Characteristics Between Mesh and Back Surface, S, if the Photo-Sensitive Element is a Photodiode, Assuming that the SiO_2 Isolating the Diode is Electrically Inactive

If the photosensitive element is a photodiode, the photocurrent through the diode is given by

$$I_{ST} = I_{CO}\left(e^{qV_{ST}/kT} - 1\right) - RH \qquad (48)$$

where I_{CO} is the saturation current of the diode, R is the retina responsivity, q is the electronic charge, k is Boltzman's constant and T is the absolute temperature

of the diode and H is the radiant power on the retina. If the SiO_2 which isolates the diodes is considered non-conducting it should charge to some steady state value and become electrically inactive. This is the way the Si behaves in a low beam velocity tube.

Rewriting equation (48) we have that

$$I_{ST} = I_{CO}\left[e^{\frac{-q\left(V_{MS}+V_{TM}\right)}{kT}} - 1\right] - RH$$

or

$$I_{ST} = -\left(I_{CO} + RH\right) + I_{CO}\, e^{\frac{-q\left(V_{MS_O} + I_{SM} R_L + V_{TM}\right)}{kT}}$$

and

$$<I_{SM}>_R = \frac{t_f}{t_R} <I_{ST}>_f$$

Therefore

$$<I_{SM}>_R = -\frac{t_f}{t_R}\left[\left(I_{CO} + RH\right) - I_{CO} < e^{-\frac{q\left(V_{MS_O} + \left(I_{SM}\right) R_L + V_{TM}\right)}{kT}} >_f\right] \quad (49)$$

The second term on the right of equation (49) tells when the signal current would bias the diode off. For a given load resistor and a given reverse bias supply V_{MS_O}, if the total signal current were to increase, it would take a less negative target to mesh voltage to forward bias the diode. If we assume that the load resistor R_L is small, then the equivalent of Figure 29 may be drawn up for the photodiode as a function of light level. This is shown in Figures 32 and 33.

If the photodiodes have a reverse impedance which is greater than the negative resistance associated with region II, a bistable solution could exist at high light levels. As we increase the photocurrent, the signal will continue to increase until we reach the peak signal, $-(\delta_{MK} - 1) I_B$. For further increases in light level, the diode would rapidly forward bias itself until the signal dropped to approximately $-(\delta_{MK} - 1) I_B \left[1 - \frac{V_{MS_O}}{V_{MK} - V_C}\right]$. Further increases in light level would not

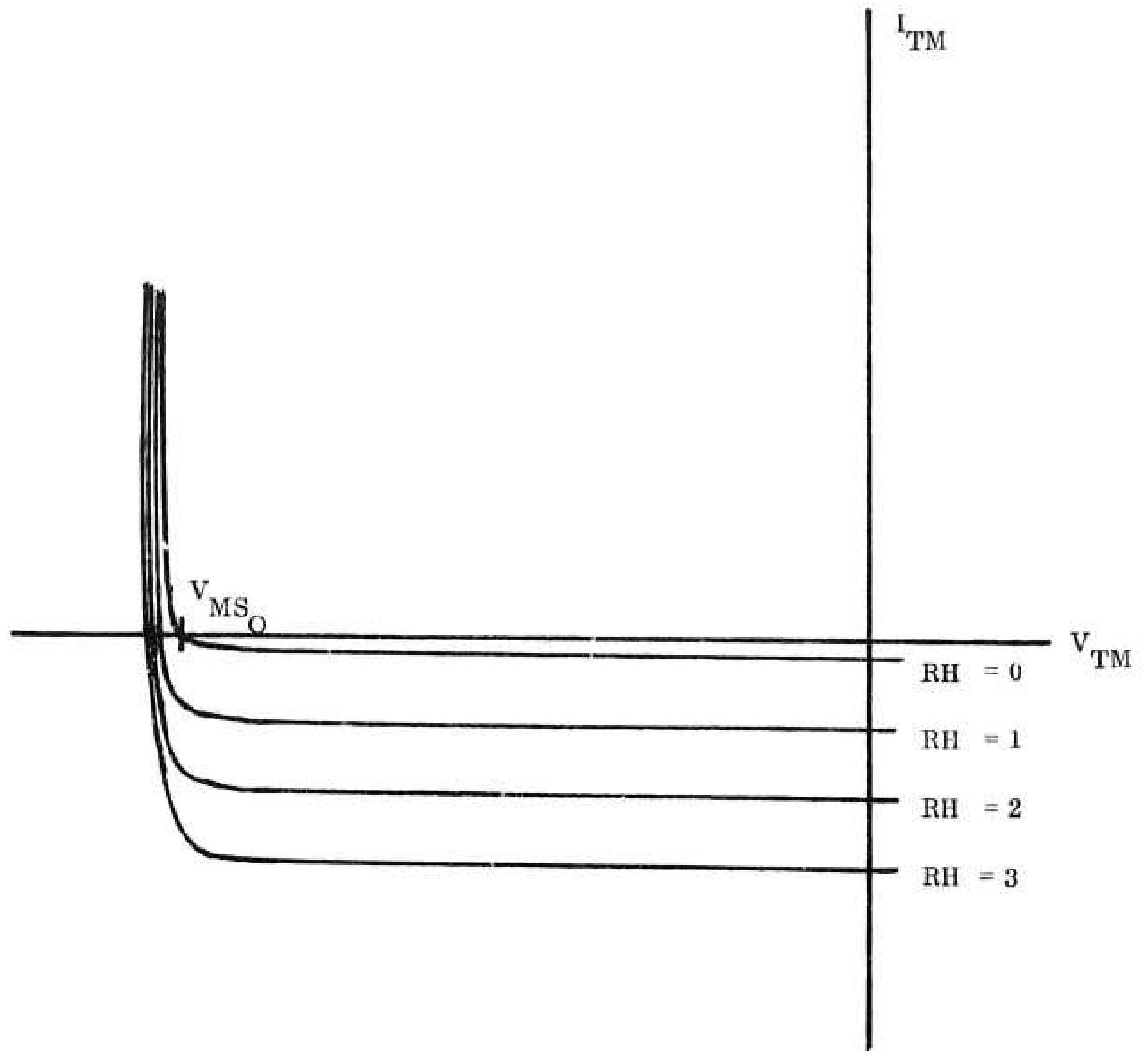

Figure 32. I_{TM} - V_{TM} Curves of the Photodiode vs. Light Level. Here V_{MS_O} is the Bias Between the Surface S and the Mesh.

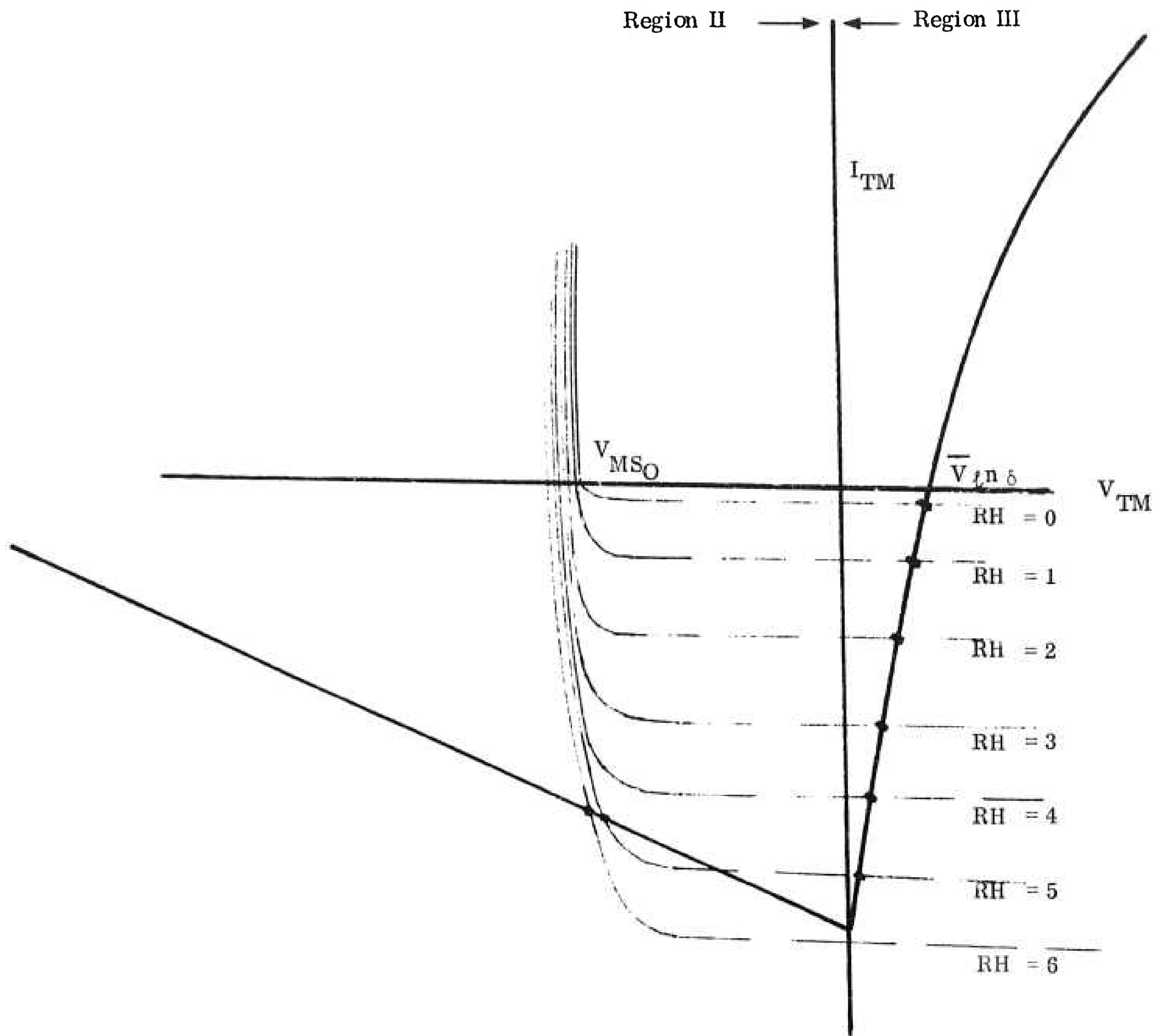

Figure 33. A Superposition of Figures 32 and 28.

significantly change the bias on the diode since it is forward biased for higher light levels. See Figure 33. As the light level were reduced, the diode would stay forward biased until the light level dropped back to a value where the signal was $-(\delta_{MK} - 1) I_B \left[1 - \frac{V_{MS_O}}{V_{MK} - V_C} \right]$ on the rising part of the curve. Thus a bistable state exists for light levels above H_O. See Figure 34. Since the diode curves are always forward biased when we are in region II of Figure 28, we cannot modulate the current significantly when we are in this region. This differs from the case of the photoconductor, which can change its voltage when biased into this region. If the photodiodes operate as described in this section, then imaging with them in a meshless tube would not be possible unless an integrated mesh were incorporated on top of the oxide surface. In this case the target to mesh I-V characteristic of Figure 28 would be that appropriate to this integrated mesh to photodiode structure. Redistribution would then become unimportant since the mesh is very close, and imaging would be accomplished by modulating the current in region III of Figure 28 or 33. The collecting walls of the meshless tube would be available for removing any unwanted secondaries which are generated by the beam off the integrated mesh surface. This could be accomplished by making the walls more positive than the integrated mesh surface. It is clear by examining Figure 33 that a tube operated in this way would have a target to mesh current which is negative and which would increase in absolute magnitude with increasing light level.

We have seen imaging in our demountable system which behaves in this manner for mesh to target spacings of 2 mils or less. This strongly suggests that good imagery could be obtained with an integrated mesh tube which would have the advantage of low microphonic noise.

It is also clear from Figure 33 that the total swing in beam current can be obtained with changing light level, if the voltage on the diode changes by $\overline{V} \ln \delta$. There is then no great advantage to be gain by having a breakdown voltage on the diode which is greater than $\overline{V} \ln \delta$ for this case.

We have also seen imaging in our demountable tube, which behaves quite differently than that described above, and which does not depend on a mesh for its existence. The physics of this new mode is discussed in Section c.

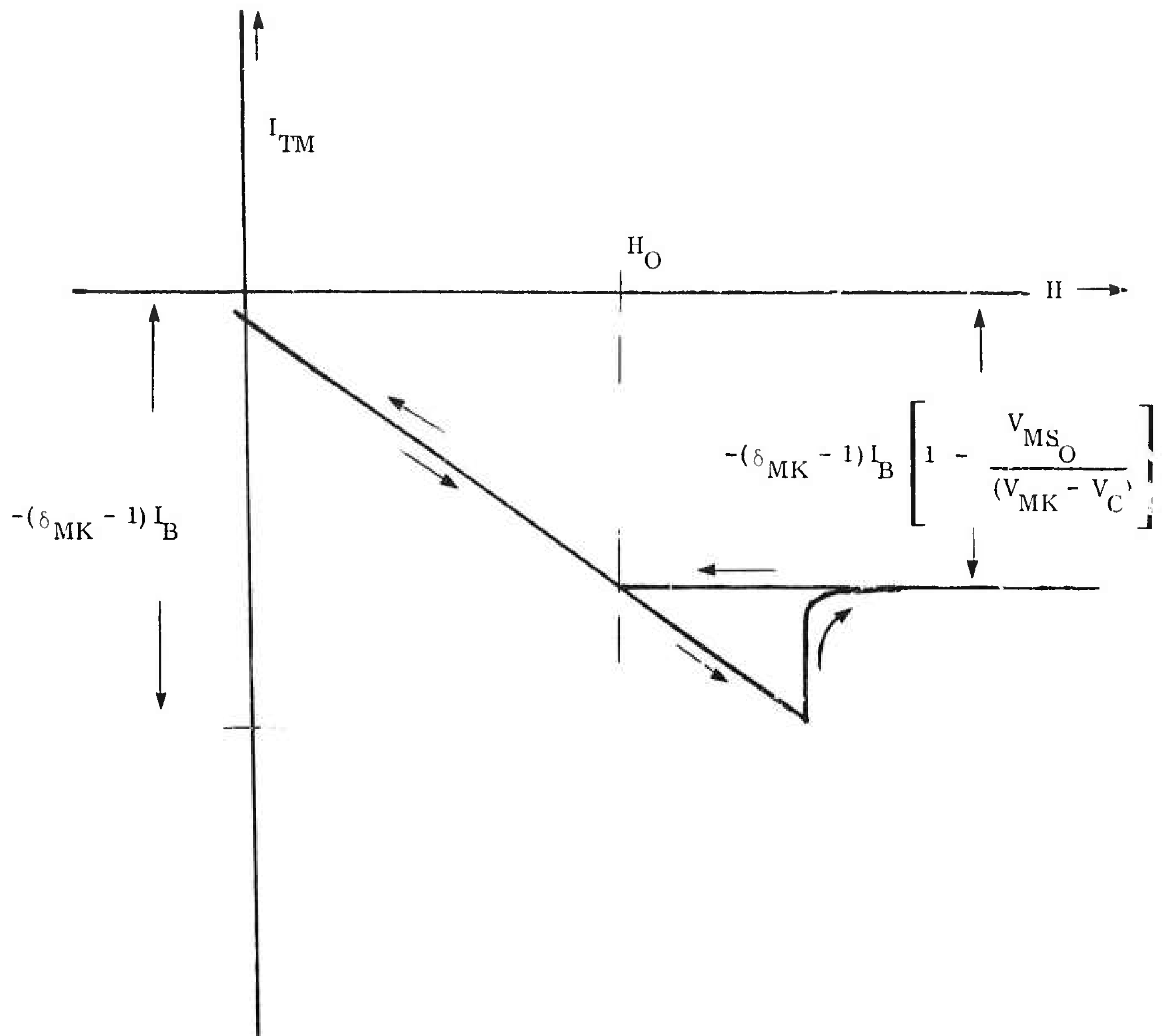

Figure 34. A Qualitative Description of I_{TM}, the Signal Current, vs. Light Level H.

c. Retina I-V Characteristics and Imaging for the Case Where the SiO_2 is No Longer Considered Inactive

This section is aimed at describing the effects which can occur as a result of having a composite surface of oxide and Pd_2Si which is exposed to the high voltage electron beam in a camera tube. When the Schottky diode array was originally conceived to be used in the tube as the photosensitive element, the oxide was introduced in order to provide isolation between the various photodiodes.

It was believed that the oxide would charge to a potential which was such that there was no net flow of carriers in or out of the surface, and then it would be electrically inactive in the circuit. This is essentially the way it behaves in the normal vidicon made up of a p-n junction array. In this case the composite surface of p Si and oxide is bombarded with a low energy electron beam and is charged to negative potentials relative to the cathode.

In our case, the array of Pd_2Si and oxide is bombarded with a high voltage electron beam which generates secondaries of differing amounts from the two surfaces. It is necessary to have a net flow of secondaries off the Pd_2Si, if it is to charge positively and reverse bias the Schottky diodes on p type Si. Therefore secondaries are of necessity involved in the process. We have by now accumulated a significant body of data which indicates that the oxide surface under these conditions is actively involved in the conduction process between mesh and Si, and is not just serving as an element of isolation between adjacent diodes. In fact, at this time let us view the composite surface as seen by the beam as shown in Figure 35. Here, the hatched areas represent the Pd_2Si diode surfaces while the grid work represents the oxide. We would like to show in this section that the data fits a model where the shaded area of the oxide grid appears to act like it has significant sheet conductance during the entire frame time when bombarded by the beam. However the white peripheral region of the oxide adjacent to the Pd_2Si is non-conducting except when the beam is passing over it. The oxide thus serves simultaneously as an element of isolation and as an integrated mesh (referred to as M2 to differentiate from regular mesh, M1). In this section, we will present the physical model whereby this can occur, and discuss the I-V relations predicted for a composite surface under

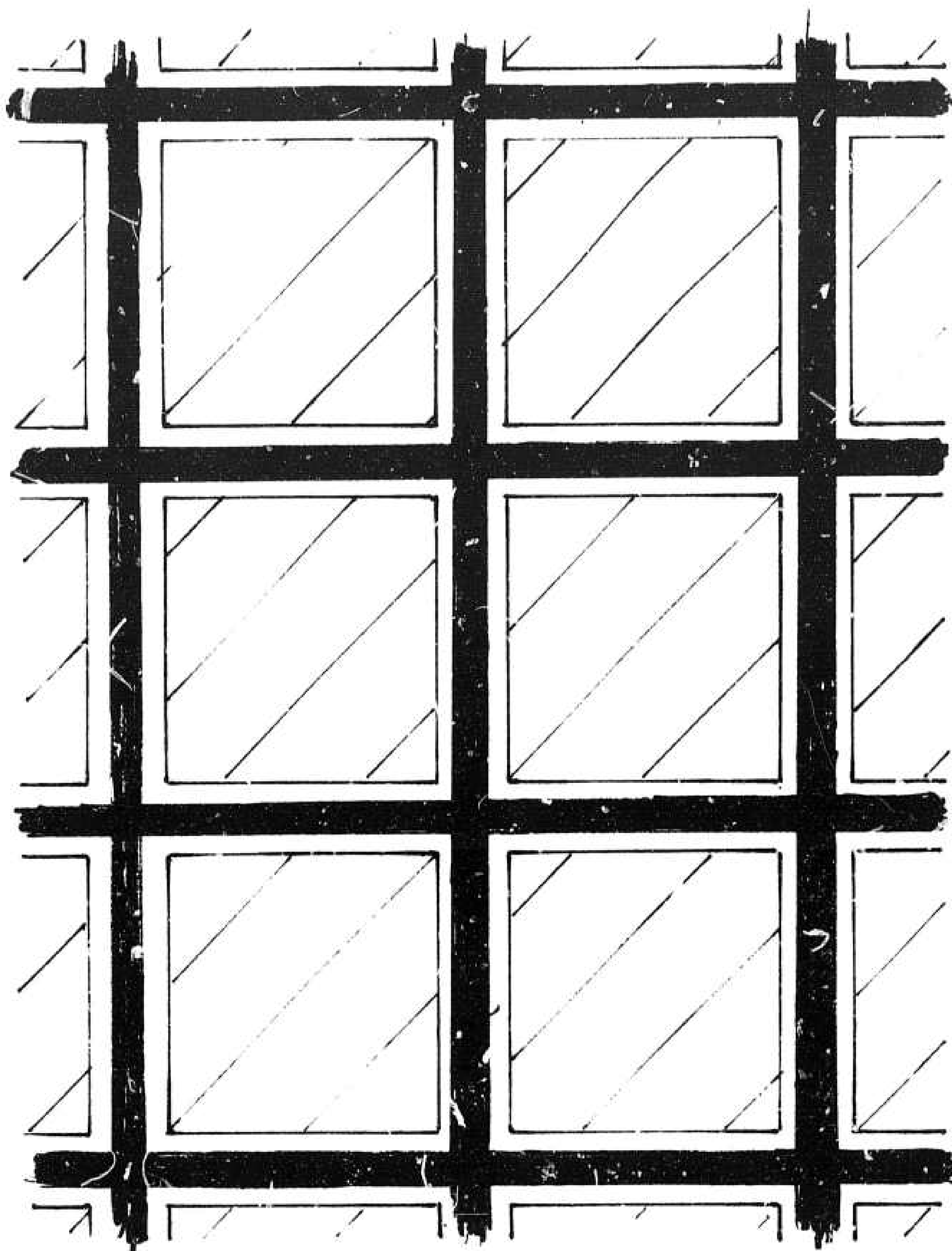

Figure 35. View of Pd_2Si - Oxide Surface as Seen by Electron Beam.

uniform illumination. Also we will discuss the various possible modes of imaging from a composite surface. Theory will be compared with experiment throughout.

i. Physical Model of Conduction Processes in the Oxide Under the Influence of the Beam

If we examine the energy distribution of electrons in the Pd_2Si under the influence of the beam, we can anticipate a situation as depicted in Figure 36a. Here E_{CT} is the bottom of the conduction band, E_{FT} is the Fermi Energy and W_{FT} is the work function of the Pd_2Si. Since there are electrons energetic enough to be removed over the work function, there must be energetic electrons between E_{FT} and W_{FT}. Once the beam is removed these energetic electrons will rapidly fall back to the Fermi level and the energy distribution will be shown in Figure 36b. Similarly if we examine the situation in the oxide, we will find at successive times after the beam has been removed, the situation depicted in Figure 37a, b, and c.

Under the influence of the beam, energetic electrons must exist in the conduction band of the oxide as in Figure 36a since secondaries can be emitted into vacuum. After the beam has been removed, these energetic electrons will rapidly relax to the bottom of the conduction band as depicted in Figure 36b. Since electrons are known to have a mobility in SiO_2, while holes are believed not to, we show the holes as rapidly becoming trapped. The electrons can remain in the state b) for a time of the order of the lifetime required for them to recombine with the trapped holes. This lifetime could be long compared to the frame time, especially if fields are established in the oxide as shown in Figure 36b. Then the conduction band electrons will be spatially removed from the positive charges and could exist for long periods of time especially at low temperatures. Under these conditions, the lifetime could easily be long compared to the frame time and the oxide could return to the state a) before it has a chance to relax to the state c). Then the oxide would appear to have a sheet conductance on the vacuum side, and the shaded area in Figure 35 would become an equipotential under the influence of the beam.

Let us now examine the conditions which exist at the interface between the oxide and the Pd_2Si. This is depicted in Figure 38 a) under the influence of the beam and b) when the beam has been removed. If the oxide is emitting secondaries into

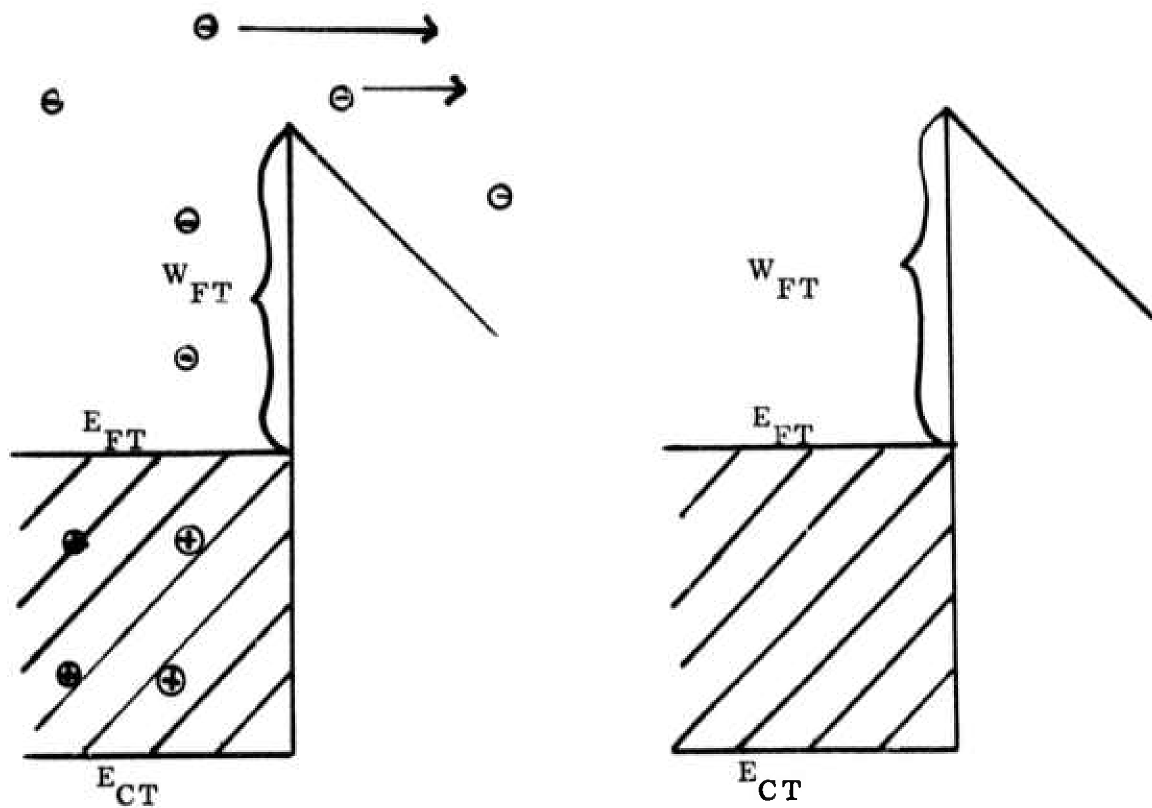

Figure 36

Energy Distribution of Electrons in the Pd_2Si

a) Under the Influence of the Electron Beam

b) With the Electron Beam Removed

W_{FT}, E_{FT}, and E_{CT} are the Work Function, Fermi Energy and Bottom of the Conduction Band, Respectively.

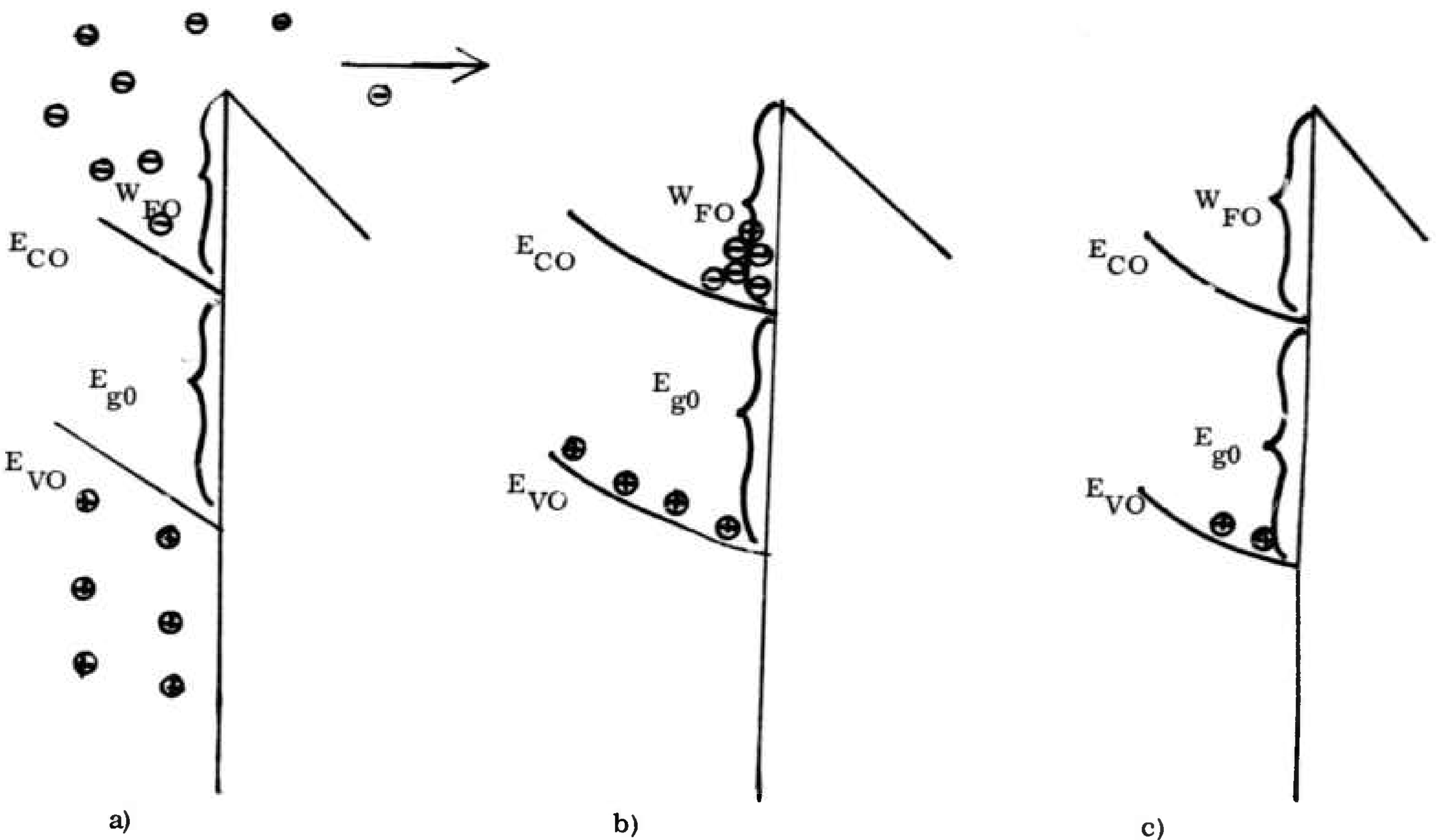

Figure 37

Energy Distribution of Electrons in the Oxide

a) Under the Influence of the Electron Beam

b) Shortly After the Beam has been Removed

c) Long After the Beam has been Removed

E_{CO} = Edge of Conduction Band

E_{VO} = Edge of Valence Band

E_{g0} = Gap Width

W_{FO} = Work Function of the Oxide

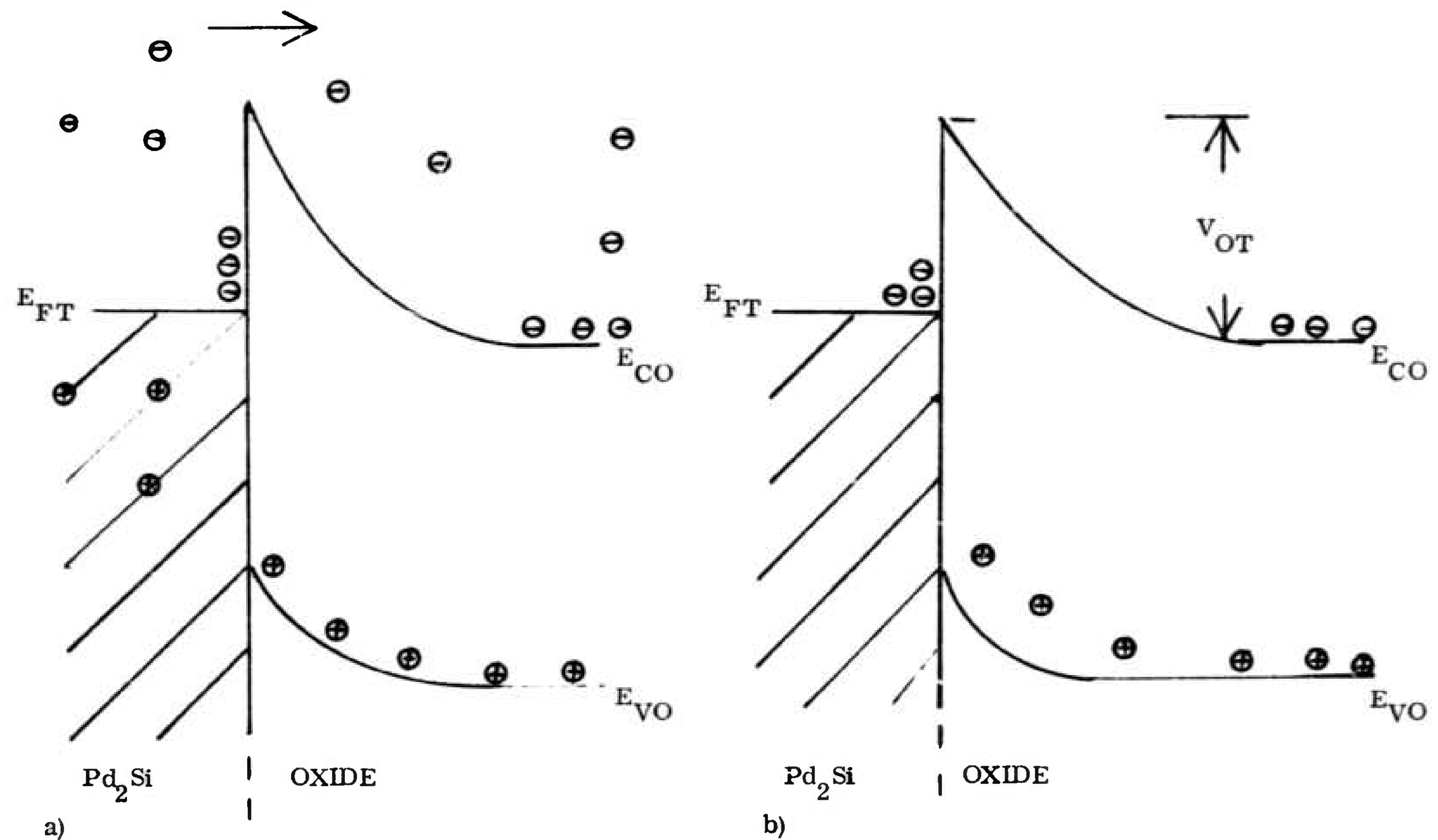

Figure 38

Metal-Oxide Interface

a) Under the Influence of the Electron Beam

b) After the Electron Beam has been Removed

V_{OT} is the potential built in at the oxide boundary as a result of scanning by the beam

vacuum, it will charge positively relative to the metal, causing a net flow of energetic electrons from the metal to the oxide. A dipole will be established at the oxide metal interface as shown until the net flow of electrons into the oxide just equals the net flow out into vacuum. When the beam is removed, this dipole will remain and the interface will appear as in Figure 38b. Since there is a large potential barrier existing at the metal oxide interface, no flow of electrons can occur across the metal to oxide interface once the beam has been removed. Referring to Figure 35 we then have the shaded conducting area of the oxide surrounded by the white non-conducting area of the oxide once the beam has been removed.

The above describes basically how the oxide can act as an integrated mesh (M2) while simultaneously offering isolation to the individual diodes. We would like to examine in more detail, the type of I-V relations we can anticipate between Si and mesh (M1) for such a structure.

ii. I-V Curves between Target Surface and Mesh (M1)

Let us assume that we have a structure as shown in Figure 35 where the Pd_2Si represented by the hatched areas will be referred to as target, T. Let this cover a fraction f_T of the entire top surface. Let the shaded areas represent the conducting oxide surface which we shall refer to as 0. Let this cover a fraction f_0 of the top surface. Let the distance between target centers be ℓ, and let the mesh, M1, be spaced a distance, d, from the composite surface. Let us suppose that a voltage, V_{TM} exists between target and mesh M1, and a voltage V_{0T} is established between oxide surface and targets. (See Figure 39.) If d is very much larger than ℓ, then the electron potential between a plane of the order ℓ out from the composite surface and d, will be given approximately by

$$\phi(Z) \approx -\left[f_T V_{TM} + f_0 (V_{TM} + V_{0T})\right]\left[1 - \frac{Z}{d}\right] \tag{50}$$

for $\ell \lesssim Z \lesssim d$

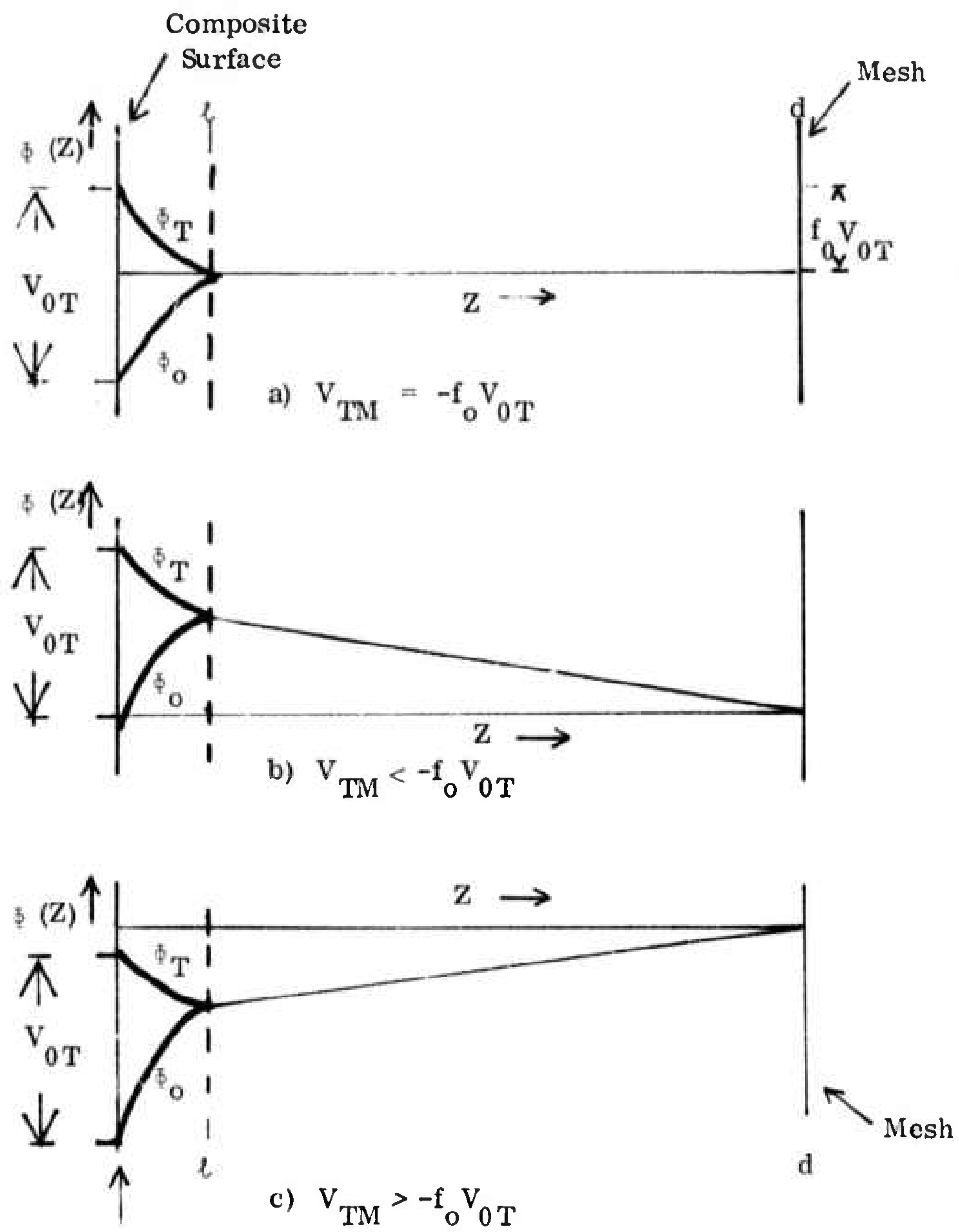

Figure 39. Electron Potential as a Function of Distance Between Composite Surface and Mesh.

(ϕ_T is potential in front of target areas, ϕ_o is potential in front of oxide areas.)

In other words for Z large compared to ℓ, the potential will only know the average of the composite surface. Specifically, let us take a case where V_{TM} equals $-f_0 V_{0T}$. Then since $f_T + f_0$ is identically equal to unity, V(Z) will be zero for $\ell \lesssim Z \leq d$. A plot of the electron potential as a function of Z for this case is shown in Figure 39a. Figure 39 b and c show how we might expect the electron potential to vary with distance for V_{TM} negative and positive respectively relative to $-f_0 V_{0T}$. In these diagrams, Φ_T and Φ_0 refer to the electron potentials in front of the central portions of the target and oxide areas respectively. For $Z \leq \ell$, we may approximate the behavior indicated in these diagrams by the following sets of equations

$$\Phi_T(Z) \approx -V_{TM}\left(1 - \frac{Z}{d}\right) + f_0 V_{0T}\left[\left(1 - \frac{Z}{\ell}\right)^2 - \left(1 - \frac{Z}{d}\right)\right] \tag{51}$$

and

$$\Phi_0(Z) \approx -V_{TM}\left(1 - \frac{Z}{d}\right) - f_0 V_{0T}\left(1 - \frac{Z}{d}\right) - f_T V_{0T}\left(1 - \frac{Z}{\ell}\right)^2 \tag{52}$$

for $\frac{Z}{\ell} \leq 1$

These equations imply that if V_{0T} is positive, there is a maximum in electron potential in front of the oxide surface for values of V_{TM} listed in equation (53). This maximum is given by

$$\Phi_{0_{max}} - \Phi_0(0) \approx f_T V_{0T}\left[1 + \frac{\left(V_{TM} + f_0 V_{0T}\right)}{f_T V_{0T}} \frac{\ell}{2d}\right]^2$$

for $-f_0 V_{0T} \geq V_{TM} \geq -\left(\frac{2d}{\ell} f_T + f_0\right) V_{0T}$

and $V_{0T} \geq 0$ (53)

If V_{0T} is negative, there would be a maximum in electron potential in front of the target area for the values of V_{TM} listed in equation (54). This maximum is given by

$$\Phi_{T_{max}} - \Phi_T(0) \approx -f_0 V_{0T}\left[1 - \left(\frac{V_{TM} + f_0 V_{0T}}{f_0 V_{0T}}\right)\frac{\ell}{2d}\right]^2$$

for $\quad -f_0 V_{0T} \geq V_{TM} \geq f_0 V_{0T}\left(\frac{2d}{\ell} - 1\right)$

and $\quad V_{0T} \leq 0 \qquad\qquad (54)$

Equations (53) and (54) imply that if $\frac{d}{\ell}$ is large, there is a large range of voltages in V_{TM}, where a maximum in electron potential occurs either in front of the oxide for V_{0T} positive, or in front of the target for V_{0T} negative. This maximum will prevent secondaries from leaving the region where it occurs, if its magnitude is greater than the energy of the secondaries. By modulating V_{0T}, we can modulate the size of this potential maximum and thus modulate the number of secondaries which can escape to the mesh M1. An estimate of the currents flowing between target and M1 and oxide and M1 can be made with the help of Figure 38 and equations (53) and (54) for the magnitudes of the potential maxima.

Let us assume that a beam current I_B arrives at the mesh M1 with a landing voltage V_{MK}. Of this, $f_M I_B$ will strike M1 where the secondary emission coefficient is δ_{MK}. $(1 - f_M) f_T I_B$ will strike the target area where the secondary emission coefficient is δ_{TK}, and $(1 - f_M) f_0 I_B$ will strike the oxide, where the secondary emission coefficient is δ_{0K}. Let the mean spread in energies of the secondaries generated from the three regions be $\overline{V}_M$, $\overline{V}_T$ and $\overline{V}_0$. We may then estimate that the following currents will flow as a function of V_{0T} and V_{TM}.

For $V_{0T} \geq 0$

a) $$\frac{I_{TM}}{I_B} \approx (1 - f_M) f_T (1 - \delta_{TK}) + f_M f_T \delta_{MK} \exp \frac{V_{TM}}{\overline{V}_M}$$

for $\quad -V_{MK} \leq V_{TM} \leq 0$

b) $$\frac{I_{TM}}{I_B} \approx (1 - f_M) f_T \left(1 - \delta_{TK} \exp \frac{-V_{TM}}{\overline{V}_T}\right) + f_M f_T \delta_{MK}$$

for $V_{TM} \geq 0$

c) $$\frac{I_{0M}}{I_B} \approx (1 - f_M) f_0 (1 - \delta_{0K}) + f_M f_0 \delta_{MK} \exp \left(\frac{V_{TM} + V_{0T}}{\overline{V}_M}\right)$$

for $-V_{MK} \leq (V_{TM} + V_{0T}) \leq -\left(\frac{2d}{\ell} - 1\right) f_T V_{0T}$

d) $$\frac{I_{0M}}{I_B} \approx (1 - f_M) f_0 \left\{1 - \delta_{0K} \exp \frac{-f_T V_{0T}}{\overline{V}_0} \left[1 + \left(\frac{V_{TM} + f_0 V_{0T}}{f_T V_{0T}}\right)\frac{\ell}{2d}\right]^2\right\}$$

$$+ f_M f_0 \delta_{MK} \exp \left(\frac{V_{TM} + V_{0T} - f_T V_{0T} \left[1 + \left(\frac{V_{TM} + f_0 V_{0T}}{f_T V_{0T}}\right)\frac{\ell}{2d}\right]^2}{\overline{V}_M}\right)$$

for $-\left(\frac{2d}{\ell} - 1\right) f_T V_{0T} \leq (V_{TM} + V_{0T}) \leq f_T V_{0T}$

e) $$\frac{I_{0M}}{I_B} \approx (1 - f_M) f_0 \left\{1 - \delta_{0K} \exp -\left(\frac{V_{TM} + V_{0T}}{\overline{V}_0}\right)\right\} + f_M f_0 \delta_{MK}$$

for $V_{TM} + V_{0T} \geq f_T V_{0T}$

Equations 55

For $V_{0T} \leq 0$

a) $$\frac{I_{TM}}{I_B} \approx (1 - f_M) f_T (1 - \delta_{TK}) + f_M f_T \delta_{MK} \exp \frac{V_{TM}}{\overline{V}_M}$$

for $-V_{MK} \leq V_{TM} \leq f_0 V_{0T} \left(\frac{2d}{\ell} - 1\right)$

b) $$\frac{I_{TM}}{I_B} \approx (1 - f_M) f_T \left\{ 1 - \delta_{TK} \exp \frac{f_0 V_{0T}}{\overline{V}_T} \left[1 - \left(\frac{V_{TM} + f_0 V_{0T}}{f_0 V_{0T}} \right) \frac{\ell}{2d} \right]^2 \right\}$$

$$+ f_M f_T \delta_{MK} \exp \frac{V_{TM} + f_0 V_{0T} \left[1 - \left(\frac{V_{TM} + f_0 V_{0T}}{f_0 V_{0T}} \right) \frac{\ell}{2d} \right]}{\overline{V}_M}$$

for $f_0 V_{0T} \left(\frac{2d}{\ell} - 1 \right) \leq V_{TM} \leq -f_0 V_{0T}$

c) $$\frac{I_{TM}}{I_B} \approx (1 - f_M) f_T \left\{ 1 - \delta_{TK} \exp \frac{-V_{TM}}{\overline{V}_T} \right\} + f_M f_T \delta_{MK}$$

for $V_{TM} \geq -f_0 V_{0T}$

d) $$\frac{I_{0M}}{I_B} \approx (1 - f_M) f_0 (1 - \delta_{0K}) + f_M f_0 \delta_{MK} \exp \left(\frac{V_{TM} + V_{0T}}{\overline{V}_M} \right)$$

for $-V_{MK} \leq V_{TM} + V_{0T} \leq 0$

e) $$\frac{I_{0M}}{I_B} \approx (1 - f_M) f_0 \left(1 - \delta_{0K} \exp\left(-\left(\frac{V_{TM} + V_{0T}}{\overline{V}_T}\right)\right)\right) + f_M f_0 \, \delta_{MK}$$

for $V_{TM} + V_{0T} \geq 0$

Equations 56

Clearly, these equations are only estimates, since the potentials will in practice change in a continuous manner as we go across a plane from a region in front of the Pd_2Si to a region in front of the SiO_2. Also they do not take into account any redistribution effects, which will certainly exist if we are in a condition such as Figure 39c, where all secondaries passing across the plane ℓ cannot make it to the mesh. Finally we have added the mesh (M1) electrons in an ad hoc way. Nonetheless they can serve as guidelines for our discussion. They should be qualitatively correct.

Curves of I_{TM}/I_B and I_{0M}/I_B are plotted in Figure 40 a and b as a function of $V_{TM}/\overline{V}$ for constant values of $V_{0T}/\overline{V}$ on the basis of equations (55) and (56), assuming the following constants.

$$\overline{V}_M \approx \overline{V}_T \approx \overline{V}_0 \approx \overline{V}, \quad \frac{\ell}{2d} << 1$$

$$f_M = 0.5 \qquad f_0 = 0.33 \qquad f_T = 0.67$$

$$\delta_{MK} = 1.0 \qquad \delta_{TK} = 1.1 \qquad \delta_{0K} = 3$$

The information contained in Figure 40 a and b can be plotted in a number of different ways, making use of the fact that

$$V_{TM} = V_{0M} - V_{0T} \tag{57}$$

Thus Figures 41 and 42 show curves of $\frac{I_{0M}}{I_B}$ vs. $\frac{V_{0T}}{\overline{V}}$ for constant values of $\frac{V_{TM}}{\overline{V}}$ and $\frac{V_{0M}}{\overline{V}}$ respectively, while Figures 43 and 44 show curves of $\frac{I_{0M}}{I_B}$ and $\frac{I_{TM}}{I_B}$ vs. $\frac{V_{TM}}{\overline{V}}$ for constant values of $\frac{V_{0M}}{\overline{V}}$. The latter two curves are

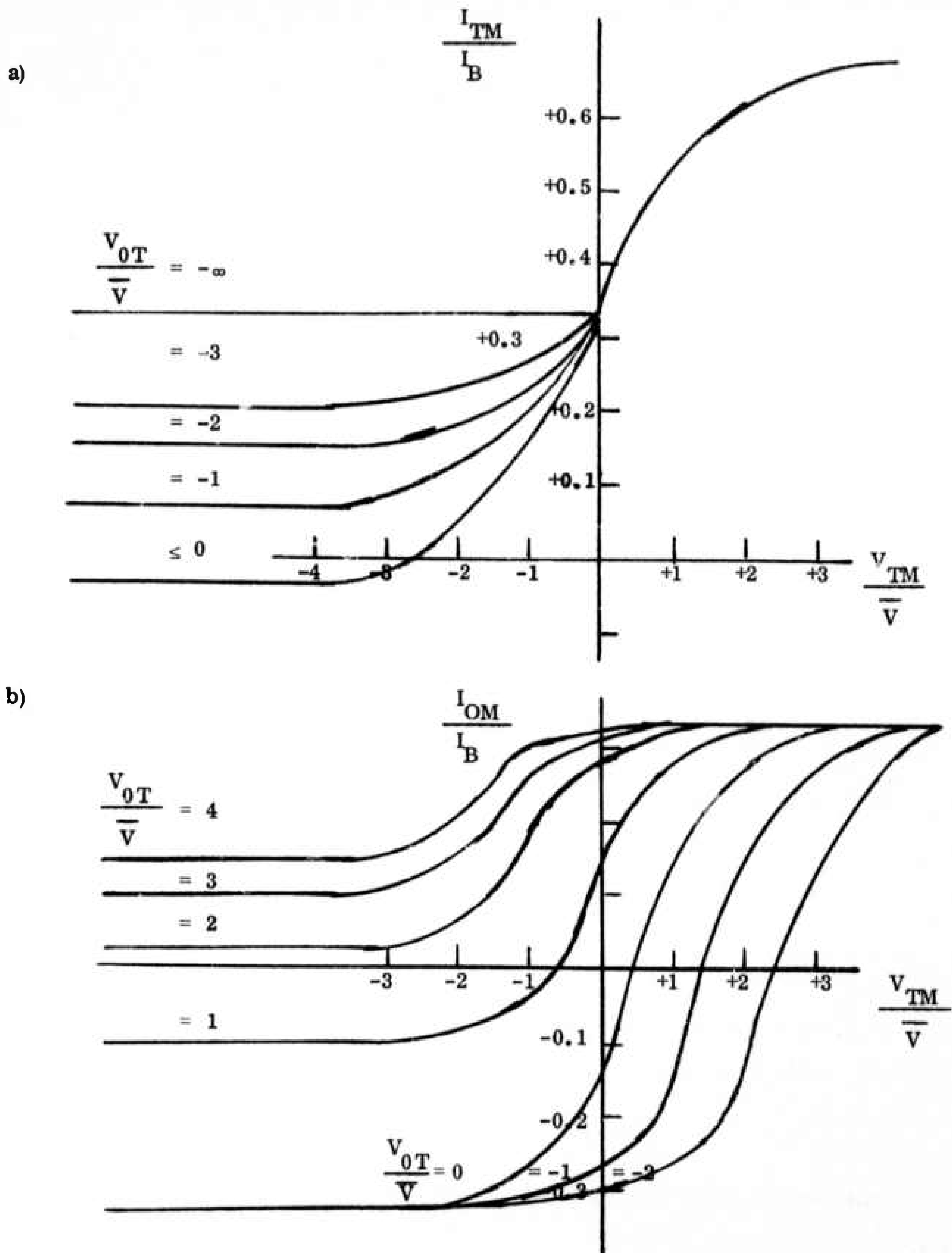

Figure 40

a) $\frac{I_{TM}}{I_B}$ vs. $\frac{V_{TM}}{\bar{V}}$ for Constant Values of $\frac{V_{0T}}{\bar{V}}$.

b) $\frac{I_{OM}}{I_B}$ vs. $\frac{V_{TM}}{\bar{V}}$ for Constant Values of $\frac{V_{0T}}{\bar{V}}$.

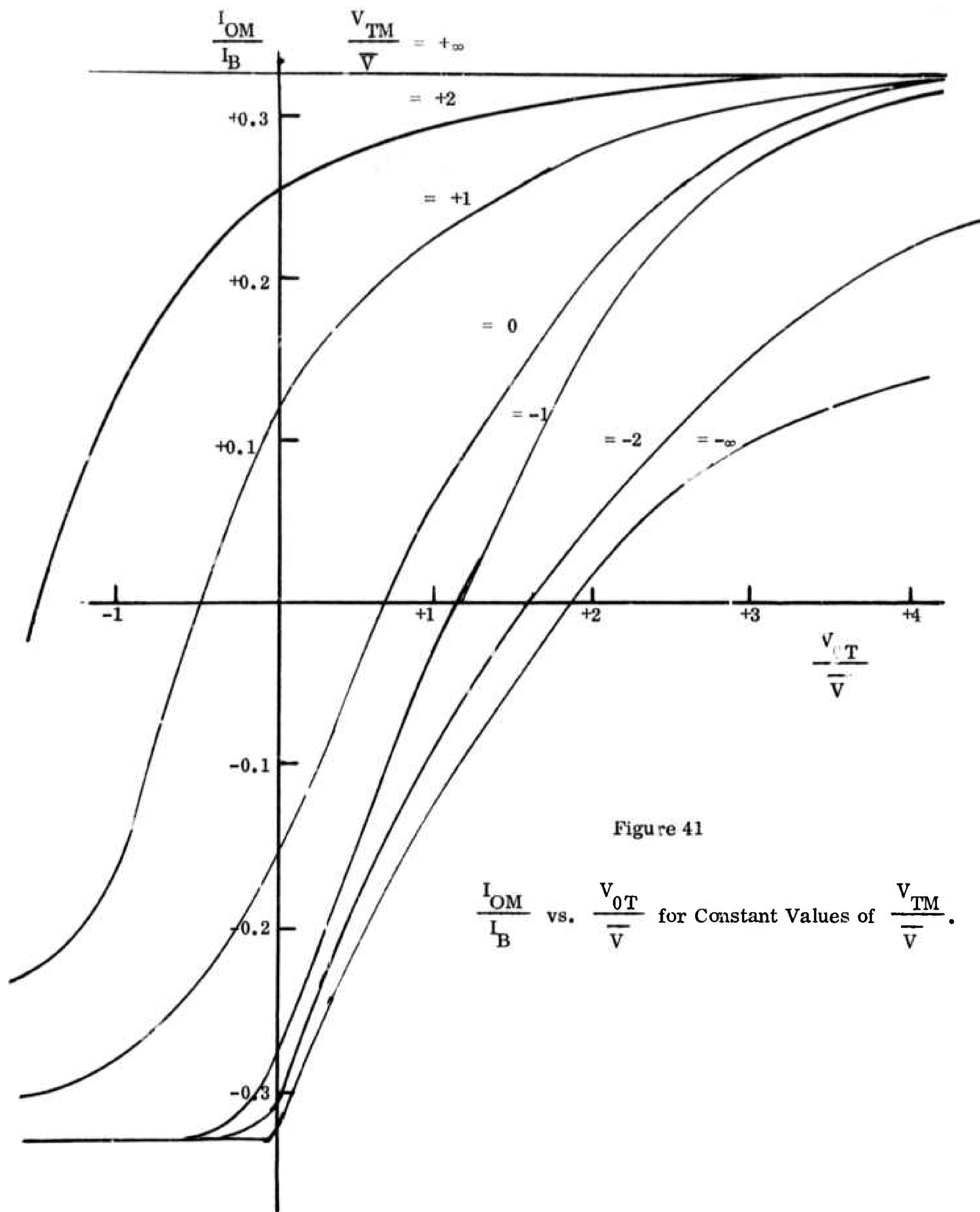

Figure 41

$\frac{I_{OM}}{I_B}$ vs. $\frac{V_{0T}}{\overline{V}}$ for Constant Values of $\frac{V_{TM}}{\overline{V}}$.

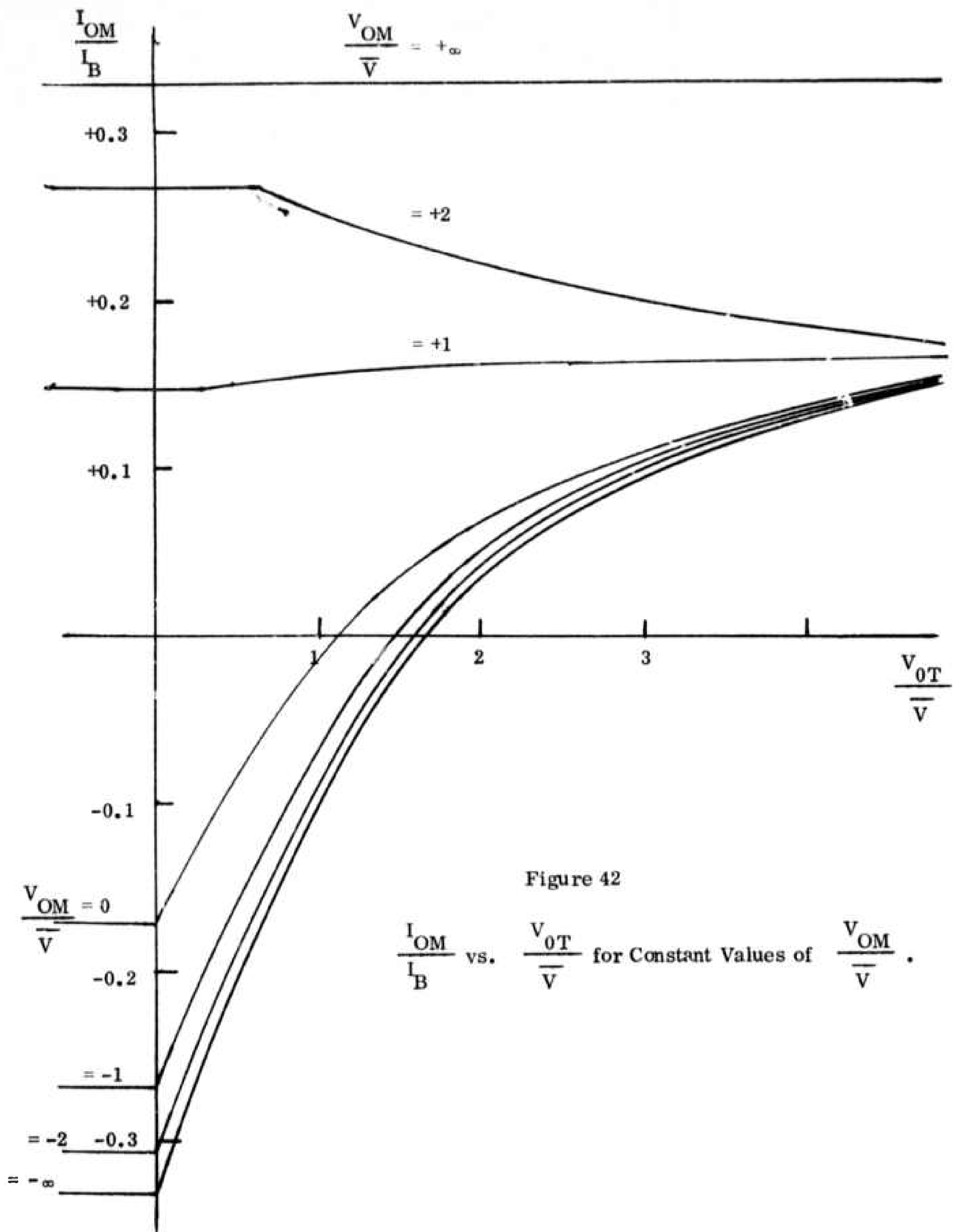

Figure 42

$\frac{I_{OM}}{I_B}$ vs. $\frac{V_{0T}}{\overline{V}}$ for Constant Values of $\frac{V_{OM}}{\overline{V}}$.

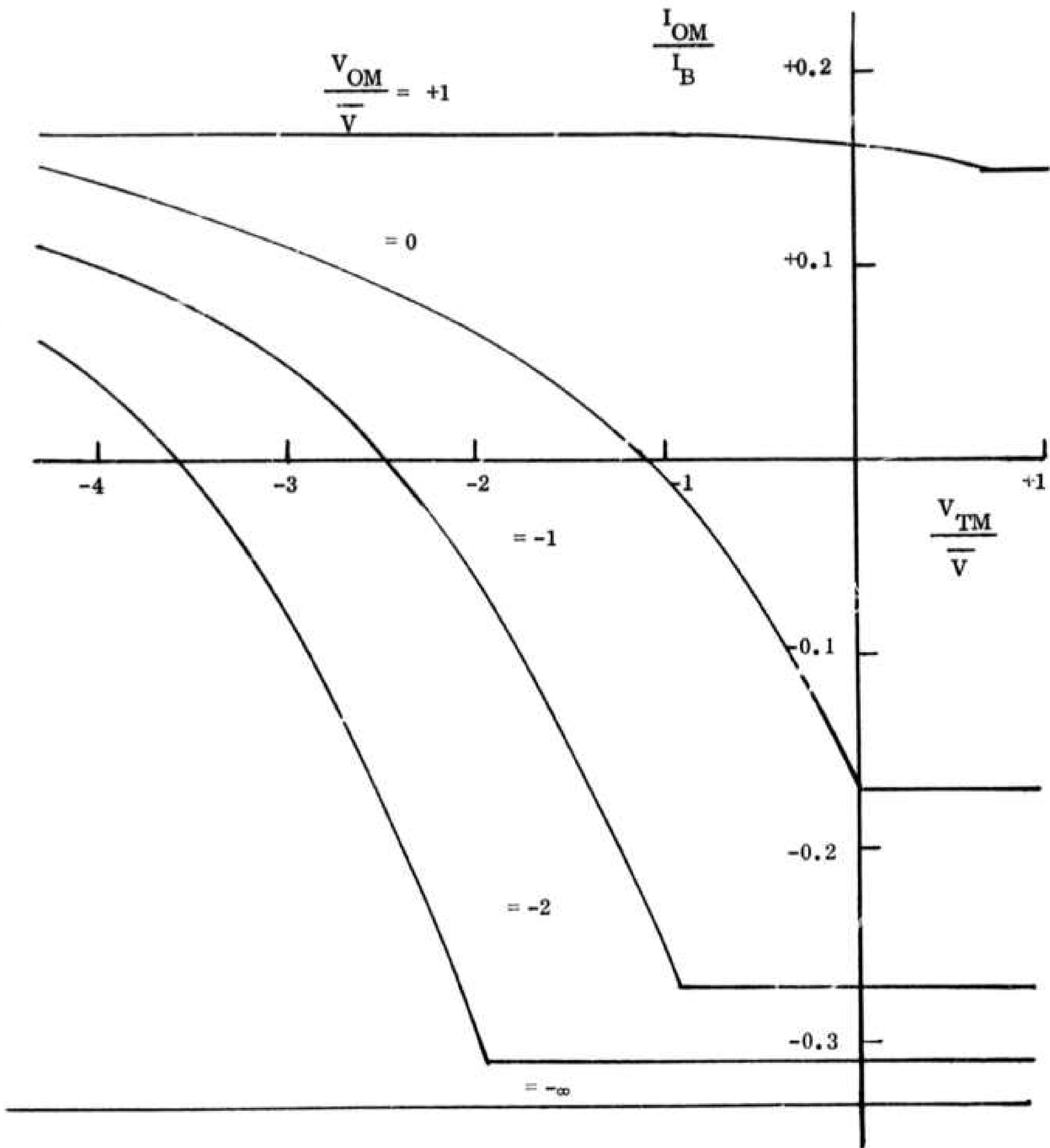

Figure 43. $\frac{I_{OM}}{I_B}$ vs. $\frac{V_{TM}}{\overline{V}}$ for Constant Values of $\frac{V_{OM}}{\overline{V}}$.

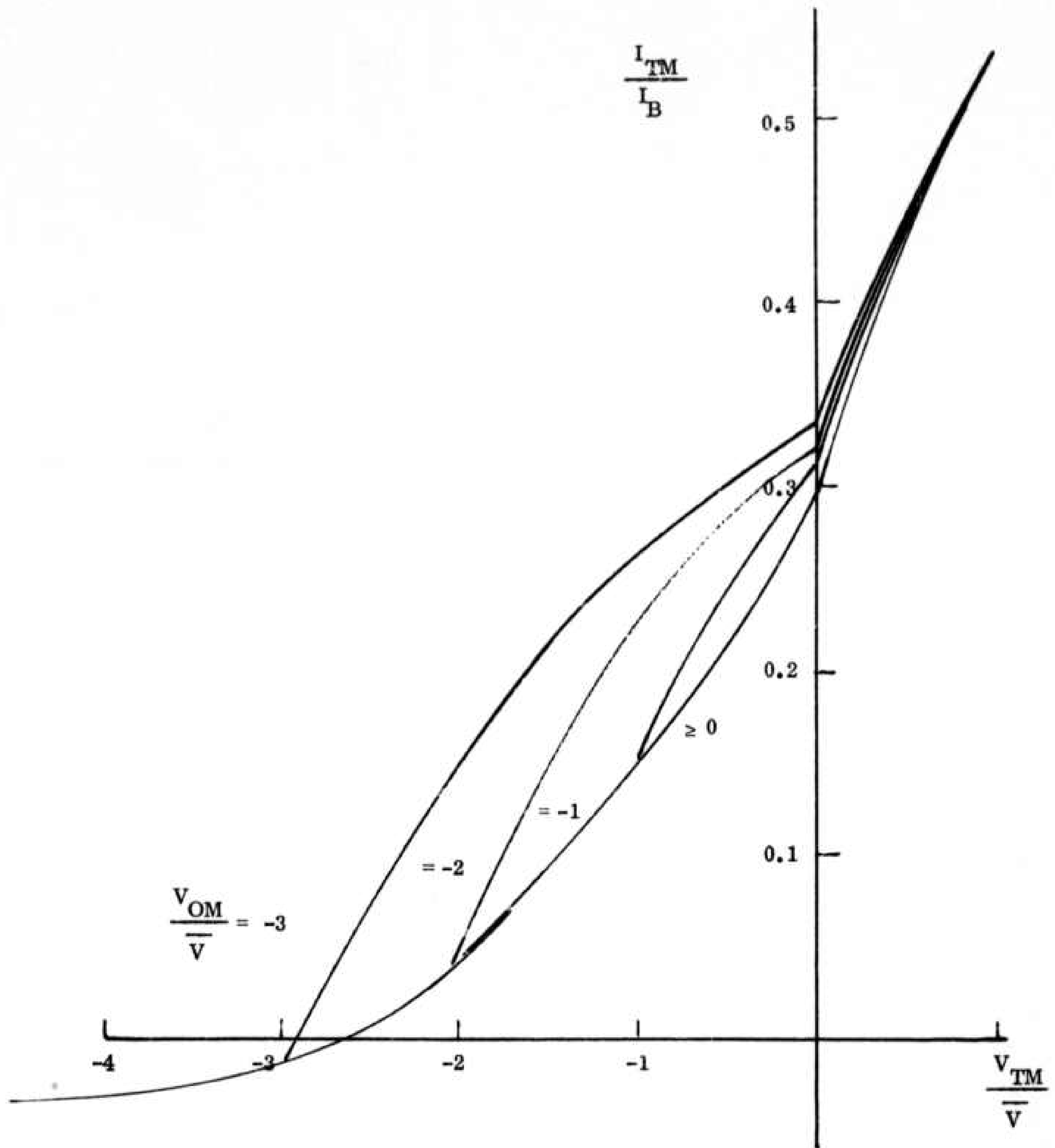

Figure 44. $\frac{I_{TM}}{I_B}$ vs. $\frac{V_{TM}}{\overline{V}}$ for Constant Values of $\frac{V_{OM}}{\overline{V}}$.

particularly significant, since we are postulating that the oxide floats to some average potential and does not deviate significantly from that over the frame time. Finally, Figure 45 shows curves of

$$\frac{I_{0M} + I_{TM}}{I_B} \quad \text{vs.} \quad \frac{V_{TM}}{\overline{V}} \quad \text{for constant values of} \quad \frac{V_{0M}}{\overline{V}} .$$

These curves are the current we would measure coming out of the mesh loop as a function of $\frac{V_{TM}}{\overline{V}}$, if we hold $\frac{V_{0M}}{\overline{V}}$ equal to a constant. It is clear that in the fourth quadrant where secondary emission occurs the behavior is drastically different depending on whether V_{TM} is greater or less than V_{0M}. At this point the oxide to target voltage changes sign. To the left of this point, we are predominantly modulating the secondaries leaving the oxide when we change V_{TM}, while to the right of this point, we are modulating the number of secondaries entering or leaving the target when we change V_{TM}.

The concepts of an oxide surface acting as an equipotential as described in the above implies that V_{0T} is on the average positive. Otherwise, the carriers would tend to leak off the oxide to the metal during the entire frame time, causing the oxide surface to return to a nonconducting state. We have nonetheless added in the curves where V_{0T} is negative for completeness. They could apply, for example, to systems where we have a metal mesh integrated onto the top of the oxide, and an external bias controlling the voltage between the two surfaces.

Before proceeding to where we bias ourselves on these curves in practice, and how they relate to imaging, we would like to recapitulate, that we have actually not assumed very much up to this point. The rather complex curves of Figures 40 to 45 are a natural consequence of having isolation between the oxide and target surface, so that a voltage V_{0T} can exist between them. This voltage will control the net secondary emission.

iii. <u>I-V Curves between Target and Oxide</u>

In order to determine where the oxide floats, and therefore where we bias ourselves on the preceding curves, we must know something about the I-V relation

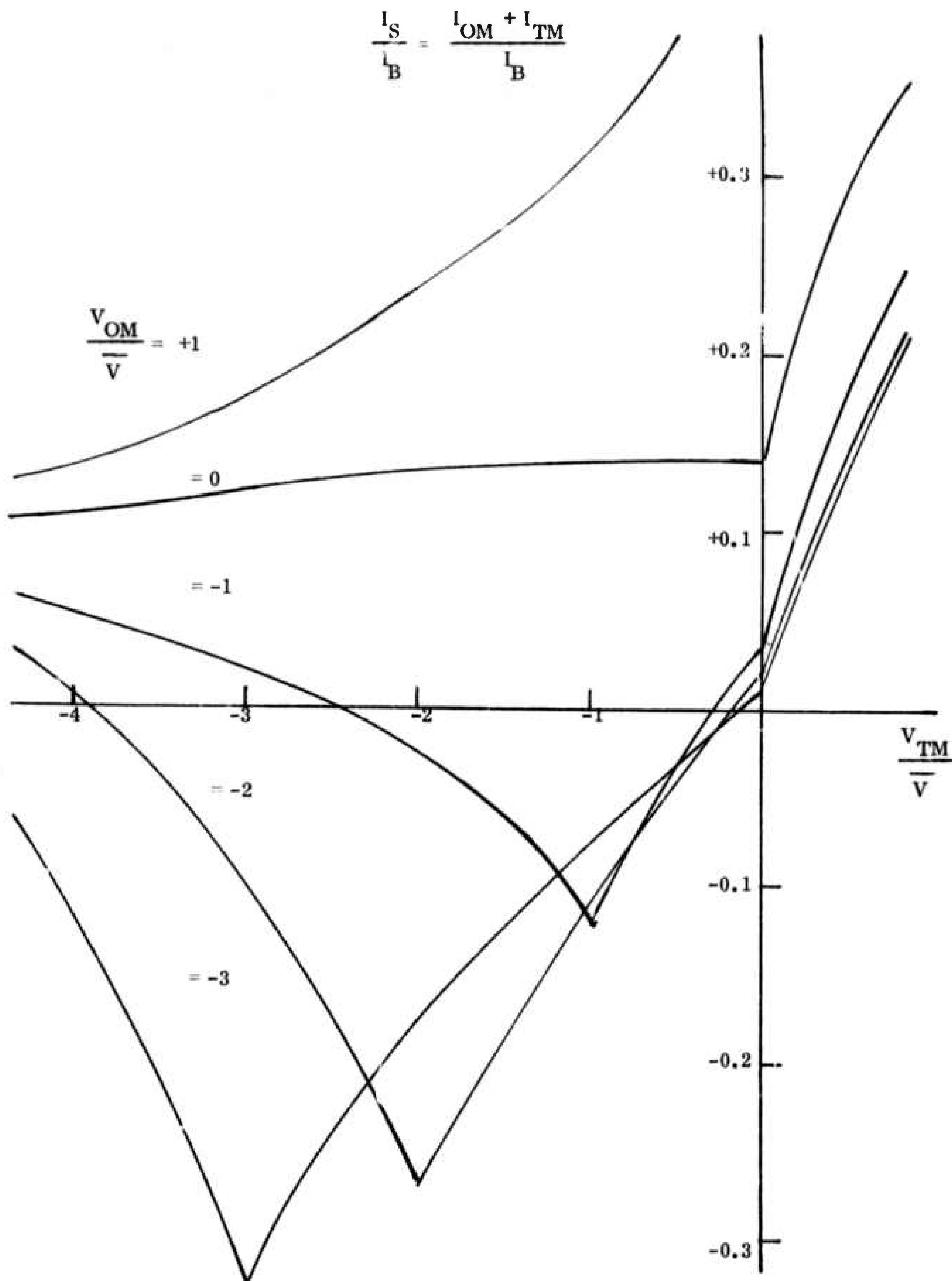

Figure 45. $\frac{I_S}{I_B} = \frac{I_{OM} + I_{TM}}{I_B}$ vs. $\frac{V_{TM}}{\overline{V}}$ for Constant Values of $\frac{V_{OM}}{\overline{V}}$.

between target and oxide under the influence of the beam. Here we can make a number of different assumptions. We will test two rather drastically different ones in order to show that the detailed nature of this assumption does not affect the qualitative results concerning the imaging properties.

First, we will assume that no current can cross this Pd_2Si to oxide boundary under the influence of the beam. Then since the oxide surface must be in a cyclic state, there can be no net current off the oxide surface during the frame time, so that the average value of I_{0M} must be zero. Referring to Figure 40b, this means that for the numbers used above, the average value of $\frac{V_{0T}}{\bar{V}}$ must be positive when $\frac{V_{TM}}{\bar{V}}$ is negative. Since $\frac{I_{TM}}{I_B}$ in Figure 40a does not show any significant dependence on $\frac{V_{0T}}{\bar{V}}$ when $\frac{V_{TM}}{\bar{V}}$ is positive, $\frac{I_{TM}}{I_B}$ would then be given by the bottom curves of Figure 40a. This is reproduced in Figure 46. In this case, this is the average current that we would measure coming off the retina as a function of V_{TM}. It is only a property of the Pd_2Si secondary emission curve, and not a property of the oxide secondary emission curve. As we will show in the section on imaging, however, the oxide properties will show up in non-uniformly illuminated retinas, even though no current can cross this boundary.

We have measured many experimental curves of the average signal current, $\langle I_S \rangle$, out of the silicon vs. V_{SM}. It would appear from this data that the assumption that no current can cross the oxide to target boundary is not a valid one. For $\frac{V_{TM}}{\bar{V}}$ very negative, the signal current would go negative, only for the secondary emission coefficient of the Pd_2Si greater than unity, if no current can cross the target to oxide boundary. The δ curve for Pd goes through unity for the cathode to target voltage V_{KT}, equal to 120 volts. For Si, the δ curve crosses unity for

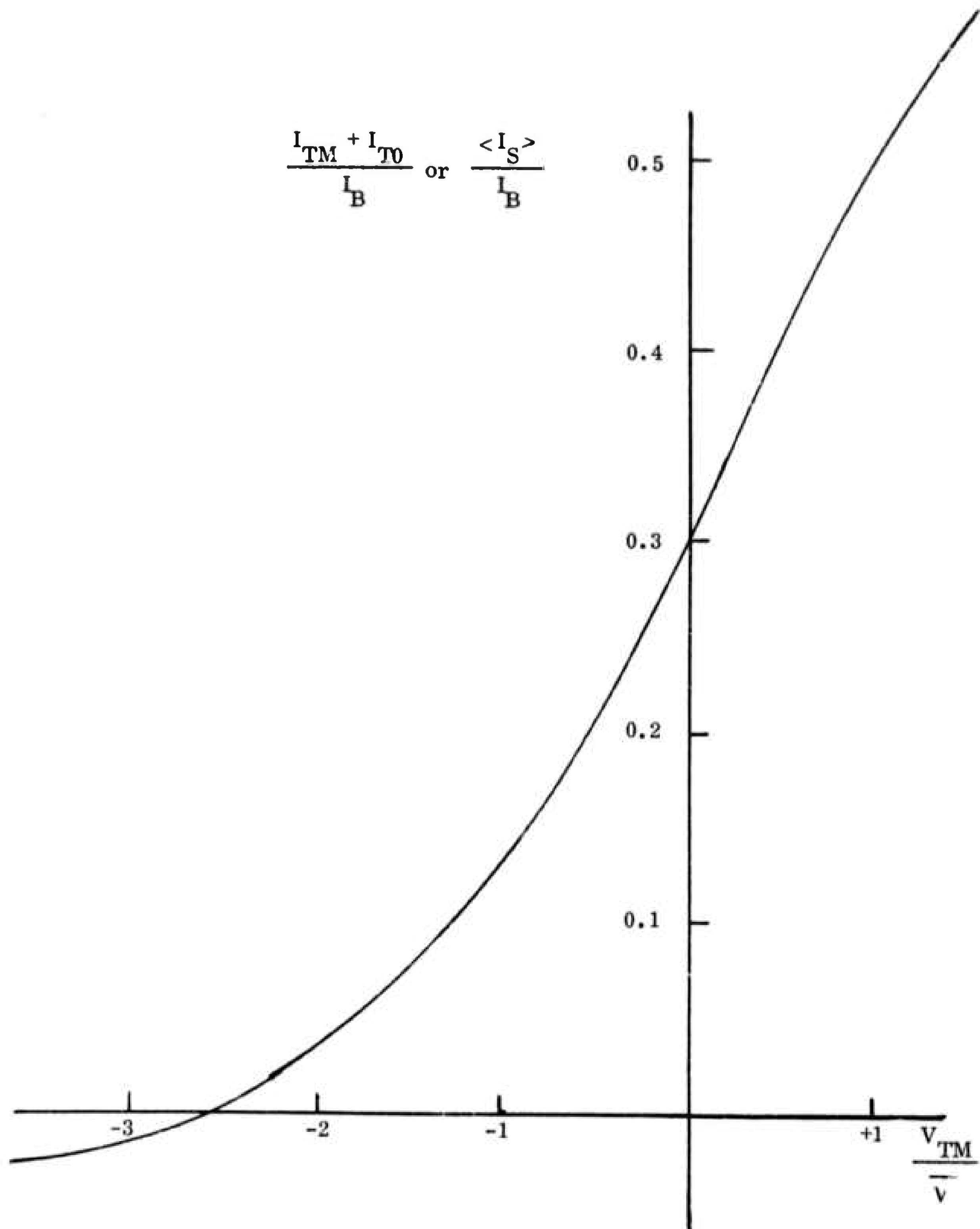

Figure 46

Average Signal Current $\frac{<I_S>}{I_B}$ vs. $\frac{V_{TM}}{\bar{V}}$ Assuming $I_{T0} = 0$.

This Curve also describes $\frac{I_{TM} + I_{T0}}{I_B}$ for any Particular Diode.

landing voltages ≈ 100 volts, while for SiO_2, it crosses unity between 30 and 50 volts. We have seen net secondary emission off the composite surface, or average signal currents which are negative, for landing voltages as low as 30 volts. We thus infer this to be D.C. conduction of electrons off the oxide surface into vacuum. If electrons cannot pass directly through the oxide from the Si, this implies that electrons must flow from the Pd_2Si to the oxide surface. Finally, we see a temperature dependence to the average secondary emission curves off the composite surface. This can be most easily and naturally explained in terms of a temperature dependence of the current which can cross this boundary.

With these experimental facts in mind, we choose as our second assumption, that the current which can flow from target to oxide under the influence of the beam is given by

$$\frac{I_{T0}}{I_B} = \frac{\left(I_{T0}\right)_S}{I_B}\left(\exp \frac{-q\left(V_{0T} - V_{0T_0}\right)}{k\,T_B} - 1\right) \tag{58}$$

This is a logical consequence of Figure 39a, if more electrons can enter the metal from the oxide than vice-versa, when V_{0T} is zero. The current flowing is then a standard diode curve, where q is the electronic charge, k is Boltzman's constant, T_B is the effective electron temperature in the oxide under the influence of the beam, I_{T0_S} is the maximum current that can flow over the barrier from the metal when V_{0T} is very positive, and V_{0T_0} is the built in voltage necessary to give no net current across the boundary. I_{T0_S} should be a property of the metal only and is probably not very temperature sensitive since electron-electron scattering probably determines its value. T_B on the other hand is determined by how fast the hot electrons can decay to the bottom of the conduction band in the oxide and is probably controlled by phonon scattering. It therefore seems likely that T_B will be larger at lower temperatures than at higher temperatures. This, in turn, implies that V_{0T_0} would be somewhat larger at lower temperatures. Figure 47 therefore gives a qualitative plot of $\frac{V_{0T}}{V}$ as we envision it, at room temperature and at nitrogen temperature.

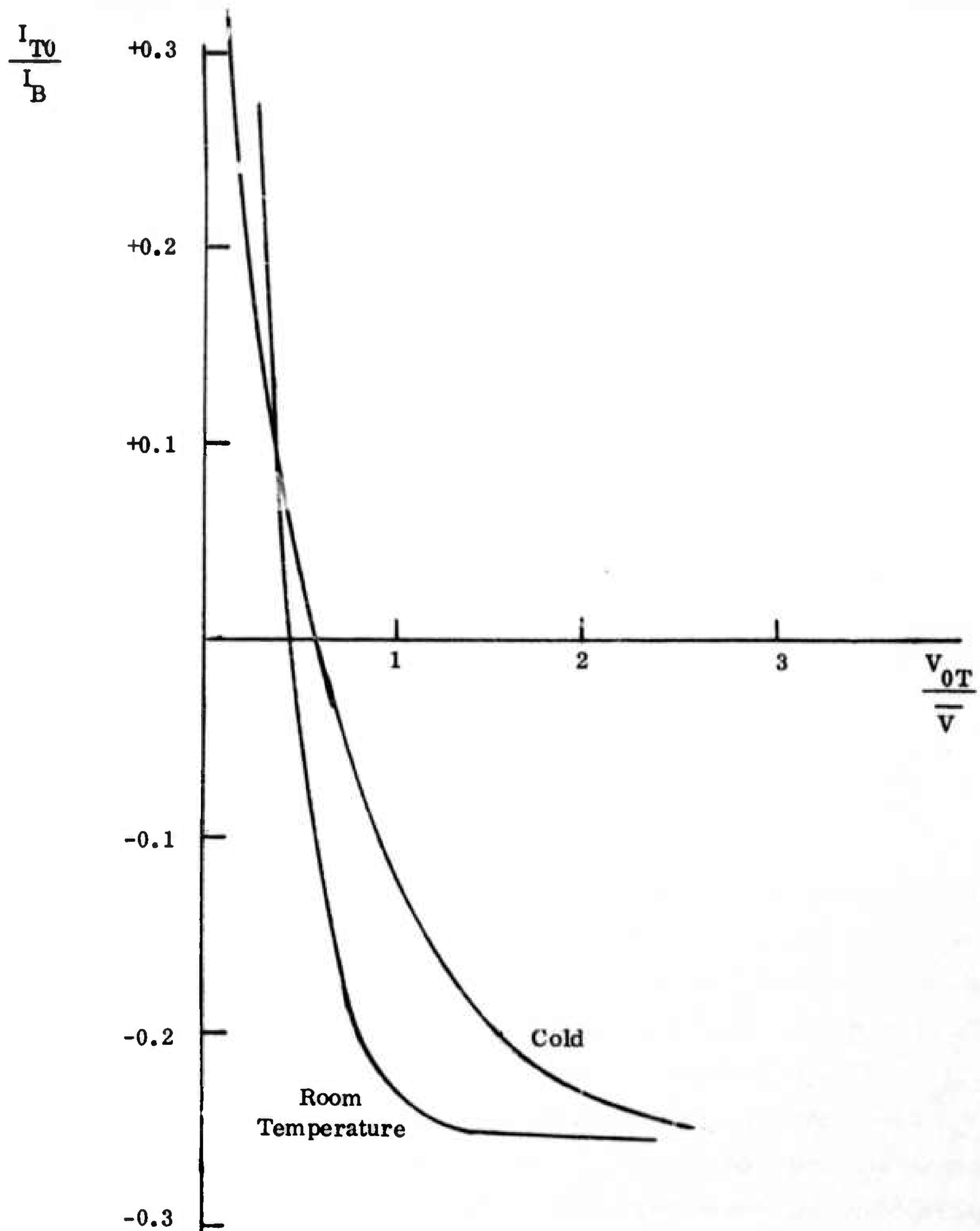

Figure 47

$\frac{I_{T0}}{I_B}$ vs. $\frac{V_{0T}}{\overline{V}}$ **Assuming a Relationship of the Form of Equation (58).**

If we are in a steady state and all diodes are uniformly illuminated, then the average value of I_{T0} must equal the average value of I_{0M}. By comparing Figures 41 and 47 we may then draw up the average value of I_{0M} vs. V_{TM}, both warm and cold. This is plotted in Figure 48. Since V_{0T} is always positive, under the assumptions of equation (58), Figure 48 may be added to the bottom curve of Figure 40a to obtain the average signal current as a function of the average value of V_{TM}. This is shown in Figure 49. These curves qualitatively resemble all of the experimental data that we have ever seen when we take into account the effects of the diode. For example, these curves may be compared with the experimental curves in Figure 50, where the effects of the diode impedance have been removed by flooding the retina with light thus forward biasing the diodes. In this case, V_{TM} may be directly compared with V_{SM} since any voltage drops across the diodes are small. Many such experimental curves have been taken, under varying conditions. They all have in common that the cold and warm curves cross at some value of $\frac{V_{SM}}{V}$. On either side of this crossover, the cold curves show a smaller absolute value of current than the warm curves. The cold curves cross through zero signal current at more negative values of V_{SM} than the warm curves. For V_{SM} very positive, the cold and warm curves both level off to about unity, while for V_{SM} negative, the cold curves saturate to a significantly lower value of secondary emission than the warm curves. All of these same things occur for the theory, if equation (58) is assumed as the type of relation for I_{T0} vs. V_{0T}, and T_B is taken as larger at the lower temperatures. We therefore assume that equation (58) is probably a reasonable description of the facts.

iv. <u>I-V Relations of the Photodiodes</u>

Finally, in order to determine the measured I-V curves between Si and mesh, we need the I-V relation of the photodiodes. Thus we assume that

$$I_{ST} = \frac{t_f}{t_R} \left[i_{CO}\left(\exp \frac{q V_{ST}}{kT} - 1 \right) - RH \right] \qquad (59)$$

for $V_{ST} \geq -V_B$

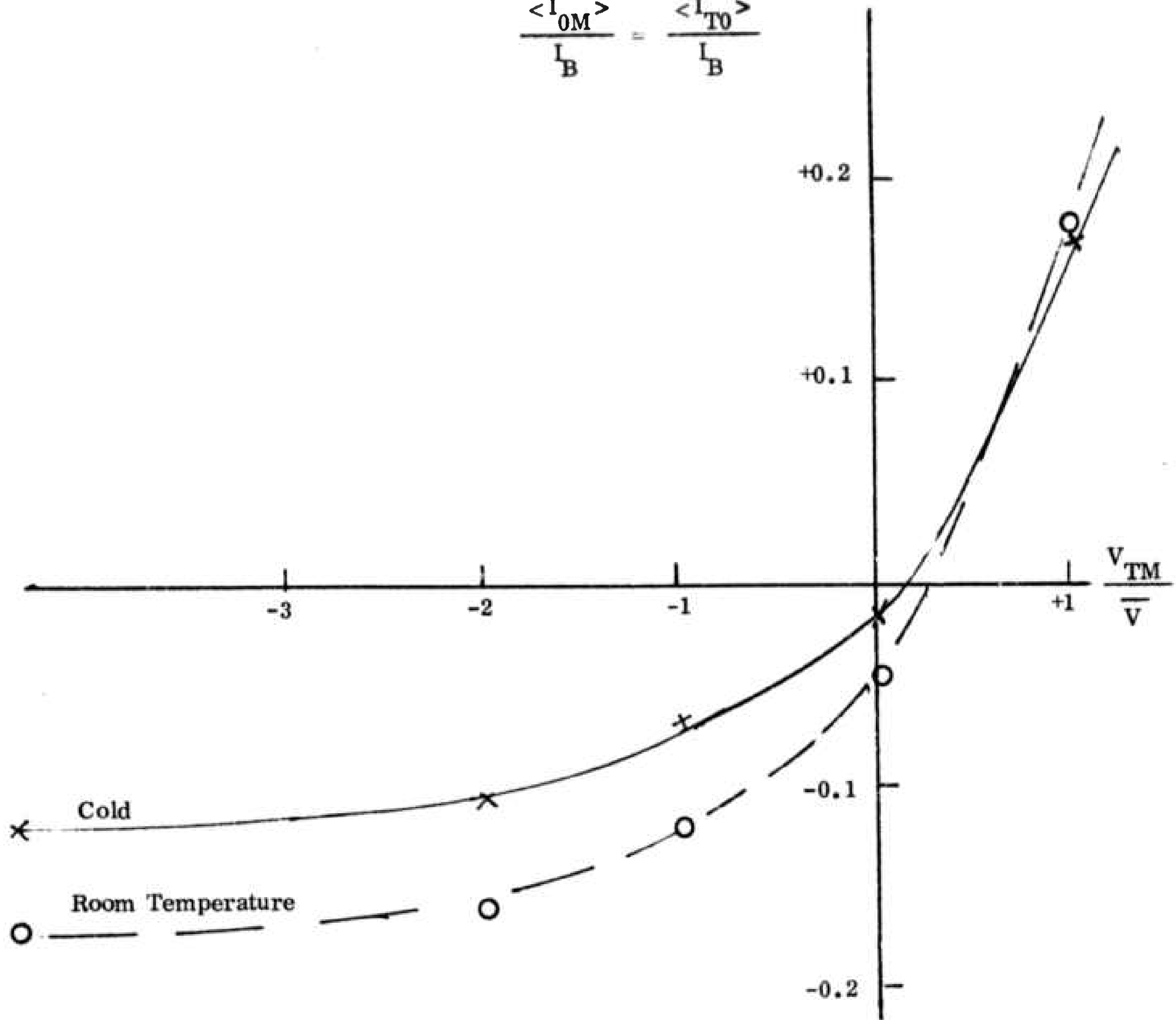

Figure 48

Average Current Off the Oxide vs. $\frac{V_{TM}}{\overline{V}}$, Assuming that I_{T0} follows Equation (58).

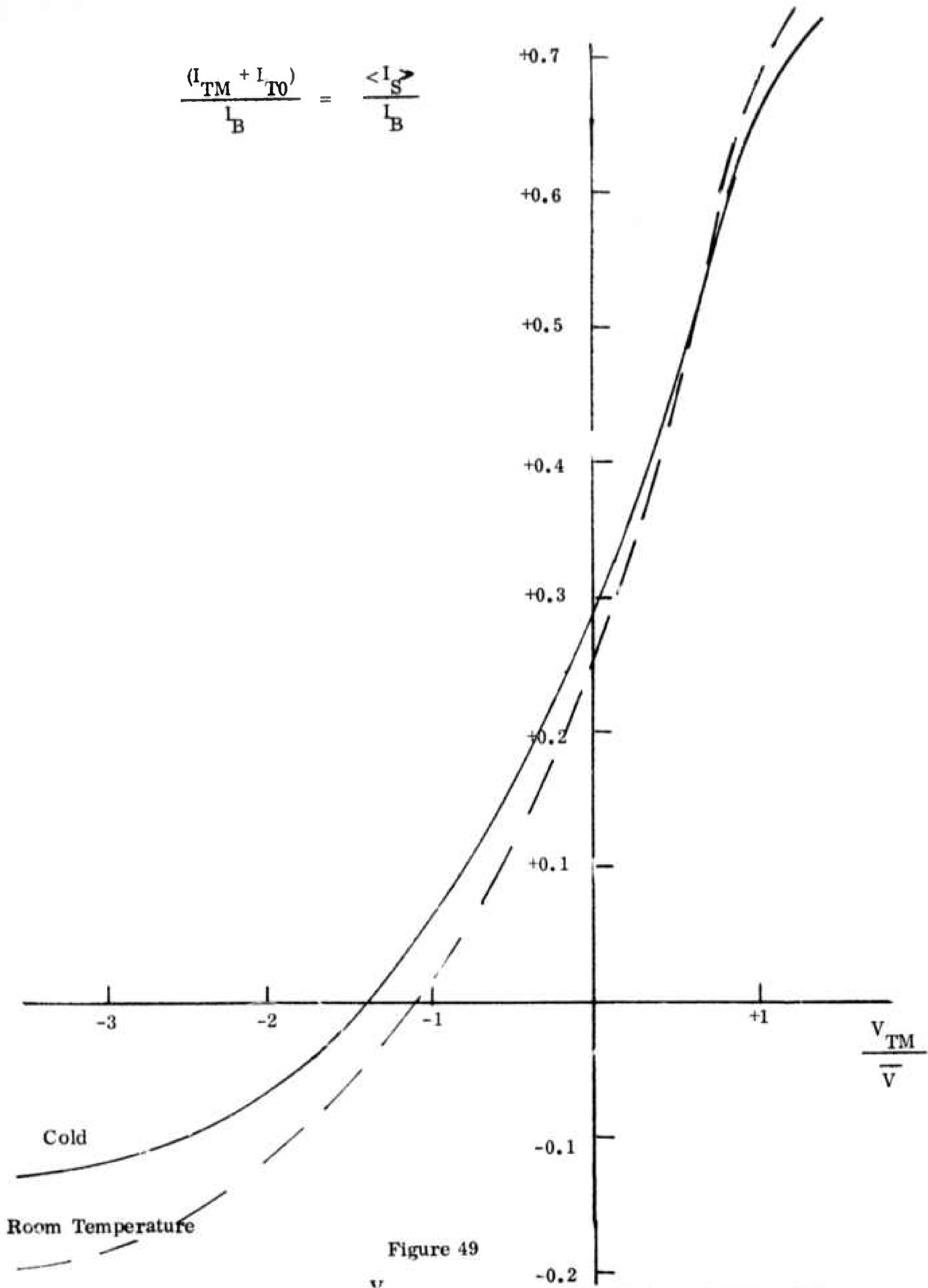

Figure 49

Average Signal Current vs. $\frac{V_{TM}}{\overline{V}}$ Assuming that I_{T0} follows Equation (58).

This Curve also describes $(I_{TM} + I_{T0})/I_B$ for any Particular Diode.

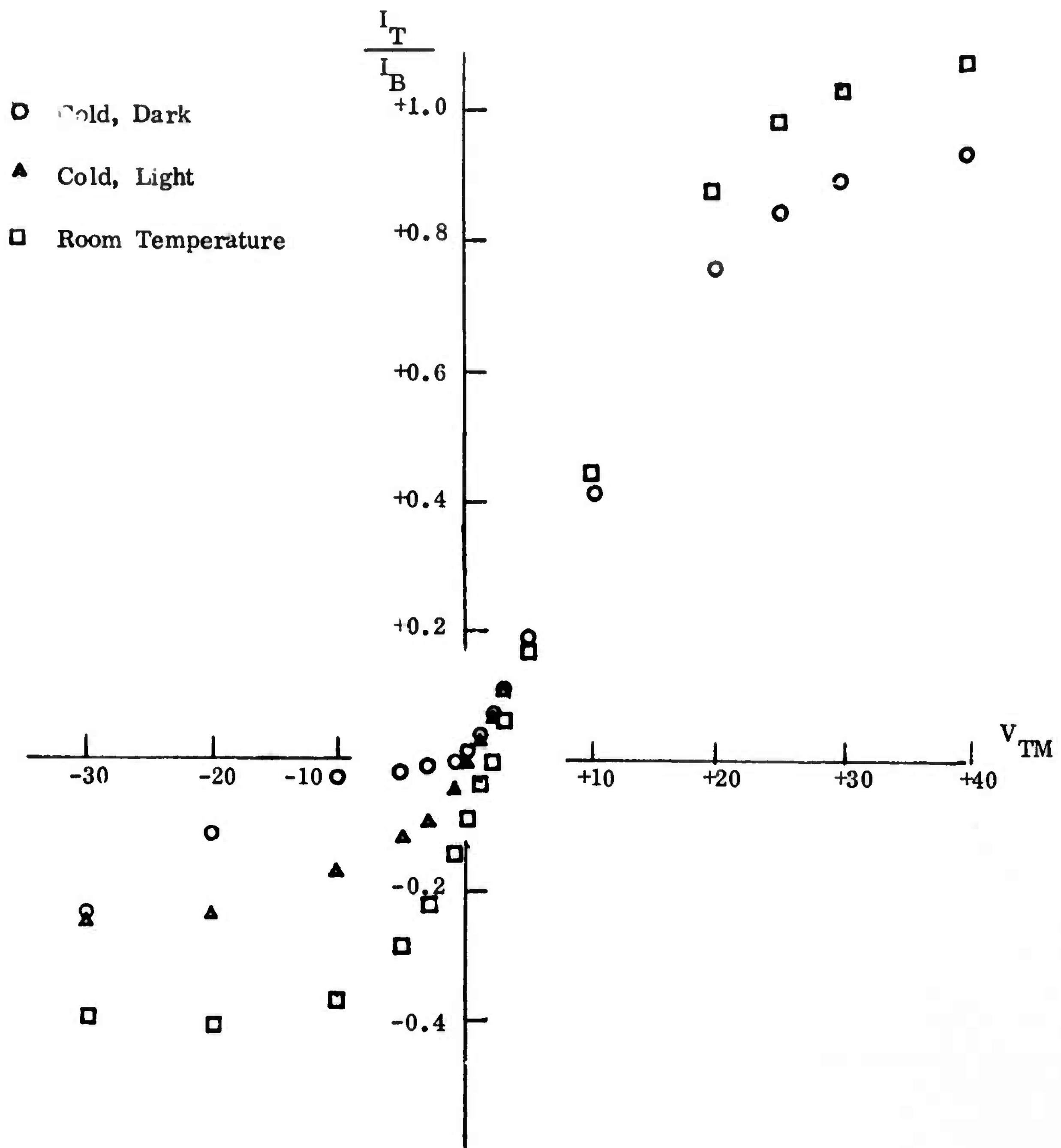

Figure 50

Experimental Data of $< I_S >$ vs. V_{TM} at Room Temperature and Cold, in the Light and in the Dark.

where t_f and t_R are the frame and read times respectively, i_{CO} is the saturation current of the diode, R is the retina responsivity and H is the radiance. Here V_B is the breakdown voltage of the diode. For $V_{ST} \leq -V_B$, it is assumed that $\frac{dI_{ST}}{dV_{ST}}$ is very large and positive. V_S is related to V_{TM} by

$$V_{ST} = V_{SM} - V_{TM} \tag{60}$$

where V_{SM} is the applied bias between Si and mesh. Thus equation (59) may be combined with (60) to give

$$I_{ST} = \frac{t_f}{t_R}\left[i_{CO}\left(\exp\frac{q(V_{SM} - V_{TM})}{kT} - 1\right) - RH\right] \tag{61}$$

$$\text{for } V_{SM} - V_{TM} \geq -V_B$$

The average value of I_{ST} must equal the average value of the signal current. Thus equation (61) may be superimposed on Figure 46 or 49 for the average signal current to determine the value of V_{TM} as a function of RH, and V_{SM}. A superposition of equation (61) and Figure 46 is thus shown in Figure 51 a and b for two different values of V_{SM}. It is clear that qualitatively similar results would occur by superimposing equation (61) with Figure 49. Let $(V_C/\overline{V})$ be the value of $\frac{V_{TM}}{\overline{V}}$ where the signal current crosses zero. Then if $\left(\frac{V_{SM} - V_C}{\overline{V}}\right)$ is less than $\frac{V_B}{\overline{V}}$, the average signal current will gradually increase with increasing light level, saturating at $0.032\ I_B$ for the case shown in Figure 51a. For $\frac{V_{SM} - V_C}{\overline{V}}$ large compared to $\frac{V_B}{\overline{V}}$, the diodes will look as shown in Figure 51b. Thus $\frac{V_{TM}}{\overline{V}}$ will equal $\frac{V_{SM}}{\overline{V}}$ for light levels such that $\frac{t_f}{t_R}\left(\frac{RH + i_{CO}}{I_B}\right) \geq 0.033$, while $\frac{V_{TM}}{\overline{V}}$ will equal $\frac{V_{SM} - V_B}{\overline{V}}$ for light levels such that $\frac{t_f}{t_R}\left(\frac{RH + i_{CO}}{I_B}\right) \leq 0.033$. An experimental dark curve of $< \frac{I_S}{I_B} >$ vs. V_{SM} is shown in Figure 50, along with the curve $\frac{I_{SM}}{I_B}$ in a strong light. As theory predicts, the current increases to more

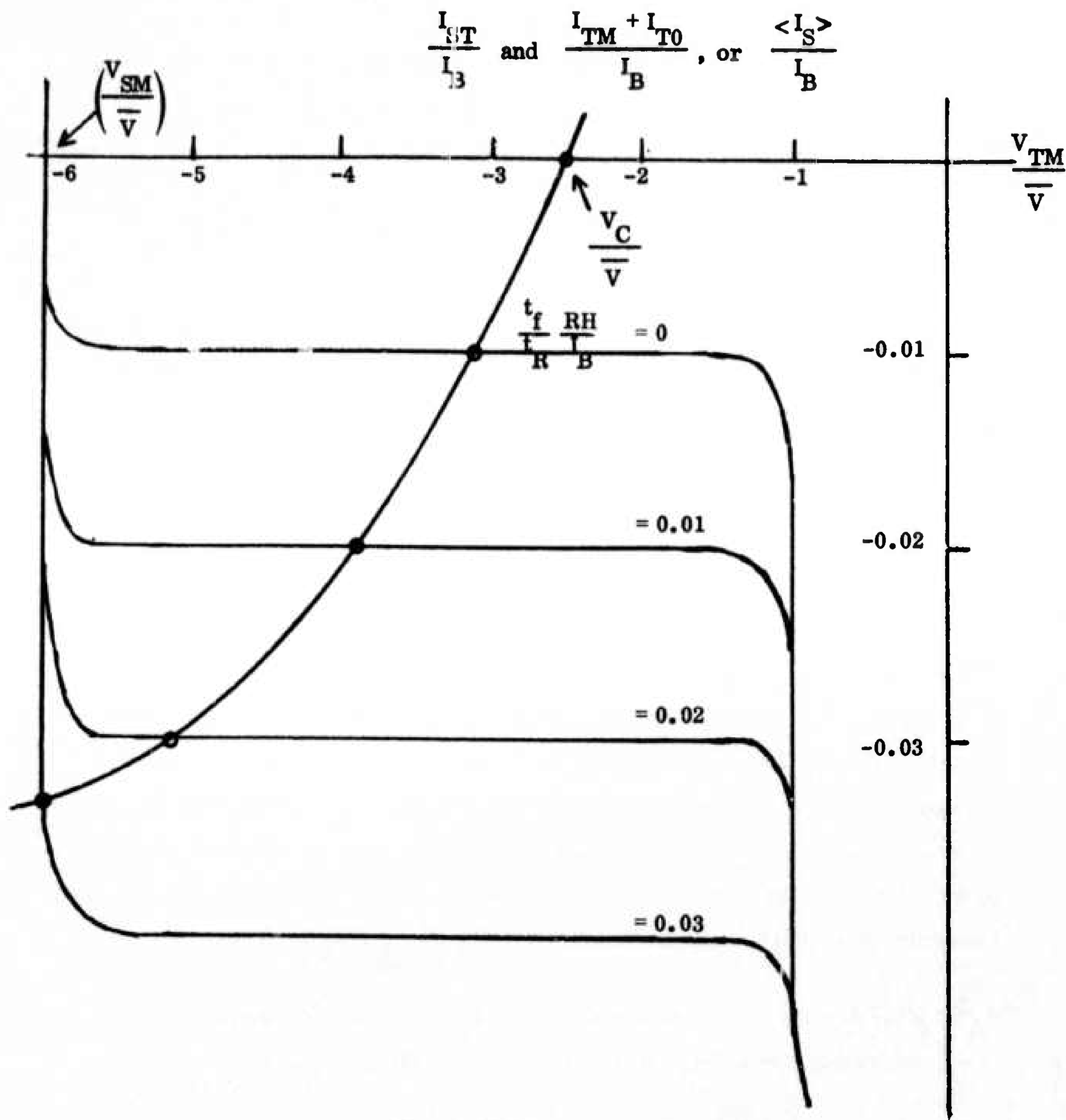

Figure 51 (a)

$\frac{I_{ST}}{I_B}$ as a Function of Light Level Superimposed on $\frac{I_{TM} + I_{T0}}{I_B}$ or $\frac{<I_S>}{I_B}$ vs. $\frac{V_{TM}}{\overline{V}}$. These curves assume $\frac{V_{SM}}{\overline{V}} = -6$, $\frac{V_B}{\overline{V}} = +5$ and $\frac{I_{T0}}{I_B} \equiv 0$. The circles give $\frac{V_{TM}}{\overline{V}}$ vs. $\frac{t_f}{t_R} \frac{RH}{I_B}$.

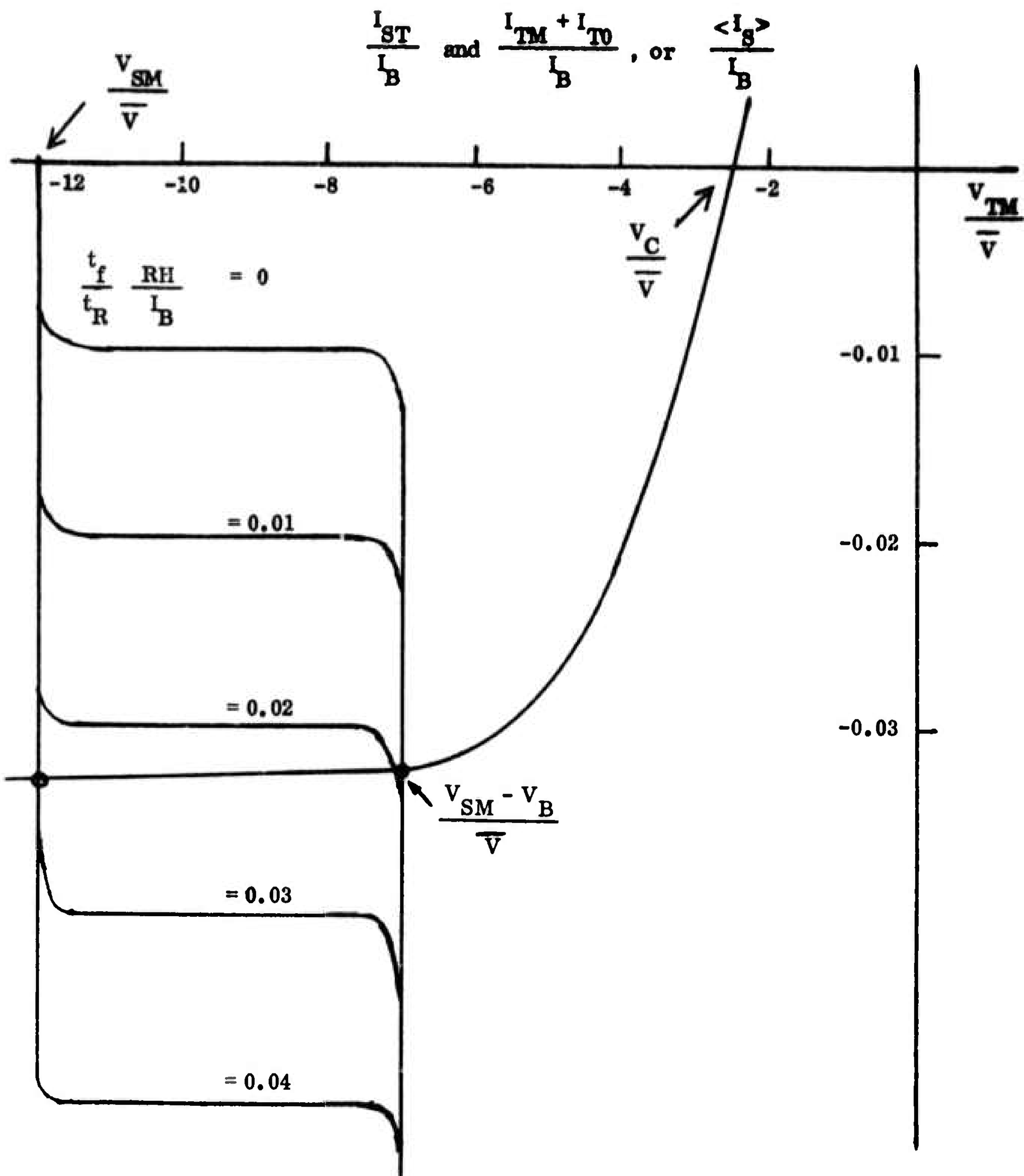

Figure 51 (b)

$\frac{I_{TS}}{I_B}$ as a Function of Light Level Superimposed on $\frac{I_{TM} + I_{T0}}{I_B} = \frac{\langle I_S \rangle}{I_B}$.

These Curves assume $\frac{V_{SM}}{\overline{V}} = -12$, $\frac{V_B}{\overline{V}} = 5$ and $\frac{I_{T0}}{I_B} \equiv 0$. For $\frac{t_f}{t_R} \frac{RH}{I_B} < 0.023$, $\frac{V_{TM}}{\overline{V}} \approx -7$. For $\frac{t_f}{t_R} \frac{RH}{I_B} > 0.023$, $\frac{V_{TM}}{\overline{V}} \approx -12$.

negative values in the light for constant values of V_{SM}, saturating when V_{SM} equals V_{TM}. It would appear from this curve that the diodes have a very high impedance out to about 10 volts, at which point they have a fairly sharp breakdown.

v. Imaging Properties of the Retina

With this much ground work on the various I-V relations, we now feel that we are in a position to discuss the rather complex imaging properties of this system. We will carry this discussion through first on the assumption that $\frac{I_{T0}}{I_B}$ is identically equal to zero, even though we do not feel that this is experimentally the case. The qualitative behavior of the imaging is not very dependent on this assumption, and it helps to simplify the discussion the first time around. We will then discuss how the results are modified if we change $\frac{I_{T0}}{I_B}$ to that given by equation (58).

- Imaging from the Composite Surface for $\frac{I_{T0}}{I_B} = 0$

In this case Figure 51 is applicable to the average signal current vs. light level. If a non-uniform light level is applied to the retina surface, each diode must independently charge through the beam current landing on its Pd_2Si surface. Thus for each diode, $\frac{I_{TM}}{I_B} \equiv \frac{I_{ST}}{I_B}$, and $\frac{V_{TM}}{\bar{V}}$ will be defined as a function of light level by Figure 50, for each diode independently. Thus diodes in the strongest light will have the most negative values of V_{TM}, while diodes in the dark will have the least negative values of V_{TM}. Referring to Figure 43, if I_{0M} were to be identically zero for each diode area independently, then V_{0M} would have to also change from dark regions to light regions in order to accommodate the changes in V_{TM} with light level. Thus V_{0M} would have to be more negative in the light areas and less negative in the dark areas. This could happen if there were no conduction along the top of the oxide surface. Then Figure 51 would tell the whole story, and imaging would occur by modulating V_{TM} and I_{TM} with light level. This would be the so-called normal or Dresner mode. The secondary emission would increase with increasing light level, or the signal current would become more negative with increasing light level.

However if the top of the oxide is conducting, under the influence of the beam, the conduction electrons will flow from the more negative to the less negative regions, their space charge easily being compensated by capacitative charging on the Si-oxide interface immediately beneath them. Thus the value of V_{0M} will be smeared out, and V_{0M} will be equipotential, determined by the average value of the light on the retina surface, or the average value of V_{TM} rather than the value determined by a local diode. V_{0M} will thus float to a value such that $\frac{\langle I_{0M} \rangle}{I_B} \equiv 0$. For example, let us suppose that we are biased as in Figure 51a, and that V_{TM} averaged over the entire scene comes out to $-3.5\,\overline{V}$. Then according to Figure 43, V_{0M} would be about $-2\,\overline{V}$ and this would be true for the entire retina surface. Then while $\langle I \rangle_{0M}$ would equal zero, we can see from Figure 51a and a curve such as Figure 43, that the dark areas would correspond to $\frac{V_{TM}}{\overline{V}} = -3$, and $\frac{I_{0M}}{I_B}$ equal to -0.09 while the very light area would correspond to $\frac{V_{TM}}{\overline{V}} = -6$ and $\frac{I_{0M}}{I_B}$ approximately equal to $+0.11$ $\frac{I_{0M}}{I_B}$ would thus be modulated with light as well as $\frac{I_{TM}}{I_B}$. The total signal current can be read off a curve such as that of Figure 45 for $\frac{V_{0M}}{\overline{V}} = -2$, and $\frac{V_{TM}}{\overline{V}}$ between -6 and -3. It is clear that the least negative values of V_{TM} corresponding to the dark areas give the most negative signal currents, while the most negative values of V_{TM} corresponding to the light areas could even read a net positive current. The change in signal current with light level is thus the opposite of that predicted by Dresner. This is then the so-called inverted mode. Experimentally the polarity of signal changes corresponding to the inverted mode has been seen in all cases except one where there was a very close mesh spacing, and it was felt that the beam did not strike the entire retina surface because of shadowing by the mesh. We will save a discussion of this until later, however, and discuss other properties of this inverted mode first.

First off, it is clear that for the case discussed, there is a built in gain in the signal current over that obtained by normal storage. When $\frac{t_f}{t_R}$ $\frac{RH}{I_B}$ changed

by 0.025 corresponding to saturation of the signal, the output signal I_S/I_B can be estimated from Figure 45 to have changed by 0.17. Therefore a gain of about 7 was achieved for the numbers used in this calculation.

If we are looking at a moving scene, but the overall light level on the target stays the same, then the value of V_{0M} will remain the same, and we should be able to track at a rate determined by the response time of the diodes. On the other hand if the overall light level on the scene changes, V_{0M} must also undergo changes to accommodate the average changes in V_{TM}. Since these changes involve changing the very large oxide to Si capacitance corresponding to that of the whole retina, they will occur rather slowly. Thus as we increase the overall light on the scene, $< V_{TM} >$ will become more negative and V_{0M} will gradually drift to more negative values. Since the values of V_{TM} corresponding to the lightest and darkest diodes do not change, we may infer from Figure 45 that the signal current read from the darkest diodes will gradually change to more negative values and the signal current read from the lightest diodes will also gradually go toward more negative values. Thus the signal current read from all the diodes will change when we change the overall scene, their average current becoming more negative with increasing overall light level. This is precisely the behavior that we see as a function of time when we change the overall light scene. It was in fact this data which indicated that all the diodes were coupled together through a common capacitance, (the oxide to Si capacitance) and led us to the concept that the oxide surface was acting as a conducting mesh.

As we continue to increase the overall light falling on the scene, V_{0M} will finally go sufficiently negative that V_{0T} will go negative on the darkest diodes. Electrons will then spill over from the oxide onto those diodes so that V_{0T} stays zero, and the current we can draw through these darkest diodes will saturate. As we increase the light level still further, diodes with slightly higher light levels will go into saturation along with the darkest diodes, and the low level contrast will be lost. Thus the picture will begin to blur out with increasing light level, as is observed.

If $\frac{V_{TM}}{\overline{V}}$ is made more negative we will finally bias ourselves into a situation

such as that shown in Figure 51b where all the diodes will carry the saturated current coming off the targets. Therefore the individual diode currents do not contain any information about the light level on the diode. However, the diodes in a strong light have V_{TM} equal to V_{SM}, while the diodes with low light levels sit with V_{TM} equal to $V_{SM} + V_B$. Since V_{TM} controls the current out of the oxide, we can still image a black and white scene even when all the diode currents are the same. This has been seen in practice. In fact, by examining Figure 45, it is clear that if V_{TM} is modulated by V_B, we will get our largest signal changes by allowing $\frac{V_{TM}}{\bar{V}}$ to be very negative. However, if the field between composite surface and mesh becomes too strong, it will pull down the potential maximum in front of the oxide as indicated in equations (53). Thus our ability to modulate the electrons will finally disappear for $\frac{V_{TM}}{\bar{V}} \leq \frac{-V_{0T}}{\bar{V}}\left(\frac{2d}{\ell} f_T + f_0\right)$. There will then be an optimum in $\frac{V_{TM}}{\bar{V}}$ for the best range of output signals. This optimum should go more negative as the mesh to target spacing increases. While this optimum will offer the best black-white contrast, it can be seen from Figure 51b that it will not allow for shades of grey, especially if the diode breakdown is steep. In other words all diodes will either read black or white. While the best black-white contrast is seen at large negative voltages, shades of grey will thus more easily be detected if we are biased as in Figure 50a. The best overall image will probably be achieved if V_{SM} sits about where the curve of $< I_S >$ vs. V_{TM} begins to saturate. See Figure 46 or 49.

- Imaging from the Composite Surface for $\frac{I_{T0}}{I_B}$ Given by Equation (58)

In actual practice, we feel that the diodes are being charged on a curve somewhat different than the one in Figure 46. This doesn't change any of the qualitative behavior described above. It would mean that it is easier to reverse bias the diodes, since the high secondary emission off the oxide is used to charge them. It should greatly improve redistribution problems since each diode can charge through the local oxide around it rather then by interacting with the remote mesh. Since the secondary emission is better, there will be an increased dynamic range. This increase in the dynamic range will reflect itself by a reduction in the

built-in gain we obtain when we go into the inverted mode. Thus the total range of output signal current that we can read by changing light level, is independent of the details of the I-V relation we assume for the PdSi-SiO_2 boundary. It is determined mainly by the change in the voltage V_{TM} that we can establish across the diodes with changing light level and the corresponding change in current off the targets and oxide into vacuum.

- <u>Conditions Required for the Two Modes of Imaging</u>

For the numbers used to calculate the curves in Figures 40-45, it is impossible to bias oneself into the Dresner mode. In order to get into the Dresner mode $\left(\frac{dI_{TM}}{dV_{TM}}\right)$ must be greater than $\left(\frac{dI_{0M}}{dV_{TM}}\right)$ at a bias condition where the diode impedance is high so that we can modulate V_{TM}. This means that $\frac{V_{SM} + V_B}{\overline{V}}$ cannot go too negative or we would be in a situation like that shown in Figure 51b where $\frac{dI_{TM}}{dV_{TM}}$ approaches zero. Also V_{SM} must be more negative than the voltage V_C where I_{TM} goes to zero, so that the diodes are reverse biased. Further $f_T(\delta_{TK} - 1)$ for the Pd_2Si would probably have to be at least comparable to $f_0(\delta_{0K} - 1)$ for the oxide so that the modulation of the current off the target could dominate. Finally the mesh spacing would have to be small so that redistribution of the electrons being modulated did not cause a blurring out of the picture. Thus the voltage range in V_{TM} and V_{MK} required to get into the Dresner mode is surely more limited and the mesh spacing is more limited than that required to get into the inverted mode.

We have seen imaging for thicknesses of the Pd_2Si ranging from 500 Å to 5000 Å, for mesh to target spacings between 2 mils and 250 mils, and for values of V_{MK} less than 100 volts and as high as 750 volts. The polarity and behavior of the imaging has always been that corresponding to the inverted mode with one exception. The opposite polarity corresponding to the Dresner mode was obtained when the mesh spacing was 2 mils V_{SM} was between -4 and -11 volts, and V_{MK} was 400 volts. For $V_{TM} < -11$ volts, the image flipped into the inverted mode. These conditions pretty much correlate with those expected from the above discussion, although there is some question whether $(\delta_{TK} - 1)$ could be high enough to get us into this mode.

For $V_{SM} < -30$ volts, the inverted image faded out. For this mesh spacing $\frac{2d}{\ell} \approx 100$. We may then infer from equation (53) that for these conditions $< V_{0T} > \approx 1/2$ volt.

It has been suggested that at the very close mesh spacings, shadowing of the electron beam by the mesh may prevent the electron beam from landing in regions immediately under the mesh wires. Thus, there may be isolated squares under the mesh holes where the oxide can conduct, each square being separated from an adjacent square by a non-conducting area. If this were the case, each square would float to a potential determined by the light pattern falling on it, and the value of V_{0M} would not have to be the same for all squares. Thus if one square were all light and another square were all dark, the current coming off the light square would be more negative than the current off the dark square. The signal current would then have a polarity corresponding to the Dresner mode, but generally we would not be modulating the current within a square. We might in this case get some peculiar edge effects in a square where we are crossing a sharp boundary between light and dark areas.

It is possible that this is going on at the close mesh spacings where we saw the polarity of the Dresner mode. However, we are then left to explain how we managed to flip into the inverted mode for V_{SM} becoming sufficiently negative.

If we look in the dead areas, where the beam does not land, V_{SM} must equal V_{TM} since no current is leaving the diodes. However the voltage between silicon and mesh will partly distribute itself across the oxide since it is non-conducting. Thus we can anticipate that

$$V_{0T} \approx \frac{-K_{0X} t_{0X} \cdot V_{SM}}{K_{0X} t_{0X} + d} \qquad (62)$$

where K_{0X} is the dielectric constant for the oxide, t_{0X} is the thickness of the oxide and d is the mesh spacing. On the other hand, by examining Figure 41, we can see that where the electron beam lands, V_{0T} will saturate as V_{TM} goes more negative. It is thus possible that as we make V_{SM} more negative, the oxide potential in the dead areas will go more positive than the oxide potential where the beam lands. Electrons can then spill into the dead areas, their space charge being neutralized by capacitative charging with holes in the Si. The oxide surface would then again become an equipotential and we would go into the inverted mode.

d. Conclusions

Our imaging results to date, seem to indicate that the oxide surface acts as a floating mesh which is capacitatively coupled to the Si substrate. While this oxide mesh is isolated from the diodes when they are not being read, we are predominantly modulating the current off of it, when the diodes are being read. The modulation of the current off the oxide is controlled by the voltage V_{TM}, once the oxide is in a cyclic state. The voltage V_{TM} is in turn controlled by the local light level. The ability to modulate the oxide current with V_{TM} was not anticipated in advance of experiment. While it greatly reduces our concerns about the redistribution of secondaries, it complicates the imaging results, mainly because the oxide to mesh potential drifts with the overall light level falling on the retina. It may be possible to minimize the effects associated with this, by making adjustments in the beam current, the frame time, and biasing voltages. This area deserves further study.

The theory also suggests that if we deliberately integrated a mesh, onto the top of the oxide, we could then control this voltage between top oxide surface and mesh by an external supply. Modulation of current off this mesh to a remote mesh could still be controlled by light falling on the diodes. However the voltage between the top of the oxide and remote mesh could now be externally controlled, so that no drifting would occur with overall light level. Since the capacitance between the integrated and the remote mesh would be low, it would be desirable from the point of view of loading to read the signal between these two leads, rather than between Si and integrated mesh where the capacitance is high.

REFERENCES

1. V. L. Dalal, J.A.P., 42, 2280 (1971).

2. F. D. Shepherd, Jr., et al., "Silicon Schottky Barrier Monolithic IRTV Focal Plans," to be published.

3. A. S. Jensen, RCA Review, Vol. XVI, pp. 216-232, June 1955.

4. S. M. Sze, "Physics of Semiconductor Devices," Wiley (1969).

5. J. P. Spratt, "Infrared Imager Test Facility," Final Report under Air Force Contract #F19628-73-C-0306, 30 September 1974.

6. V. Garuts and C. Samuel, "Measuring Conventional Oscilloscope Noise," Tekscope, April 1969.

7. M. P. Lepselter and S. M. Sze, B.S.T.J., 47, 195 (1968).

8. R. Kollath, Handbook Physics, Vol. XXI, Springer (Berlin), 1956.

9. J. Dresner, RCA Review, 22, 305 (1961).

APPENDIX

EFFECT OF MESH CAPACITANCE ON PREAMPLIFIER INPUT

The following equivalent circuit can be used to described the effect of mesh to target capacitance on the input capacitance to the preamp.

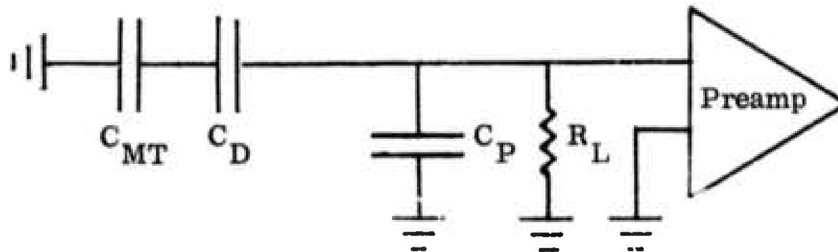

C_{MT} = mesh to target capacitance

C_D = capacitance of the metal-silicon diodes

C_P = parasitic capacitance to ground between retina and preamplifier input

R_L = input load resistor

$$\text{Thus, } C_{in} = C_P + \frac{C_{MT}\, C_D}{C_D + C_{MT}}$$

or, since $C_D >> C_{MT}$

$$C_{in} \approx C_P + C_{MT}$$

So that C_{in} increases if C_{MT} increases. For example, with a 1-inch diameter retina-mesh combination, a 0.020 inch mesh retina spacing will introduce less than 10 pf capacitance, but a 0.002 inch spacing will introduce nearly 100 pf.

Since the preamp measures the voltage to ground across R_L, the effect of close mesh spacing on the bandwidth is the same as an increased parasitic capacticance, i.e.,

$$\text{bandwidth} = B = \frac{1}{2\pi R_L (C_P + C_{MT})} .$$

Preceding page blank

Thus the mesh spacing should be kept as large as possible commensurate with the need to prevent redistribution of secondary electrons.